FEUP

"High Pressure–High Temperature Viscosity Modeling of Hidrocarbons and Synthetic Mixtures Present on Petroleum Reservoirs "

PhD thesis
on
Chemical Engineering

by

José Manuel de Castro Miranda do Vale Machado

Supervision
Maria Eugénia Rebello de Almeida Macedo

LSRE
Laboratory of Separation and Reaction Engineering

Departamento de Engenharia Química
Faculdade de Engenharia
Universidade do Porto

Acknowledgements

The author wishes to express its indebtment to European Commission -EVIDENT project, Contract No: JOF3-CT97-0034 for the financial support of the work presented.

This work was carried out at the Laboratory of Separation and Reaction Engineering (LSRE) headed by Professor Alírio E. Rodrigues. The author expresses his deep gratituted for the constant interest and scientific example.

The author wishes also to express his gratitude to all the EVIDENT Project partners, for their goodwill and cooperation with the FEUP team, as well as for all the co-workers in the Evident Porto Team – Professor Maria Eugénia Macedo, Dr. Laurent Trassy, Dr. Marcelo Zabaloy, José Joaquím Machado and Eliana Abreu, for their deep commitment and team spirit.

A special thanks to Claus Zéberg-Mikkelsen (Technical University of Denmark) for having provided, within the framework of the European project EVIDENT, a database used for calculations

For all friends and family that endured the effort of finishing and writing the present work.

A last word of appreciation is due to my PhD supervisor, Professor Maria Eugénia Macedo, for all the support and trust along the years.

Abstract

The present work was conducted within the framework of the EU EVIDENT (Extended VIscosity and DENsity Technology) project. The main goal of the project was to attain a better understanding of deep off-shore petroleum reservoir's viscosity and density, which are critical variables for the project and operation of extraction equipments. Conditions in such petroleum wells are characterized as High Temperature High Pressure (HPHT). Under such conditions a scarcity of data and robust and accurate models for viscosity are encountered. The goal of the work carried out was to obtain a model for viscosity, based on Molecular Dynamic (MD) simulation techniques.

As a first approach, a wide literature search was carried out on the available models, evaluating both their ranges in pressure, temperature and density, but also on the phases that the models were able to simulate.

After, and to obtain a better understanding of molecular simulation techniques, a description of the methodology of MD is presented, along with results obtained during this work for the Lennard-Jones model fluid.

The conclusion of the work performed in MD simulations, namely in computer processing time and calculation speed, led to the development of an alternative strategy, using Equivalent Analytical Relationships (EAR's) based on MD data. A full viscosity equation of state was developed based on EAR's obtained by adjusting MD data.

This model was first applied to a large pure component viscosity database, and then extended to mixtures. Due to the limited range of application, compared to the goals of the project, extrapolation schemes were also devised, to extend the temperature and density applicability range of the model, limited by the MD data used to develop the EAR's.

The model was finally tested with pure and multi-component mixture data, and its performance benchmarked against other models presented in the literature, demonstrating its good qualitative and quantitative behavior with low values of average absolute-value percent relative deviation for most of the systems studied.

Resumo

O trabalho apresentado foi executado no âmbito do projecto europeu EVIDENT (Extended Viscosity and DENsity Technology), cujo objectivo consistiu na procura de uma melhor compreensão sobre comportamento da viscosidade e densidade em fluidos petrolíferos em reservatórios marítimos de grande profundidade, uma vez que estas variáveis são críticas no projecto e operação de equipamentos de extracção. As condições neste tipo de poços de petróleo são caracterizados pelas suas condições extremas de alta temperatura e alta pressão (ATAP). Para estas condições operacionais, verifica-se uma grande escassez de dados e de modelos de simulação de viscosidades. O objectivo dos trabalhos desenvolvidos é então a obtencão de um modelo de simulação para viscosidade, baseado em técnicas de simulação molecular (SM).

Como primeira aproximação ao objectivo do trabalho, foi realizada uma pesquisa bibliográfica sobre modelos disponíveis, avaliando tanto as gamas de pressão, temperatura e densidade, como o tipo de fases que os modelos conseguem simular.

Seguidamente, e para obter um melhor entendimento das técnicas de simulação molecular, é apresentada uma descrição da metodologia de SM, assim como resultados de simulação obtidos para o fluido de Lennard-Jones.

A conclusão do trabalho realizado sobre SM, nomeadamente no que respeita a tempos e velocidades de computação, levou ao desenvolvimento de uma estratégia alternativa, usando Relações Analíticas Equivalentes (REA), baseadas em dados resultantes de SM. Uma equação de estado para cálculo de viscosidades foi desenvolvida, tendo como base as REA obtidas por ajuste de dados de SM.

O modelo obtido foi primeiramente aplicado a uma base de dados de viscosidades de componentes puros, e posteriormente aplicado a misturas. Devido aos limites de aplicação, comparativamente aos objectivos do projecto, foram desenvolvidas técnicas de extrapolação, para estender a gama de aplicação no que diz respeito às gamas de temperatura e densidade resultantes dos dados de SM usados para o desenvolvimento das RAE.

O modelo foi por fim testado com dados de viscosidade para compostos puros e misturas multi-componente, e a sua performance comparada com modelos presentes na literatura, tendo demonstrado o seu bom comportamento qualitativo e quantitativo com valores de desvios médios significativamente baixos para a maior parte dos sistemas estudados.

Resumé

Ce travail a été réalisé dans le cadre du projet européen EVIDENT (Extended VIscosity and DENsity Technology). L'objectif principal de ce projet est de parvenir à une meilleure connaissance des variations de la viscosité et de la densité des réserves pétrolières localisées dans les grands fonds marins (offshore). Ces deux propriétés sont en effet essentielles pour le dimensionnement des unités d'extraction. Les puits de pétrole offshore sont dits "HPHT" car ils sont caractérisés par de Hautes Pressions et de Hautes Températures. Dans de telles conditions, les données expérimentales de viscosité sont rares et peu de modèles sont suffisamment robustes et précis pour estimer cette propriété. Le but des travaux entrepris est de développer un modèle capable d'estimer la viscosité en conditions extrêmes en utilisant des techniques de simulation par dynamique moléculaire (DM).

Dans un premier temps, une recherche bibliographique approfondie a été menée afin de recenser les modèles décrits dans la littérature. Une évaluation de leur domaine de validité en pression, température et densité ainsi qu'un recensement des états physiques de la matière que ces modèles pouvaient représenter ont été réalisés.

Dans un deuxième temps, afin de mieux comprendre les techniques de simulation moléculaire, une description de la méthodologie employée en dynamique moléculaire (DM) est présentée. Nous donnons alors les résultats obtenus au cours de ce travail pour un fluide modèle de Lennard-Jones.

Les conclusions du travail de simulation par DM relatives au temps et la vitesse de calcul nous ont conduit à développer une stratégie alternative basée sur la définition de relations analytiques équivalentes (RAE) construites sur des données obtenues par DM. Par ajustement de données issues de la DM, une équation permettant d'estimer la viscosité a été développée.

Ce modèle a d'abord été appliqué aux corps purs avant d'être étendu aux mélanges. A cause du domaine restreint des données de DM utilisées pour développer les RAE, le champ d'application du modèle mis au point est limité, en comparaison aux objectifs du projet. Pour palier à cet inconvénient, des méthodes d'extrapolation en température et en densité ont également été développées.

Le modèle final a été testé sur des données de corps purs et de mélange. Ses performances sont supérieures aux autres modèles de la littérature démontrant ainsi son bon comportement qualitatif et quantitatif puisque de petits écarts absolus ou relatifs sont obtenus pour la plupart des systèmes étudiés.

Index

1. Introduction

1.1 MOTIVATION

The depletion of world fossil fuel reserves has been leading oil and natural gas companies to search and exploit natural reservoirs at consecutively higher depths. Deep offshore petroleum reservoir exploration constitutes challenging engineering problems.

These reservoirs lay at depths of 2 to 3 thousand meters below the sea surface, under pressures ranging up to 1000 bar. Recent foundings point to the existence of rich gas condensates in these reservoirs. In the oil business, their common name is "deep off-shore reservoirs".

Nevertheless, the cost of an extra North See well can cause the abandonment of exploration, for economic reasons: the cost of 1 "deep off-shore" well is equivalent to 5 "off-shore" wells and close to 100 "on shore" wells.

Due to this reason, the recovery efficiency is therefore a paramount factor for an acceptable return on the investment.

To attain such high levels of efficiency, extraction technologies such as "CO2 enhanced oil recovery" by gas injection are applied, and an accurate prediction of physical properties and geological conditions that influence the transport properties of both phases must be available, so that the best extraction "strategy" can be simulated in reservoir simulators before the actual extraction operation can take place.

In this way, the development of models that can predict these physical properties with acceptable accuracy is fundamental both during simulation and extraction operations, namely on the development of the extraction equipment.

Viscosity has in this context a paramount role, as it will determine in great extent the dynamics of the fluids being extracted and the forces acting on the extraction equipment and reservoir wells.

Nonetheless, and when compared with other physical properties, a relative scarcity of experimental data and predictive models is found. When available, these models or datasets are referred to narrow ranges of conditions (Pressure-Temperature-Density-Phase State) to be used in the "operation envelopes" of deep offshore wells – High Pressure (~100 MPa) and High Temperature (~373 K) (HPHT).

The existing models are most often of empiric nature, usually based on correlated data. Their range of applicability in P-T and the phase type that the models can represent are also narrow and their accuracy limited and dependent of the reference fluids.

To cope with such limitations, a consortium of University Laboratories and companies joined forces in a JOULE Project, supported by the European Union – EVIDENT – **E**xtended **VI**scosity and **DEN**sity **T**echnology. Universities such as University of Porto (FEUP) - Portugal, Université de Pau - France, Hariott-Watt University – Edinburgh - UK, Technical University of Denmark (DTU) - Denmark, the company ELF-TOTAL in France and the *Institut Français du Pétròle* – Paris - France, collaborated for 3 years to produce both accurate and wide-range models as well as a comprehensive database of experimental viscosity data in deep off-shore conditions of petroleum reservoir fluids (HPHT).

The FEUP team was assigned with the task to develop a model based on molecular theory. The study presented in this thesis is therefore a reflection of the work done for the Project by the author.

A comment should be made at this point, regarding the orientation followed during the PhD studies by the author: The EVIDENT Project had very specific goals and each team had specific development tasks to perform and a Project schedule to respect. The work performed under these circumstances requires a "Project Management" approach, regarding scientific and strategic decisions made during an on-going project. In so many occasions, the "scientific curiosity" of the author had to be replaced by the professional project-oriented attitude on the choice of the "road to follow".

1.2 OBJECTIVES

The main objective of this thesis is the development of a viscosity model, based on Molecular Dynamics, able to simulate deep off-shore viscosity behaviour of multi-component mixtures containing hidrocarbons and other compounds present in deep offshore petroleum wells.

In chapter 2, an assessment of the existing models able to represent Newtonian fluid viscosity of pure components and mixtures, both with theoretical and semi-theoretical background, is presented. Their main features are analyzed, namely applicability in terms of fluid state, as well as the range in terms of temperature, pressure and density. Calculation comparisons are presented for selected models that showed the best predictive features.

In chapter 3, an overview on Molecular Dynamic (MD) techniques is presented, as well as the theoretical background for Equilibrium Molecular Dynamic (EMD) simulation. Results for EMD simulations performed for the model fluid of Lennard-Jones are presented and compared with the ones presented in the literature. The results and conclusions of this chapter, regarding the applicability of MD simulation to petroleum reservoir simulators are presented, as well as considerations regarding the quality pertaining to the method, and their computing power and time requirements.

In chapter 4, an alternative to MD simulations is presented. The development of a model based on MD simulation results for the Lennard-Jones fluid is presented, as well as the results of its tests with a large pure component viscosity database, containing typical reservoir compounds. The model developed is based on the Equivalent Analytical Relationships (EAR) technique, using background data from previous MD simulations from the literature. A thorough analysis, both on its qualitative and quantitative behaviour is presented and its results and limitations discussed.

In chapter 5, the implementation of extrapolation schemes to the model is proposed, due to range limitations in terms of temperature and density. A qualitative and

quantitative assessment is presented for the model incorporating these extrapolation features, and the resulting final model is extended to mixtures, using the One Fluid Approach applied to its internal parameters (ε and σ). Interaction parameters are also implemented, and the resulting model tested, firstly against a database of binary, ternary, quaternary and quinary mixtures, and subsequently against data for synthetic mixtures representing real reservoir fluids. As a final performance test, the results of the model are compared to an alternative model proposed by our EVIDENT partners from DTU in Denmark, and results and main features discussed.

The main conclusions of this work are latter presented in chapter 6, with suggestions for further work.

2. Evaluation of Existing Models

2.1 INTRODUCTION AND GENERAL REMARKS

The objective of this chapter is to present an assessment of the existing models to represent Newtonian fluid viscosity of pure components and mixtures, both with theoretical and semi-theoretical background, proposed in the literature.

Due to the relative scarcity of theoretical-based models available in the literature, we have decided to take into account some empirical methods. Nevertheless, we have limited our research field to methods not based on "corresponding states theory" in view that this being the objective of the the work carried out by the DTU modeling team , partner in the Evident Project.

We have to emphasize that the main criterion of selection was the predictive character of the method. In fact, if there is a great number of solutions proposed in the literature to represent the fluid viscous behavior, the majority of the methods require, for reliability sake, the fitting of parameters to existing measurements. If this procedure can be accomplished for pure compounds or simple mixtures, it is not reasonable to imagine such a way of dealing with complex mixtures containing hundreds of components like petroleum fluid "cuts".

As a starting point to the model revision and selection, we have considered the extensive review article from Monnery, Svrcek and Mehrotra (1995), where the authors describe and compare the different approaches available for the viscosity modeling.

The main problems met during this study were linked to:

- the scarcity of high pressure reliable data available in the literature – as opposite to the amount of data published for low and atmospheric pressures is quite important;
- the specificity of models which are, in general, dedicated on one hand to gases, on the other to liquids;
- the determination of pure compound properties (molecular weight, density or specific volume, viscosity) which are not always available;
- the strong relationships between density and viscosity. The use of kinematic viscosity rather than dynamic viscosity, which is sometimes proposed, does not appear to be a feasible solution.

The purpose of this chapter is to show some of the solutions proposed in the literature, to evaluate their quality and to define their limitations. Before presenting the results, it has to be underlined that none of the methods can offer a general answer, and that in all the cases we were unable to test models with the totality of experimental viscosity database.

Although there is no global way to solve the problem, we can propose different solutions in relation with the fluid state.

For very dense fluids (i.e., liquids), we have not found theoretical based models developed for high pressures. One explanation for this situation can be the relative limited number of high-pressure data available in the literature. The answer suggested here is first to model the mixture viscosity under low pressures with a semi-theoretical model (Reaction Rate Theory models) and secondly to extend the method application to high pressures with a correlation (Kanti *et al.*, 1989). In order to evaluate the quality of the results, we consider another solution for liquid mixtures proposed by Orbey and Sandler (1993). This method is totally empirical but has the advantage to limit the pure compound datum input to normal boiling temperature.

For dilute and dense gases, Chung *et al.* (1984; 1988) proposed a model based on Chapman-Enskog viscosity equation. This model can be extended to liquids but important deviations can be expected in those conditions.

The comparison of liquid viscosity methods and their extension to high pressures constitute the first part of this chapter. In a second section, we present the model of Chung *et al.* (1984; 1988), established for gases and extended to liquids.

2.2 MODELS FOR LIQUIDS

2.2.1 The Reaction Rate Theory - Application to viscosity phenomenon

2.2.1.1 The Reaction Rate Theory

Initially, the Reaction Rate Theory, or "Activated Complex" theory, was introduced to model chemical reaction behaviours. Due to its very simple approach, this concept has been widely used to describe a large number of other chemical and physical phenomena. The idea is that any given evolution process can be identified as an equilibrium between reactants and products. To go from one side to the other, the system is passing through a transition state, $[AB]^*$, called "Activated Complex" (Figure 2.1):

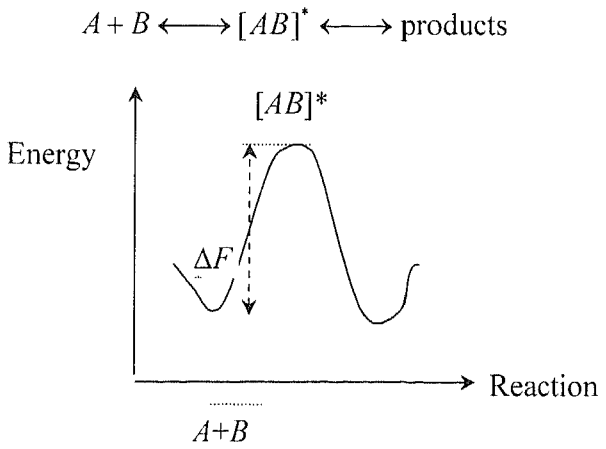

Figure 2.1 - Energy profile in the Reaction Rate Theory.
Reproduced from Powell *et al.* (1941)

The aim of the Reaction Rate Theory is to express the proportion of "Activated Complex", which is able to reach the final state.

Such as it was formulated originally, it is common use to consider the partition function of "Activated Complex" destruction as similar as a transitional degree of freedom in the direction of the product formation. Also, to simplify the problem, one can suppose that the pathway in the two directions (reactants $\Rightarrow$ products and products $\Rightarrow$ reactants) is symmetrical. Thus, the Reaction Rate can be expressed as a function of reactant concentration, C_0, of temperature, T, and of Activation Energy, ΔF^*:

$$\text{Reaction Rate} = C_0 \frac{kT}{h} \exp\left[-\frac{\Delta F^*}{RT}\right] \qquad (1)$$

All the models based on Reaction Rate Theory consider equation 1. They only present differences in the way of expressing C_0.

2.2.1.2 Application of the Reaction Rate Theory to viscosity:

Eyring and coworkers (Powell *et al.*, 1941), proposed to model transport phenomena using the same approach. For viscosity, they consider a reticular model constituted by two molecule layers where all the sites are not occupied (Figure 2.2).

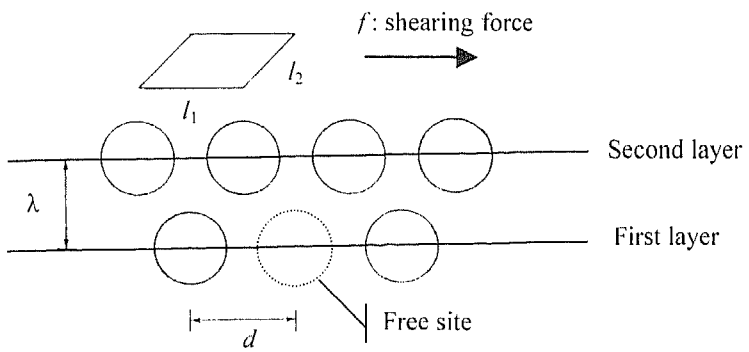

Figure 2.2 - Eyring's model for fluid flow. Reproduced from Powell *et al.* (1941)

If a molecule in the liquid moves from one equilibrium site to another, the molecule has to overcome an activation energy barrier. If there is no shear force, the activation energy is the same in the forward (formation of the "Activated Complex") and backward (destruction of the "Activated Complex") directions, i.e. ΔF^*. On the other side, if a shearing force f is applied across the two layers, the molecular movement frequencies in the two directions are different.

The dynamic viscosity is expressed as the shearing force, f, divided by the velocity gradient, $\left(\frac{\Delta u}{\lambda}\right)$, between the two molecule layers, that is to say:

$$\eta = \frac{f\lambda}{\Delta u} \tag{2}$$

where λ is the distance between two molecule layers. The velocity difference Δu takes only into account the frequencies of molecule movements in the forward and the backward directions (respectively, k'_f and k'_b) and the mean distance, d, to move from an occupied site and a vacant position:

$$\Delta u = d\left(k'_f - k'_b\right) \tag{3}$$

For the expression of k'_f and k'_b, we have to consider each molecule as a reticular segment (Figure 2.2) occupying the elementary surface (l_1*l_2). The work, ε_a, done by the shear force, f, to allow a molecule to reach the "Activated Complex" state is thus:

$$\varepsilon_a = f\left(l_1 * l_2\right)\frac{d}{2} \tag{4}$$

i.e., the frequencies of movements will be expressed by:

Forward direction: $k'_f = \frac{kT}{h}\exp\left(-\frac{\Delta F^* - \varepsilon_a}{RT}\right)$ (5)

Backward direction: $k'_b = \frac{kT}{h}\exp\left(-\frac{\Delta F^* + \varepsilon_a}{RT}\right)$ (6)

The combination of expressions 2 to 6, leads to the final expression:

$$\eta = \frac{h N_a}{V}\exp\left(\frac{\Delta F^*}{RT}\right) \quad (7)$$

where we assume, as close approximation, that the term $\frac{d^2 l_1 l_2}{\lambda}$ can be considered as the volume $\frac{V}{N_a}$ of a molecule (Powell *et al.*, 1941).

In the one fluid approach, expression 7 is used both for pure compounds and for mixtures, i.e.,

Pure compound *i*: $\eta_i = \frac{h N_a}{V_i}\exp\left(\frac{\Delta F_i^*}{RT}\right)$ (8)

Mixture: $\eta_{mix} = \frac{h N_a}{V_{mix}}\exp\left(\frac{\Delta F_{mix}^*}{RT}\right)$ (9)

where it is possible to consider the mixture activation molar free energy, ΔF_{mix}^* equal to the sum of the pure compounds activation molar free energies multiplied by their respective mole fraction and a term of excess activation molar free energy:

$$\Delta F_{mix}^* = \sum_{i=1}^{p} x_i \Delta F_i^* + \left[\Delta F^*\right]^{Excess} \quad (10)$$

The simultaneous use of equations 8, 9 and 10, yields the following expression for the mixture dynamic viscosity η_{mix}:

$$\ln(\eta_{mix}V_{mix}) = \sum_{i=1}^{p} x_i \ln(\eta_i V_i) + \frac{[\Delta F^*]^{Excess}}{RT} \quad (11)$$

which is also equivalent for mixture kinematic viscosity, ν_{mix}, to:

$$\ln(\nu_{mix}M_{mix}) = \sum_{i=1}^{p} x_i \ln(\nu_i M_i) + \frac{[\Delta F^*]^{Excess}}{RT} \quad (12)$$

The implicit condition to go from equation 11 to equation 12 is to use the following mixing rules for molecular weight and molar volume, assuming ideal behavior of components in the mixture:

$$M_{mix} = \sum_{i=1}^{p} x_i M_i \quad (13)$$

$$V_{mix} = \sum_{i=1}^{p} x_i V_i \quad (14)$$

It is obvious that with equations 11 and 12, one can obtain different ways to express $[\Delta F^*]^{Excess}$.

2.2.1.3 Other approaches

We have taken into account three predictive methods based on the Reaction Rate Theory. They are all based on group contribution approaches, like the UNIFAC model (Fredenslund *et al.*, 1975). In fact, Eyring and coworkers (Powell *et al.*, 1941) had already tried to correlate the activation energy, for which experimental value is impossible to define, to more common used properties such as heats of vaporization.

If the results were satisfactory for some of the compounds studied by the authors, Wu (1986) noted that for a more extensive database, the results obtained were very poor and did not justify at all the correlation parameters proposed by Eyring and coworkers (Powell *et al.*, 1941).

Wu (1986) proposed the first model studied in this section.

Rather than comparing activation energies and heats of vaporization, the author determined directly $\left[\Delta F^{*}\right]^{Excess}$ from the molar free energy of mixing. After an analysis of the results obtained for n-alkane-n-alkane binary systems (in fact, the residual contribution to the excess molar free energy is equal to zero, since the interaction energy parameters for n-alkane-n-alkane systems are negligible), Wu (1986) suggested to multiply the combinatorial term of UNIFAC by a scaling factor equal to 3.71. In that condition the expression of the activation energy is given by:

$$\left[\Delta F^{*}\right]^{Excess} = -\left(3.7\ \Delta F^{Excess}_{Combinatorial} + \Delta F^{Excess}_{residual}\right) \qquad (15)$$

If the original structure of UNIFAC was kept, interaction parameters were fitted to experimental viscosity data points available in the literature.

The second model analysed was presented by Chevalier (1988). This approach is quite similar to Wu's model (Wu, 1986). If no scaling factor is introduced ahead of the combinatorial term, the method requires interaction parameters between methyl (CH_3-) and methylene (-CH_2-) alkane groups but also between alkane groups (CH_3- and -CH_2-) and cyclane group (-$[CH_2]_{Cycl}$-). In order to simplify the method, the number of surface and volume factors was reduced and the molecule cut was simplified. The authors justify the introduction of a minus sign forward the residual term in order to account for the difference between activation energy and excess molar free energy (Meyer *et al.*, 1971):

$$\left[\Delta F^{*}\right]^{Excess} = \Delta F^{Excess}_{Combinatorial} - \Delta F^{Excess}_{residual} \qquad (16)$$

For this model, the original structure of UNIFAC was also kept, but all the interaction energy parameters were fitted to the low-pressure experimental viscosity data published by Chevalier *et al.* (Chevalier *et al.*, 1990).

The approach of Cao *et al.* (1992; 1993 a, b) is differing from the original formulation of Eyring and coworkers (Powell *et al.*, 1941) (equations 11 and 12) since the authors used the statistical mechanical lattice theory (Guggenheim, 1952) and the local composition concept in its development. The concept of group solution is included from the beginning and not at the end such as it happens with the methods of Wu (1986) and Chevalier *et al.* (1988).

These authors consider that there are two degrees of freedom of molecular movement due to the activation process and suppose that the activation energy of a molecule *i* is directly proportional to its potential energy in the liquid mixture. In order to avoid the classical fitting procedure of interaction energy parameters, Cao *et al.* (1993b) decided to use directly vapor-liquid equilibrium (VLE) parameters from the UNIFAC original method (Fredenslund *et al.*, 1977). An empirical correlation (equation 20) was nevertheless introduced to attain reliable predictions. Under these conditions, equations 11 and 12 were changed to:

$$\ln(\eta_{mix} V_{mix}) = \sum_{i=1}^{p} \left[\phi_i \ln(\eta_i V_i) - 2\phi_i \ln\left(\frac{\phi_i}{x_i}\right) \sum_{k\ groups} \vartheta_k^{(i)} \left(\Xi_{ki} - \Xi_{ki}^{(i)}\right) \right] \quad (17)$$

and,

$$\ln(\nu_{mix} M_{mix}) = \sum_{i=1}^{p} \left[\phi_i \ln(\nu_i M_i) - 2\phi_i \ln\left(\frac{\phi_i}{x_i}\right) \sum_{k\ groups} \vartheta_k^{(i)} \left(\Xi_{ki} - \Xi_{ki}^{(i)}\right) \right] \quad (18)$$

with:

$$\Xi_{ki} = -\frac{Q_k}{R_k} N_{ki}^{vis} \sum_{m\ groups} \theta_{mk} \ln(\Psi_{mk}) \quad (19)$$

$$N_{ki}^{vis} = Q_k \left(\frac{q_i - r_i}{2} - \frac{1 - r_i}{z} \right) \quad (20)$$

where the parameter definition of z, q_i, r_i, ϕ_i, Q_k, R_k, θ_{mk}, $\vartheta_k^{(i)}$ is identical to that used in original UNIFAC model (Fredenslund *et al.*, 1975).

2.2.1.4 Comparison of the results under atmospheric pressure and at ambient temperature

The goal of the work carried out in the present chapter was to estimate the predictive capabilities of the methods previously described under atmospheric pressure and, for most of the data, at 298.15 K. Such as it is shown in equations 11, 12, 17 and 18, in order to calculate mixture viscosities it is compulsory to introduce some properties of pure compounds. If molecular weight can be easily assessed for all the molecules, a different situation arises when assessing viscosity (kinematic or dynamic) or molar volumes.

The problem is really acute for dynamic viscosity relations (equations 11 and 17) where it is necessary to introduce both density and dynamic viscosity for each component of the mixture. It is clear that the choice of kinematic viscosity calculation (equations 12 and 18) limits the problematic input data to pure compound kinematic viscosities. For the comparison performed using low-pressure data, experimental property measurements were available for each system component. This situation allows us to focus on the unique predictive quality of the models, without any perturbation due to the determination of input parameters.

In a situation where the pure compound viscosity data should be deficient, it is eventually possible to use the viscosity correlations proposed by Cao *et al.* (1992) for a large variety of molecules. Another alternative could be the use of the group contribution method developed by Van Velzen *et al.* (1972) which is very well described in Reid *et al.* (1987).

The results obtained are in most of the cases very satisfactory (See Table 2.1). The parameter fitting procedure applied for Wu's model (1986) and for the method of Chevalier *et al.* (1988) leads to very accurate predictions. However, the results given by Wu's method for aromatic-alkane systems were very different from those presented by the author (Wu, 1986). One can suppose that one explanation for these important deviations is a wrong transcription of the interaction parameters in the UNIFAC parameter table.

Nevertheless, we can expect with Wu's method (1986) results of the same quality of those obtained with the method of Chevalier *et al.* (1988). It is very interesting to note that the introduction of new interaction groups in Chevalier's method (1988) does not give any advantage for the modeling of n-alkane-n-alkane and cyclane-n-alkane systems.

The solution proposed by Wu (1986) to use a scaling factor ahead of the combinatorial term seems, in that case, more appropriate. The results given by the method of Cao *et al.* (1993a, b) are also good although the behavior of the model seems less reliable for systems containing aromatic-cyclane interactions and when the size difference between molecules of the system is increasing. Nevertheless, this last method is the most widely used due to the use of already available VLE UNIFAC interaction parameters (Fredenslund *et al.*, 1977).

Table 2.1 - Comparison of the performance of different models for the prediction of binary systems kinematic viscosities at atmospheric pressure.

				AAD (%)		
Binary	**System**	**P (MPa)**	**NDP**	**Wu (1986)**	**Chevalier *et al.* (1988)**	**Cao *et al.* (1993a, b)**
n-alkane	n-alkane	0.101325	144	0.4	0.4	2.1
Substituted alkane	n-alkane	0.101325	68	2.5	2.9	3.9
Cyclane	n-alkane	0.101325	45	3.6	4.1	3.0
Aromatic	n-alkane or aromatic	0.101325	233	-	1.4	7.3
Aromatic	Cyclane	0.101325	25	-	1.91	10.62

Due to the use of low-pressure models such as the UNIFAC method, all the models previously described are unable to represent high-pressure viscosities. We have also to underline that the temperature range of application of these models is very narrow. Thus, in order to account for the simultaneous effects of pressure and temperature, it is necessary to use correlations, as presented in the next section.

2.2.2 Empirical and semi-empirical correlations

2.2.2.1 Kanti's method (Kanti et al., 1989)

This method was originally developed for petroleum fluid applications. The idea was to carry out predictions with a minimum of input data, and more precisely to use petroleum cuts measurements obtained in the production field. To predict the dynamic viscosity of a given fluid, under pressure P and at a temperature T, it is only necessary to hold a value of the dynamic viscosity fluid under a pressure of one bar and at an arbitrary reference temperature T_0. If this correlation is purely empirical, it has the advantage to use only nine universal constants α, β, χ, δ, ε, φ, κ, λ and ς, given in Table 2.2.

$$\ln\left[\frac{\eta(P,T)}{\eta(1,T_0)}\right] = \left(\alpha\xi^2+\beta\xi+\chi\right)\ln\left[1+\frac{(P-1)}{\delta\xi^2+\varepsilon\xi+\varphi}\right] + \left(\kappa\psi^2+\lambda\psi+\varsigma\right)\left(\frac{1}{T}-\frac{1}{T_0}\right) \tag{21}$$

with,

$$\xi = \psi+\left(\kappa\psi^2+\lambda\psi+\varsigma\right)\left(\frac{1}{T}-\frac{1}{T_0}\right) \tag{22}$$

$$\psi = \ln\left[\eta(1,T_0)\right] \tag{23}$$

Table 2.2 - Parameters α, β, χ, δ, ε, φ, κ, λ and ς given by Kanti *et al.* (1989)

α = 0.275832	β = 0.533739	χ = 1.838385
δ = 40.59832	ε = 236.3475	φ = 1610.261
κ = 6.729026	λ = 481.5716	ς = 1278.456

The parameters α, β, χ, δ, ε, φ, κ, λ and ς were fitted to a database containing dynamic viscosity data for n-alkanes and n-alkyl-benzenes from atmospheric pressure up to a thousand bar.

Et-Tahir (1993) and Baylaucq (1996) showed that the use of Kanti's method (Kanti *et al.*, 1989) could lead to very accurate predictions, for pure compounds but also for binary and ternary hydrocarbon systems, at the condition to hold the fluid experimental dynamic viscosity under a pressure of one bar and at T_0. The use of Kanti's model with experimental reference viscosity data, in order to adjust the correlation, is also called "Self-reference Model".

The global deviations obtained following this procedure are reported in Table 2.3.
We have nevertheless to remark that our study was limited to binary and ternary systems for which experimental dynamic viscosities under one bar were available, that is to say essentially data from the Laboratory of University of Pau (Evident Partner).

The results, presented in Table 2.3, are particularly satisfactory for all the systems studied. Nevertheless, the systematic study carried out by Baylaucq (1996) with the ternary system "n-heptane / methyl-cyclohexane / 1-methylnaphtalene", allowed us to observe that the accuracy of Kanti's method (Kanti *et al.*, 1989) is higher for alkanes than for cyclanes and aromatics.

Nevertheless, it is clear that the "Self-reference Model" is an excellent solution to apply to petroleum fluids for the determination, within experimental precision, of the dynamic viscosity of heavy cuts under high pressures.

Table 2.3 - Results of Self-reference model (Kanti *et al.*, 1989) for the prediction of dynamic viscosities under high pressures.

System	NDP	AAD (%)
n-heptane / methyl-cyclohexane	119	4.9
n-heptane / 1-methylnaphtalene	119	10.0
Methyl-cyclohexane / 1-methylnaphtalene	119	7.8
Toluene / 2,6,10,14-tetramethylpentadecane	84	4.9
Toluene / 1-methylnaphtalene	85	9.6
Toluene / 2,2,4,4,6,8,8- heptamethylnonane	85	6.8
n-heptane / n-decane	11	3.4
n-decane / n-hexadecane	51	2.8
n-heptane / methyl-cyclohexane / 1-methylnaphtalene	357	6.1
n-decane / n-dodecane / n-tetradecane / n-hexadecane	17	5.3

In order to give a total predictive character to Kanti's method (Kanti *et al.*, 1989), we tried to associate it with a model derived from the Reaction Rate Theory, such as Cao's equations (Cao *et al.*, 1993a, b).

First, pure compound kinematic viscosities were calculated at a fixed temperature T_0. For most of the compounds, the correlations proposed by Cao *et al.* (1992) were used. Nevertheless, Cao's parameters were not available for 2,6,10,14-tetramethyl pentadecane, 1-methylnaphtalene and 2,2,4,4,6,8,8-heptamethyl nonane.

For these compounds, the following procedure was adopted:

(i) Critical parameters and acentric factor of 2,6,10,14-tetramethylpentadecane and 2,2,4,4,6,8,8-heptamethylnonane were calculated with the group contribution method proposed by Avaullée *et al.* (1997);

(ii) The estimation of the molar liquid volume, at a temperature T_0, for 2,6,10,14-tetramethylpentadecane, 1-methylnaphtalene and 2,2,4,4,6,8,8-heptamethyl nonane was done using the Rackett correlation modified by Spencer and Danner (1972);

(iii) The dynamic viscosity at T_0 for these three compounds was obtained with the group contribution method of Van Velzen *et al.* (1972) (See Reid *et al.*, 1987).

Then, the calculation of the kinematic viscosities of 2,6,10,14-tetramethyl pentadecane, 1-methylnaphtalene and 2,2,4,4,6,8,8-heptamethylnonane was achieved with the values of dynamic viscosities and molar volumes obtained as described previously.

With the kinematic viscosity of pure compounds, it is possible to obtain the kinematic value for the viscosity of the mixture under atmospheric pressure and at a temperature T_0 (Cao *et al.*, 1993a, b). The use of the experimental density of the mixture at T_0 associated with Kanti's method (Kanti *et al.*, 1989) gives us an estimative of the fluid dynamic viscosity.

It should be noticed that the application of this procedure is limited by the knowledge of the density of the hydrocarbon phase under atmospheric pressure and at a temperature T_0.

It is clear that Kanti's method (Kanti *et al.*, 1989), such as Baylaucq (1996) and Werner (1996) have underlined, is mainly available for fluids with moderate viscosities. For fluids with high viscosities such as asphaltenes, and also for fluids of weak viscosity such as gases, one can expect important deviations.

2.2.2.2 The Orbey and Sandler Model (1993)

One of the main problems concerning the models associated to the Reaction Rate Theory is the determination of the pure compound properties. As an alternative to these models, Orbey and Sandler (1993) proposed an empirical model that only requires the normal boiling point as input datum.

First, the authors developed a correlation to reproduce the temperature variation of the dynamic viscosity for propane, within the experimental accuracy:

$$\ln\left(\frac{\eta}{\eta_{ref}}\right)_{propane} = -1.6866 + 1.4010\left(\frac{T_b}{T}\right) + 0.2406\left(\frac{T_b}{T}\right)^2 \qquad (24)$$

where η_{ref} is an arbitrary dynamic viscosity reference value for propane.

The observation of reduced dynamic viscosity evolution in n-alkane homologous series leaded the authors to propose the following expression:

$$\ln\left(\frac{\eta}{\eta_{ref}}\right)_{n-alkane} = \Omega \ln\left(\frac{\eta}{\eta_{ref}}\right)_{propane} \qquad (25)$$

where Ω is a parameter which is specific for each compound.

In order to give a complete predictive feature to their method, Orbey and Sandler (1993) decided to keep the same value of η_{ref} for both propane and higher molecular weight n-alkanes. In these conditions, Ω is also expressed as a function of normal boiling point:

$$\Omega = 0.143 + 0.00463\, T_b - 0.00000405\, T_b^2 \qquad (26)$$

Orbey and Sandler (1993) suggested the use of $\eta_{ref} = 0.225\,10^{-3}$ Pa.s, for n-alkane series, but noted that η_{ref} value differs from one homologous series to another. In this review, we suppose that the η_{ref} n-alkane value is universal.

For normal boiling temperature, we used the available values from the Thermodynamic Research Center (TRC) Thermodynamic Tables (1987) which are usually well accepted for petroleum applications. The normal boiling temperatures of 2,6,10,14-tetramethylpentadecane and 2,2,4,4,6,8,8-heptamethylnonane respectively, Tb = 578.52 K and Tb = 517.57 K) were estimated from low-pressure data using an extrapolation method proposed by Coniglio (1993). The mixing rule for the mixture normal boiling point determination is the following:

$$(T_b)_{mix} = \left[\sum_{i=1}^{p} x_i (T_b)_i^3\right]^{1/3} \qquad (27)$$

For comparison purposes, we consider equations 24 to 27 and a dynamic viscosity reference of $\eta_{ref} = 0.225\,10^{-3}$ Pa.s .

Under atmospheric pressure, Table 2.4 shows that both Orbey and Sandler (1993) and Cao's (Cao *et al.*, 1993a, b) methods yield equivalent global results for alkane-alkane systems. In the case of cyclane-n-alkane, aromatic-aromatic and cyclane-aromatic systems, one can observe (that the results of Orbey and Sandler model (1993) are very poor. It seems that the chosen universal value of η_{ref} does not suit properly to systems containing aromatics and cyclanes.

One can note that expressions 24 to 27 do not take into account the pressure effect, and thus, are only valid under atmospheric pressure. In order to extend the model applicability to high pressures, Orbey and Sandler (1993) suggested the introduction of a new one-parameter pressure correlation:

$$\ln\left(\frac{\eta(P)}{\eta(P_{sat})}\right)=\frac{P}{\Theta} \tag{28}$$

where η(Psat) is determined with expressions 24 to 27 and Θ is a constant approximately equal to:

$$\Theta = 10^{8}\ \text{Pa} \tag{29}$$

Table 2.4 - Comparison of the models of Orbey and Sandler (1993) and of Cao *et al.* (1993a, b) for viscosity prediction of binary systems at atmospheric pressure.

				AAD (%)	
Binary	Systems	P (MPa)	NDP	Cao *et al.* (1993a, b)	Orbey and Sandler (1993)
n-alkane	n-alkane	0.101325	144	2.1	1.8
substituted alkane	n-alkane	0.101325	68	3.9	5.6
cyclane	n-alkane	0.101325	45	3.0	22.8
aromatic	n-alkane or aromatic	0.101325	233	7.3	10.8 (74 pts)
Aromatic	Cyclane	0.101325	25	10.62	33.6

Table 2.5 presents a comparison of the global results for the model constituted by equations 24 to 29 with those obtained with the model associating Kanti's correlation (Kanti *et al.*, 1989) and Cao's method (Cao *et al.*, 1993a, b). The lack of available fluid density data in the database reduces the comparison to a very limited number of systems.

Table 2.5 - Comparison of the model of Kanti *et al.* (1989) associated to the method of Cao *et al.* (1992, 1993a, b) and the model of Orbey and Sandler (1993) for the prediction of dynamic viscosities at high pressures.

		AAD (%)	
System	**NDP**	**Kanti et al. (1989) + Cao et al. (1992, 1993a, b)**	**Orbey and Sandler (1993)**
n-heptane / methyl-cyclohexane	126	8.1	15.0
n-heptane / 1-methylnaphtalene	126	12.2	17.4
methyl-cyclohexane / 1-methylnaphtalene	126	11.8	17.6
Toluene / 2,6,10,14-tetramethyl pentadecane	89	13.3 (44pts)	20.9
Toluene / 1-methylnaphtalene	90	18.4 (45pts)	12.7
Toluene / 2,2,4,4,6,8,8- heptamethyl nonane	90	22.3 (45pts)	19.8
n-pentane / n-decane	5	-	4.4
n-hexane / benzene	60	-	22.3
n-heptane / n-decane	12	-	14.9
n-decane / n-hexadecane	54	-	3.7
n-heptane / methyl-cyclohexane / 1-methylnaphtalene	378	7.8	33.7
n-butane / n-hexane / n-decane	5	-	8.7
n-pentane / n-hexane / n-heptane / n-decane	4	-	21.0
n-decane / n-dodecane / n-tetradecane / n-hexadecane	18	-	9.3

As could be expected, the deviations obtained are in general bigger than those calculated with the "Self-reference Model" (Table 2.3). Nevertheless, the results for the systems "n-heptane / methyl-cyclohexane", "n-heptane / 1-methylnaphtalene" and "methyl-cyclohexane / 1-methylnaphtalene" are quite satisfactory compared to the values of Table 2.3. This good behavior of the model is confirmed by the very satisfactory results obtained for the ternary mixture "n-heptane / methyl-cyclohexane / 1-methylnaphtalene".

The weakness of the method seems to be the calculation of the pure compound viscosities of 2,6,10,14-tetramethylpentadecane and 2,2,4,4,6,8,8-heptamethyl nonane. The lack of accuracy of the group contribution method of Van Velzen *et al.* (1972) to describe isomers and substituted molecules leads to very important deviations for the calculation of the kinematic viscosity of the fluid under atmospheric pressure and at T_0.

The general behavior that can be observed for the Orbey and Sandler (1993) model is that it gives better results with alkane-alkane systems than with systems containing other hydrocarbons molecules. An explanation of this effect is certainly the choice of a unique viscosity reference value, η_{ref}, for all the hydrocarbon compounds. We have to emphasize that due to the deviations observed with the method of Orbey and Sandler (1993) for the calculation of low-pressure viscosity data (Table 2.4), it was impossible to expect more accurate results at high pressures.

One can also observe that the model associating Kanti's correlation (Kanti *et al.*, 1989) and Cao's method (Cao *et al.*, 1993a, b) gives better results for the binary systems "n-heptane / methyl-cyclohexane", "n-heptane / 1-methylnaphtalene", "methyl-cyclohexane / 1-methylnaphtalene" and also for the ternary mixture "n-heptane / methyl-cyclohexane / 1-methylnaphtalene". For the other systems, the deviations obtained with the two methods are very similar.

Even if the approach of Orbey and Sandler (1993) is simpler than the other proposed in the literature, the results obtained, except for alkane-alkane systems, seem not acceptable for engineering purposes.

The same limitation remarks done for Kanti's method (Kanti *et al.*, 1989) can be applied to Orbey and Sandler's model (1993). Nevertheless, even if the problem of high viscosity compounds is not solved, these authors tried to incorporate in their model diluted gases illustrating their proposal with a carbon dioxide example.

Since the viscous behavior of CO_2 and hydrocarbons is different, it is impossible to model carbon dioxide with the same approach. In order to solve the problem, Orbey and Sandler (1993) suggested considering separately hydrocarbon phase and carbon dioxide. The viscosity of the dense phase is still represented by the model composed by equations 24 to 29. Special correlations were developed for carbon dioxide depending on the position in the (P, T) domain by reference to the critical state. Thus, for supercritical CO_2, the authors proposed the following dynamic viscosity relation:

$$\eta_{CO_2} = [0.00197 + 0.000044\,T] + [0.00502 - 0.00000102\,T]\,P \qquad (30)$$

The viscosity of the pseudo-binary CO_2-hydrocarbon phase is then obtained with a linear mixing rule:

$$\eta_{mix} = \sum_{i=1}^{p} x_i \eta_i \qquad (31)$$

The results are very satisfactory (approximately, 4.4% of average absolute deviation for 70 experimental data points) for the binary system carbon dioxide-n-decane studied by the authors. Nevertheless, as a limitation of the model, we must underline that a serious coherence problem appears, due to the definition of variable x_i in equations (27) and (31), when the model is extended to ternary and even more complex mixtures.

All the models reviewd before are dedicated to the representation of liquid phase viscosity. Very few of them are able to take into account the fact that a large variety of gases is often dissolved into the fluid, and when this phenomenon is considered, such as in Orbey and Sandler (1993) model, they are very difficult to be generalized. Another way to model petroleum fluid viscosity, is to consider models based on "the kinetic theory of gases" and try to extend these methods to dense fluids.

2.3 MODEL FOR DILUTED AND DENSE GASES

Chung *et al.* (1984; 1988) proposed a very interesting approach, based on the Chapman-Enskog (CE) modification of "the kinetic theory of gases" expression, i.e.:

$$\eta_{CE} = \frac{0.5}{16} \frac{(\pi m k T)^{1/2}}{\pi \sigma^2 \Omega^*} \tag{32}$$

where m is the mass of the molecule, k is the Boltzmann constant, σ is the potential distance and T is the absolute temperature.

The factor Ω^* is defined as the collision integral related to the choice of the potential model. Due to the complexity of the rigorous expression of Ω^*, some empirical correlations are proposed in the literature. For the well known Lennard-Jones potential, Neufeld *et al.* (1972) have suggested to correlate Ω^* as a function of reduced temperature T^* using the following relation:

$$\Omega^* = \frac{A}{(T^*)^B} + \frac{C}{\exp(DT^*)} + \frac{E}{\exp(FT^*)} + G(T^*)^B \sin\left[S(T^*)^W - H\right] \tag{33}$$

where the parameters of equation 33 are given in Table 2.6. The reduced temperature, T^*, is expressed as a function of the Boltzmann constant and the potential energy parameter ε:

$$T^* = \frac{kT}{\varepsilon} \tag{34}$$

Table 2.6 - Parameters of the correlation of Neufeld *et al.* (1972) for the collision integral Ω^* calculation.

A = 1.16145	B = 0.14874	C = 0.52487	D = 0.77320	E = 2.16178
F = 2.43787	G = -6.435 10^{-4}	H = 7.27371	S = 18.0323	W = -0.76830

The application of the equations 32 to 34 is limited to simple molecular gases. To extend it to polyatomic molecular gases, Chung *et al.* (1984, 1988) proposed to multiply equation 32 by an empirical factor F_c in order to account for molecular structure and polar effects:

$$\eta_0 = 2.66910^{-6} \frac{(MT)^{1/2}}{\sigma^2 \Omega^*} F_c \tag{35}$$

with,

$$F_c = 1 - 0.2756\omega + 0.059035\mu_r^4 + \kappa \tag{36}$$

where M is the molecular weight in g.mol^{-1}, ω is the acentric factor, μ_r is a dimensionless dipole moment and κ is a correction factor for hydrogen bonding effects of associating substances (thus, except for methanol and water, all the values of κ, for petroleum fluid components, are equal to zero).

To calculate σ, T^* and κ, the following relations were used:

$$\sigma = 0.809 V_c^{1/3} \tag{37}$$

$$T^* = \frac{k}{\varepsilon} T = 1.2593 \frac{T}{T_c} \tag{38}$$

$$\mu_r = 131.3 \frac{\mu}{(V_c T_c)^{1/2}} \tag{39}$$

where T_c is the critical temperature in K and V_c is the critical volume in cm^3.mol^{-1}. The values for the dipole moment μ (in Debye) are those given in Reid *et al.* (1987).

With equations 35 to 39, the model application is limited to dilute gas viscosity. For dense fluids, Chung *et al.* (1984; 1988) used an empirical correction to account for the fact that the fluid has a high density.

The equation of the dynamic viscosity η (in Pa.s) is then written as:

$$\eta = \eta_0 \left(\frac{1}{\Gamma_1} + \alpha_6 Y \right) + \eta_1 \tag{40}$$

The expressions of Y, Γ_1 and η_1 are given as functions of the density ρ (in mol.cm^{-3}) and the reduced temperature T^*:

$$\Gamma_1 = \frac{\frac{\alpha_1}{Y}\left[1-\exp(-\alpha_4 Y)\right] + \alpha_2 \Gamma_2 \exp(\alpha_5 Y) + \alpha_3 \Gamma_2}{\alpha_1 \alpha_4 + \alpha_2 + \alpha_3} \tag{41}$$

$$\Gamma_2 = \frac{1-0.5\,Y}{(1-Y)^3} \tag{42}$$

$$Y = \frac{\rho V_c}{6} \tag{43}$$

$$\eta_1 = 3.634410^{-6} \frac{(M T_c)^{1/2}}{V_c^{2/3}} \alpha_7 Y^2 \Gamma_1 \exp\left(\alpha_8 + \frac{\alpha_9}{T^*} + \frac{\alpha_{10}}{(T^*)^2} \right) \tag{44}$$

where the factors α_1, α_2, α_3, α_4, α_5, α_6, α_7, α_8, α_9 and α_{10} are functions of ω, μ_r and κ:

$$\alpha_i = a_0(i) + a_1(i)\omega + a_2(i)\mu_r^4 + a_3(i)\kappa \tag{45}$$

The parameters a_0 (i), a_1 (i), a_2 (i) and a_3 (i) are given in Table 2.7.

Table 2.7 - Parameters a_0 (i), a_1 (i), a_2 (i) and a_3 (i) for the calculation of factors α_i in relation (45).

i	a_0 (i)	a_1 (i)	a_2 (i)	a_3 (i)
1	6.32402	50.41190	-51.68010	1189.0200
2	0.0012102	-0.0011536	-0.0062571	0.037283
3	5.28346	254.20900	-168.48100	3898.27000
4	6.62263	38.09570	-8.46414	31.41780
5	19.74540	7.63034	-14.35440	31.52670
6	-1.89992	-12.53670	4.98529	-18.15070
7	24.27450	3.44945	-11.29130	69.34660
8	0.79716	1.11764	0.012348	-4.11661
9	-0.23816	0.067695	-0.81630	4.02528
10	0.068629	0.34793	0.59256	-0.72663

In order to extend their model to mixtures, Chung *et al.* (1984; 1988) proposed the following mixing rules:

$$\sigma_{mix}^3 = \sum_{i=1}^{p}\sum_{j=1}^{p} x_i x_j \sigma_{ij}^3 \tag{46}$$

with $$\sigma_{ij} = \xi_{ij}\left(\sigma_i \sigma_j\right)^{1/2} \tag{47}$$

$$\frac{\varepsilon_{mix}}{k} = \frac{\sum_{i=1}^{p}\sum_{j=1}^{p} x_i x_j \left(\frac{\varepsilon_{ij}}{k}\right)\sigma_{ij}^3}{\sigma_{mix}^3} \tag{48}$$

with $$\frac{\varepsilon_{ij}}{k} = \zeta_{ij}\left[\frac{\varepsilon_i}{k}\frac{\varepsilon_j}{k}\right]^{1/2} \tag{49}$$

$$\left(V_c\right)_{mix} = \left(\frac{\sigma_{mix}}{0.809}\right)^3 \tag{50}$$

$$\left(T_c\right)_{mix} = 1.2593\,\frac{\varepsilon_{mix}}{k} \tag{51}$$

$$\omega_{mix} = \frac{\sum_{i=1}^{p}\sum_{j=1}^{p} x_i x_j \omega_{ij}\,\sigma_{ij}^3}{\sigma_{mix}^3} \tag{52}$$

with $$\omega_{ij} = \frac{1}{2}\left(\omega_i \omega_j\right) \tag{53}$$

$$M_{mix} = \left[\frac{\sum_{i=1}^{p}\sum_{j=1}^{p} x_i x_j \left(\frac{\varepsilon_{ij}}{k}\right)\sigma_{ij}^2\, M_{ij}^{1/2}}{\left(\frac{\varepsilon_{mix}}{k}\right)\sigma_{mix}^2}\right]^2 \tag{54}$$

where

$$M_{ij} = \frac{2\,M_i\,M_j}{M_i + M_j} \tag{55}$$

$$\kappa_{mix} = \sum_{i=1}^{p}\sum_{j=1}^{p} x_i x_j \kappa_{ij} \tag{56}$$

with

$$\kappa_{ij} = \left(\kappa_i \kappa_j\right)^{1/2} \tag{57}$$

$$\mu_{mix}^4 = \frac{\sum_{i=1}^{p}\sum_{j=1}^{p} x_i x_j \mu_i^2\,\mu_j^2}{\left(\frac{\varepsilon_{ij}}{k}\right)\sigma_{ij}^3}\left(\frac{\varepsilon_{mix}}{k}\right)\sigma_{mix}^3 \tag{58}$$

$$\left(\mu_r\right)_{mix} = 131.3\,\frac{\mu_r}{\left[\left(V_c\right)_{mix}\left(T_c\right)_{mix}\right]^{1/2}} \tag{59}$$

where binary interaction parameters ξ_{ij} and ζ_{ij} are set equal to unity for most of the systems.

The parameters T_c, V_c and ω used for pure compounds were taken from a file provided by the DTU Evident team. For 2,6,10,14-tetramethylpentadecane and 2,2,4,4,6,8,8- heptamethylnonane, these parameters were calculated with the group contribution method recently proposed by Avaullée *et al.* (1997).

One should note that if the model of Chung *et al.* (1984; 1988) requires a limited input of data (only T_c, V_c, ω and μ), the knowledge of the phase density is compulsory to calculate dynamic viscosity. The lack of available fluid density data in the database reduces this study to a very limited number of systems.

The global results obtained are reported in Table 2.8.

Since this model was established for gases, it was possible to predict the behavior for the systems "Methane / ethane" and "Carbon dioxide / ethane". The results show that the deviations are small (Table 2.8). Results for the mixture "Carbon dioxide / n-decane" are of significant lower quality.

If the model of Chung *et al.* (1984, 1988) does not give satisfactory predictions for liquid binary mixtures, it is important to note that the accuracy of its results is very near from that of a model specifically developed for the liquid phase such as the Orbey and Sandler method (1993) (Table 2.5).

The quality of the results obtained for the ternary mixture "n-heptane / methyl-cyclohexane / 1-methylnaphtalene" is however very good when compared to those calculated for binary systems. For this system, Orbey and Sandler method (1993) (Table 2.5) gives deviations three times larger than those of the model of Chung *et al.* (1984; 1988).

Table 2.8 - Results of the model of Chung *et al.* (1984, 1988) for the prediction of dynamic viscosities of systems at high pressures.

System	NDP	AAD (%)
Methane / ethane	103	2.9
Carbon dioxide / ethane	94	8.4
Carbon dioxide / n-decane	83	23.8
n-heptane / methyl-cyclohexane	126	17.0
n-heptane / 1-methylnaphtalene	126	15.8
Methyl-cyclohexane / 1-methylnaphtalene	126	31.2
Toluene / 2,6,10,14-tetramethylpentadecane	44	24.9
Toluene / 1-methylnaphtalene	45	10.7
Toluene / 2,2,4,4,6,8,8- heptamethylnonane	45	22.7
n-heptane / methyl-cyclohexane / 1-methylnaphtalene	378	12.5

2.4 CONCLUSIONS

In this chapter, we presented some available solutions in order to model viscosity phenomenon. If the number of viscosity models existing in the literature is quite important, very few of them can be used for complex mixtures. Conscious of the difficulties to use a parameter fitting procedure for petroleum fluid viscosity modelling, the main selection criterion has been to be attentive to the predictive features of the methods.

Despite the large database provided by the DTU Evident team under the scope of the EVIDENT Project, the scarcity of simultaneous density and viscosity measurements reduced our study to a few systems. We have to emphasize that the most interesting data, both for the accuracy and the wideness of pressure range, were provided by the Evident team of Pau (Et-Tahir *et al.*, 1993) and (Baylaucq *et al.*, 1996).
The solutions that we can propose for the viscosity modelling are mostly partial. They depend essentially of the fluid state domain (liquid or gas) considered.

For liquids, the following remarks can be stated:

- The "Self-reference" model, proposed by Kanti *et al.* (1989), is a very accurate method for the calculation of moderate fluid viscosity. The knowledge of a viscosity datum point under atmospheric pressure, easily obtained with a basic analysis of the fluid properties, is sufficient to model dynamic viscosity up to a thousand bar.

- The association of Kanti's correlation (Kanti *et al.*, 1989) with a Reaction Rate Theory model (e.g., Cao *et al.*, 1992, 1993a, b), gives satisfactory results if the determination of pure compound properties (T_c, P_c, ω and v_i) is really accurate. In the opposite situation, the calculation of branched alkane viscosities with the group contribution method of Van Velzen *et al.* (1972) shows that a bad evaluation of pure compound properties can lead to very important deviations for the mixture.

As a limit of the two methods previously mentioned, we have to notice that none of them is able to account for the large amount of gas which is often dissolved into the liquid phase. In order to solve this problem, we show the results of a totally empirical model proposed by Orbey and Sandler (1993). The deviations obtained with a carbon dioxide-n-decane system are very good but the generalization of the method seems very difficult.

For gas mixtures, the method of Chung *et al.* (1984, 1988), based on a modified expression of the "kinetic theory of gases", gives satisfactory results, but for the system carbon dioxide-n-decane the model provides deviations bigger than 20%. If its application to liquids is not satisfactory, the results obtained are equivalent to those given by a dense phase model such as the Orbey and Sandler method (1993).

If model deviations are often bigger than 15%, it should be underlined that accuracy of the majority of literature data vary within 5% and 15% (See Monnery *et al.*, 1995).

The capital problem of the analysed models is mainly the model specificity (liquid or gas). Thus, it seems that even if the results of Chung *et al.* model (1984, 1988) are not very satisfactory for liquid mixtures, this method is the most reliable for petroleum fluid viscosity modelling.

As a general conclusion, it is clear that a model capable of modelling viscosity on any phase, in a wide range of temperature and pressure with good predictive capability and a solid theoretical background is not available in the open literature. In fact, the studied models have quite narrow ranges of applicability and are usually bounded to a specific phase, even if extension methods (most of the times of empirical nature) are proposed.

Bearing in mind these conclusions, it was decided to develop an approach to the problem in hands, based on molecular simulation techniques, as detailed in the next chapter.

2.5 LIST OF SYMBOLS

AAD Average absolute deviation;

h Plank constant;

k Boltzmann constant;

m mass of a molecule;

M_{mix} molecular weight of the liquid mixture in $g.mol^{-1}$;

M_i molecular weight of the liquid pure component *i*;

N_a Avogadro number;

NDP Number of data points

P pressure in Pa;

P_{sat} saturation pressure;

R universal gas constant: $R = 8.31441\ J.K^{-1}.mol^{-1}$;

T temperature in K;

T_c critical temperature;

T_b normal boiling temperature;

T^* reduced temperature equal to $T^* = \frac{k\,T}{\varepsilon}$;

V_{mix} molar volume of the liquid mixture in $m^3.mol^{-1}$;

V_i molar volume of the liquid pure component *i*;

V_c critical volume in $cm^3.mol^{-1}$;

x_i molar fraction in component *i*;

Greek symbols

ε potential energy parameter;

μ dipole moment in Debye;

σ potential distance in ångstrom;

η_{mix} dynamic viscosity of mixture in $N.s/m^2$ (or Pa.s);

η_i dynamic viscosity of component *i*;

ν_{mix} kinematic viscosity of the mixture expressed in $m^2.s^{-1}$;

ν_i kinematic viscosity of the liquid pure component *i*;

ω acentric factor;

ΔF^*_{mix} activation molar free energy for the mixture.

2.6 REFERENCES

- Avaullée, L., Trassy, L., Neau, E., Jaubert, J. N. Fluid Phase Equilib., 139, 155-170 1997.
- Baylaucq, A., *Etude des variations en fonction de la pression de la viscosité dynamique du ternaire heptane + méthylcyclohexane + 1-méthylnaphtalène – Mesures et modélisation*, Thèse, Université de Pau, France, 1996.
- Cao,W., Fredenslund, A., Rasmussen, P. Ind. Eng. Chem. Res., 31, 2603-2619, 1992.
- Cao, W., Knudsen, K., Fredenslund, A., Rasmussen, P. Ind. Eng. Chem. Res., 32, 2077-2087, 1993a.
- Cao, W., Knudsen, K., Fredenslund, A., Rasmussen, P. Ind. Eng. Chem. Res., 32, 2088-2092, 1993b.
- Chevalier, J.L., Petrino, P., Gaston-Bonhomme, Y. Chem. Eng. Sc., 43, 1303-1309, 1988.
- Chevalier, J.L., Petrino, P., Gaston-Bonhomme, Y. J. Chem. Eng. Data, 35, 206-212, 1990.
- Chung, T.H., Lee, L.L., Starling, K.E. Ind. Eng. Chem. Res., 23, 8-13, 1984.
- Chung, T.H., Ajlan, M., Lee, L.L., Starling, K.E. Ind. Eng. Chem. Res., 27, 671-679, 1988.
- Coniglio, L., *Estimation des propriétés thermophysiques des hydrocarbures lourds, Thèse*, Université d'Aix-Marseille III, France, 1993.
- Et-Tahir, A., *Détermination des variations de la viscosité de divers hydrocarbures en fonction de la pression et de la température – Etude critique de modèles répresentatifs*, Thèse, Université de Pau, France, 1993.
- Fredenslund, A., Jones, R. L., Prauznitz, J.M., AIChE J., 21, 1086-1099, 1975.
- Fredenslund, A., Gmehling, J., Rasmussen, P., Vapor-liquid equilibrium using UNIFAC, Elsevier, New-York, 1977.
- Guggenheim, E.A., Mixtures. The theory of equilibrium properties for some simple classes of mixtures, solutions and allois, Clarendon Press, Oxford, 1952.
- Kanti, M., Zhou, H., Ye, S., Boned, C., Lagourette, B., Saint-Guirons, H., Xans, P., Montel, F. J. Phys. Chem., 93, 3860-3864, 1989.
- Meyer, R., Meyer, M., Metzger, J., Péneloux, A. J. Chem. Phys., 68, 406, 1971.
- Monnery, W.D., Svrcek, W.Y., Mehrotra, A.K. Can. J. Chem. Eng., 73, 3-40, 1995.
- Neufeld, P.D., Janzen, A.R., Aziz, R.A. J. Chem. Phys., 57, 1100, 1972.
- Orbey, H., Sandler, S.I. Can. J. Chem. Eng., 71, 437-446, 1993.
- Powell, R.E, Roseveare, W.E., Eyring, H. Ind. Eng. Chem., 33, 430-435, 1941.
- Reid, R.C., Prausnitz, J.M., Poling, B.E., The Properties of Gases and Liquids, 4th edition, MacGraw-Hill, New-York, 1987.
- Spencer, C.F., Danner, R.P. J. Chem. Eng. Data, 17, 236-241, 1972.

- TRC Thermodynamic Tables, Thermodynamic Research Center, Texas A & M University System, College Station, Texas.
- Van Velzen, D., Cardozo, R.L., Lankencamp, H. Ind. Eng. Chem. Fundam., 11, 20-25, 1972.
- Werner, A., Viscosité des fluides riches en produits lourds – mesure et modélisation, Thèse, Université de Pau, France, 1996.
- Wu, D.T. Fluid Phase Equilib., 30, 149-156, 1986.

2.7 TABLE OF CONTENTS

2.7.1 List of Tables

2.7.2 List of Figures

3. Viscosity Simulation: Molecular Dynamics Approach

3.1 INTRODUCTION TO MOLECULAR SIMULATION

After the accomplishment of the first task of the project, dedicated to the evaluation of existing models for the representation of viscosity at high pressures and high temperatures, it was possible to observe that none of the tested models were fully applicable at the required conditions. Furthermore, one of the main conclusions taken from the analysis of the existing models is that they are generally very specific and not suitable for HPHT petroleum fluid viscosity simulation. Most of them were developed either for liquid or for gas phase but none for both. The limits of these theoretical, semi-empirical and totally empirical models gave the motivation to investigate new approaches based on computer simulations.

In the present chapter we will concentrate our attention on the real goal of our work, which is the development of codes in order to model viscous behaviour with a Molecular Dynamics approach. This task is a great challenge because of the relative scarcity of published work in this domain. One should also underline that until the end of the last decade, the way to estimate viscosity was not well defined (Equilibrium Molecular Dynamics [EMD] or Non-Equilibrium Molecular Dynamics [NEMD]) and subject to polemical discussions. It is now almost a certitude that these two methods are giving equivalent results and are complementary rather than contradictory. In this work, for a question of time, attention is focused on the EMD method.

It is well known since the work of Metropolis (on Monte Carlo) and Alder and Wainwright (1970) (on Molecular Dynamics) that equilibrium properties can be estimated with computer simulations applied to Statistical Mechanics. These two methods differ in their own fundaments. The former is based on statistical sampling (stochastic technique) carried out in given ensembles (*NVT*, *NPT*, $N\mu T$...) and for the later, the problem can be considered from a classical mechanics point of view (deterministic approach).

The determination of the macroscopic properties of a *N*-body system can be done by means of arithmetic averages of instantaneous values over either some large number of steps of the random walk in the case of Monte-Carlo method or some large number of steps of the trajectory in the phase space for Molecular Dynamics approach. If it can be expected from both methods equivalent results for simple thermodynamic properties - if the sampling is done carefully - only MD allows the determination of transport properties - diffusion, viscosity and thermal coefficients (Haile, 1992).

In the work presented in this chapter, some "runs" with Lennard-Jones fluids for 108, 256, 500 and 864 particles were performed. If these activities are quite distant from the initial project objective, they were nevertheless absolutely necessary in order to assess the quality of the simulations and the reliability of the code. A great part of the work was dedicated to assess, first the quality of the equilibrium state, secondly the precision of the calculation and finally to improve the efficiency of the code.

For Lennard-Jones fluids, one can note that the results obtained are in global statistical agreement with the simulations presented in the literature (Erpenbeck, 1988; Schoen, 1985). After these validation tests, one can imagine, in the future, the introduction of more elaborated potential functions in order to model real molecules.

3.2 THEORETICAL BACKGROUND – MECHANISTIC APPROACH

3.2.1 Thermodynamics and Statistical Mechanics

In general terms, the representation of equilibrium properties of matter (solid, liquid or gas) is commonly done by the use of a macroscopic approach (i.e., classical thermodynamics). In fact, thermodynamics gives us some exact mathematical relations between many properties and has the useful advantage "leapfrog" the assessement of the real nature of the matter (particles or continuum). If this later characteristic ensures the universality of its equations, it has a noticeable drawback that thermodynamics is not providing any physical interpretation of its relations. On the contrary, statistical mechanics assumes the existence of atoms and molecules to calculate and interpret observable quantities from a molecular point of view. Thus, statistical mechanics provides formalism for the calculation of thermodynamic quantities from the analysis of microscopic behaviour.

Due to the huge amount of molecules that composes an observable piece of matter (of the order of 10^{23}), it is evident that considering, in a simulation, each macroscopic system particle apart is totally impossible. As an alternative, one can suggest that a statistical treatment of the problem can be significantly more practical. Thus, it is simpler to limit the number of system particles to a finite value and to link up the system results to macroscopic observable properties by the production of a configuration set distributed according to some statistical distribution functions. Computers by means of Monte Carlo or Molecular Dynamics methods (or other simulation methods such as Brownian Dynamics or General Langevin Dynamics) are charged to carry out this duty.

3.2.2 Molecular Dynamics and Classical Mechanics

The basis of Molecular Dynamics is that the time evolution of an interacting molecule set is followed by the integration of their equations of motion (Haile, 1992).

Molecular Dynamics uses a classical mechanics approach. More precisely, for a system constituted of *N* particles, *N* equations of the type can be considered:

$$\mathbf{F}_i = \dot{\mathbf{p}}_i = \frac{d\,\mathbf{p}_i}{dt} \tag{1}$$

where $\mathbf{p}_i$ is the momentum of the particle *i* and $\mathbf{F}_i$ the force acting on this particle (all the symbols noted with bold letters are vector quantities). One can recognize in equation 1, a general form of Newton's second law.

As Newton's second law is somewhat difficult to extend to non-cartesian coordinate systems, it is often preferable to adopt more convenient formulation of classical mechanics. Rather than keeping a formulation in terms of force such as it is done in the Newtonian approach, Lagrangian and Hamiltonian ones propose expressions of classical mechanics based on, respectively, potential energy and total energy. The Hamiltonian formulation, because of its close link with the total energy, offers the best compromise for quantum mechanics and statistical mechanics expressions.

Hamiltonian equations of motion are written (Haile, 1992):

$$\frac{\partial H\left(\mathbf{p}^N, \mathbf{q}^N\right)}{\partial \mathbf{p}_i} = \dot{\mathbf{q}}_i \quad \text{and} \quad \frac{\partial H\left(\mathbf{p}^N, \mathbf{q}^N\right)}{\partial \mathbf{q}_i} = -\dot{\mathbf{p}}_i \tag{2}$$

where the Hamiltonian, $H\left(\mathbf{p}^N, \mathbf{q}^N\right)$, depends on the position $\mathbf{q}$ and the momentum $\mathbf{p}$ of each of the *N* system particles. The Hamiltonian can be related to kinetic (K) and potential energies (U) of the system by means of (Haile, 1992):

$$H\left(\mathbf{p}^N, \mathbf{q}^N\right) = K + U = E_{tot} \tag{3}$$

Due to the fact that the Hamiltonian, $H(\mathbf{p}^N, \mathbf{q}^N)$, does not depend explicitly on time, equation 3 is an equivalent form of the well known energy conservation equation.

In a cartesian frame, the Hamiltonian formulation of classical mechanics includes 6*N* first order differential equations (2 x 3*N* equations). In fact, during a simulation, the system computed trajectory is sampling a 6*N*-dimensional phase space (3*N* for position **q** and 3*N* for momentum **p**).

3.2.3 Quantum Mechanics - Classical approximations

Two questions can naturally come to mind when one is referring to molecular systems. The first is relative to the size scale at which the process occurs and the second holds in the way to treat multi-body systems (molecules are constituted of nuclei and electrons).

The underlying idea in the classical mechanics approach is that the energy spectrum is supposed to be a continuum. The work carried out at the beginning of the 20th century on microscopic systems proved the contrary and gave birth to a new branch of physics: quantum mechanics. In quantum mechanics, the notion of energy quantization is introduced, following the Schrödinger formalism, via the classical wave equation. This procedure leads to the well known time-independent Schrödinger equation (Haile, 1992):

$$\hat{H}\,\psi(\mathbf{q}^N) = E_{tot}\,\psi(\mathbf{q}^N) \tag{4}$$

where $\psi(\mathbf{q}^N)$ is a spatial wave-function and $\hat{H}$ is the Hamiltonian operator of the system, denoted by:

$$\hat{H} = \frac{\hbar^2}{2}\sum_{i=1}^{N}\frac{1}{m_i}\frac{\partial^2}{\partial \mathbf{q}_i^2} + V(\mathbf{q}^N) \tag{5}$$

In Molecular Dynamics, rather than using Newton's laws, equations 4 and 5 should be considered in the case of systems at the atomistic level. In order to introduce complexity with the quantum approach, a simple validity test of the classical mechanics laws is given by the de Broglie thermal wavelength Λ, defined as (Haile, 1992):

$$\Lambda = \sqrt{\frac{2\pi\hbar^2}{m_{At} k_B T}} \tag{6}$$

where m_{At} is the atomic mass and T the absolute temperature. The classical mechanics approximation is justified when Λ is small compared to the mean nearest distance between two neighbours, and this criterion is verified for most of the elements heavier than Argon.

The second problem to solve concerns the treatment of multi-particle systems: the matter is constituted of nuclei and electrons and, as far as it is known, none of these elements have the same configuration and momentum at a given time. Thus, in the case of a multi-molecular system, we have to integrate the position and the motion of nuclei but also of electrons. In these conditions, the Hamiltonian operator $\hat{H}$ should take the following form:

$$\hat{H} = \frac{\hbar^2}{2}\sum_{i=1}^{N_{Nu}} \frac{1}{(m_{Nu})_i}\frac{\partial^2}{\partial \mathbf{q}_i^2} + \frac{\hbar^2}{2}\sum_{k=1}^{N_{El}} \frac{1}{m_{El}}\frac{\partial^2}{\partial \mathbf{q}_k^2} + \sum_{i=1}^{N_{Nu}}\sum_{j>i}^{N_{Nu}} \frac{Z_i Z_j e^2}{|\mathbf{q}_i - \mathbf{q}_j|} + \sum_{k=1}^{N_{El}}\sum_{l>k}^{N_{El}} \frac{e^2}{|\mathbf{q}_k - \mathbf{q}_l|} - \sum_{i=1}^{N_{Nu}}\sum_{k=1}^{N_{El}} \frac{Z_i e^2}{|\mathbf{q}_i - \mathbf{q}_k|} \tag{7}$$

where Z_i is the charge of nucleus i and $\mathbf{q}_k$ the position vector of electron k. In equation 7, we can identify, from the left to the right, the nucleus kinetic term, the electronic kinetic term, the nucleus potential term, the electronic potential term and finally a cross potential term (nucleus-electronic), respectively.

The observation of equation 7 gives us an idea of how the Schrödinger equation of the Hamiltonian operator of a molecular system is extremely difficult to solve. The study of the works published in the literature about simulations of molecular systems shows that only the nucleus positions are taken into account. Thus, one has to consider what are the conditions to reduce atomic or molecular configuration to nucleus positions.

In order to achieve this simplification, several approximations are necessary. First step, within the Born-Oppenheimer approximation, and due to the difference of size and mass between nuclei and electrons, it is possible to express the molecular system wave function as the product of a nucleus part and of an electronic contribution (Haile, 1992):

$$\psi(\mathbf{q}^N, \mathbf{q}^N) = \psi_{Nu}(\mathbf{q}^N)\,\psi_{El}(\mathbf{q}^N; \mathbf{q}^N) \tag{8}$$

where the electronic wave function $\psi_{El}(\mathbf{q}^N; \mathbf{q}^N)$ depends also on the nucleus position because of the circumvolution of electrons about the kernels.

Due to the rapid motion of electrons (compared to nucleus), the position and the momentum of electrons is averaged out, i.e. the electronic contribution to kinetic energy in equation 7 disappears. At the opposite, even if due to the electronic configuration average, potential terms depend only explicitly on nucleus position, the highest reactivity of electrons, compared to nuclei, makes the potential part of the molecular system Hamiltonian essentially electronic. Thus, in those conditions, the resolution of equation 7 for a molecular system is reduced to find the solution of the nucleus Hamiltonian (equation 5).

3.2.4 Forces - Potential function

If the kinetic part of the Hamiltonian is very well defined, this is not the case of the potential contribution. In fact, the rough treatment of potential terms of equation 7 appears totally idealistic. It is therefore better to solve this problem in terms of global forces that are acting on each atom or molecule. This means that determining the system potential energy by Molecular Dynamics is equivalent to choose a global potential expression depending on the position of nuclei. When the choice of the potential function has been accomplished, forces are derived as the gradients of the potential with respect to atomic displacements:

$$\mathbf{F}_i = \frac{\partial}{\partial \mathbf{q}_i} U\left(\mathbf{q}^N\right) \tag{9}$$

A potential function is usually built from the relative position of atoms with respect to each other. Thus, $U\left(\mathbf{q}^N\right)$ has to account for interactions between two, three, four,....n atoms. The potential consequently defined appears too complex to be easily handled with computers. In fact, potential energy evaluation represents the most time consuming part of the calculation from a computing point of view.

In order to simplify the problem, potential function is commonly restricted to pairwise interactions between particles *i* and *j*:

$$U\left(\mathbf{q}^N\right) = \sum_{i=1}^{N} \sum_{j>i}^{N} \phi\left(\left|\mathbf{q}_i - \mathbf{q}_j\right|\right) \tag{10}$$

Nevertheless, the pairwise approximation (equation 10) could appear to be quite abusive with respect to the analysis of the influence of the ternary interaction term between particles *i*, *j* and *k*. Various kind of many-body interaction potentials can be investigated in order to improve the realism of the pairwise interaction approximation.

For spherical particles several pairwise potential function models have been proposed in the literature. The most commonly used, in terms of the efficiency-simplicity ratio, is the Lennard-Jones 12-6 potential (Haile, 1992):

$$\phi_{i,j}\left(\left|\mathbf{q}_i - \mathbf{q}_j\right|\right) = 4\varepsilon\left[\left(\frac{\sigma}{\left|\mathbf{q}_i - \mathbf{q}_j\right|}\right)^{12} - \left(\frac{\sigma}{\left|\mathbf{q}_i - \mathbf{q}_j\right|}\right)^{6}\right] \tag{11}$$

where, σ is the potential distance and ε the minimum energy of the potential function. These two parameters are characteristics of the particle under study.

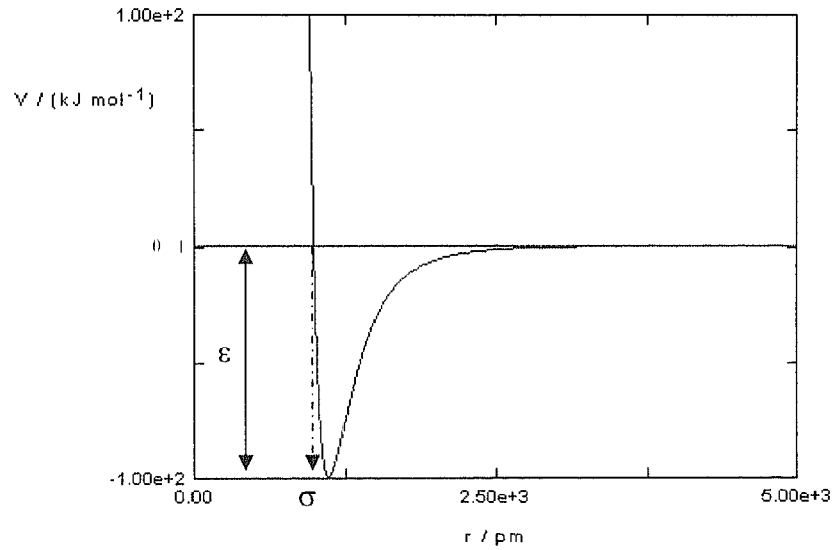

Figure 3.1 - Graphic representation of the Lennard-Jones potential function, with ε = 100 kJ mol^{-1} and σ = 1000 picometers.
Reproduced from Atkins and de Paula (2005).

The repulsive part (exponent twelve term) is dominating at short distance. Its role is to account for the repulsion between atoms when they are brought very close to each other. In fact, when the electronic clouds surrounding atoms start to overlap, the energy of the system increases tremendously, as stated in the Pauli principle. The attraction term (exponent six term) gives cohesion to the system. Its origin corresponds to the Van der Waals dispersion forces that are initiated by dipole-dipole interactions. If these forces are rather weak, they have a longer action range compared to repulsive forces.

The Lennard-Jones potential function, despite its extreme simplification of the attraction-repulsion processes, stays nowadays the standard potential that is used on most of the research where the focus is on fundamental issues. The simulation work done with Lennard-Jones systems is able to help the understanding of basic points in many areas.

3.3 MOLECULAR DYNAMICS TECHNIQUES

After the considerations referred on the previous section, a tool is now available to carry out a Molecular Dynamics simulation for *N*-body systems, but some questions remain. These questions are mainly linked to the way to handle the finiteness of simulated systems by comparison to the huge amount of particles contained in a piece of macroscopic matter. On one hand, to be realistic, large enough systems have to be considered in order to reduce statistic errors. On the other hand, it is reasonable to limit the number of particles of the cell at the smallest acceptable value, to avoid very high computing times. Finally, it has to be decided in what conditions and how to solve equations of motion.

3.3.1 Periodic boundary conditions

A simulation in Molecular Dynamics will be typically performed on cells containing hundreds of particles (at the limit, a few thousands). However, even for the biggest cell that one can imagine, no system should be large enough to model matter at the macroscopic scale. As a consequence of this limitation, the number of molecules placed at the border of the cell can never be negligible compared to the total number of molecules included in the cell, and this outcome is affecting the homogeneity of the simulation conditions. So, what should we do at the boundaries of the cell in order to avoid these surface effects?

A solution to this problem is given by the use of periodic boundary conditions (PBC). With periodic boundary technique, particles are enclosed in a cubic box of finite dimension *L*, and this cell is replicated to infinity by translation of the original cell along each of the space directions. As a consequence of PBC, (Figure 3.2) the number *N* of particles of a cell is constant; when a particle leaves the central cell, its image automatically enters in.

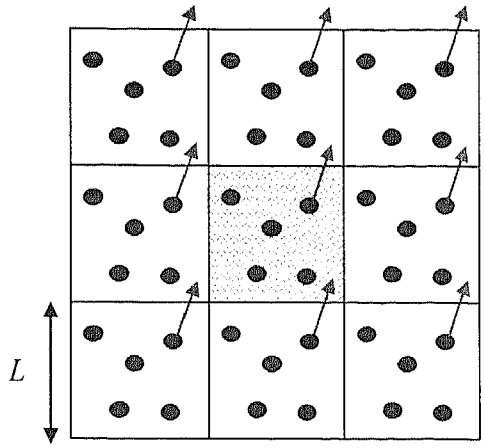

Figure 3.2 - Application of periodic boundary conditions.

The particle of the central cell (shadowed) and all its images are moving together.

The key point of PBC is that now, each particle *i* in the central box should be thought as interacting not only with other particles *j* contained in this box, but also with their images situated in nearby boxes.

3.3.2 Potential cut-off and minimum distance criterion

The Lennard-Jones model (equation 11) has an infinite action range. If the interactions are going through box boundaries, it means that it has to be considered for the force estimation an infinite number of neighbours for each particle *i*.

The analysis of Lennard-Jones function shows that the attractive part of the potential becomes very quickly negligible (at around three times the potential distance σ). With the use of the whole potential, it is expected then to spend most of the computing time calculating pairwise interactions for particles having almost no influence on each other.

In order to avoid this "expensive" situation, a common solution consists in introducing an arbitrary cutoff radius R_{cut} (Figure 3.3) after which the potential is no longer acting. Thus, two particles separated by a distance equal or larger than a cut-off distance R_{cut}, do not interact with each other. If the cut-off trick is very useful in terms of time computing, this procedure has nevertheless an influence on the calculation of quantities that depend on the particle separation (mainly, internal energy and

pressure). Consequently, these quantities have to be corrected in order to account for non-zero pairwise interactions beyond the radius cut-off.

The potential cut-off is also useful to avoid seeing a particle interacting with its own image. A consequence of such a situation could be the instability of the algorithm charged to solve equations of motion.

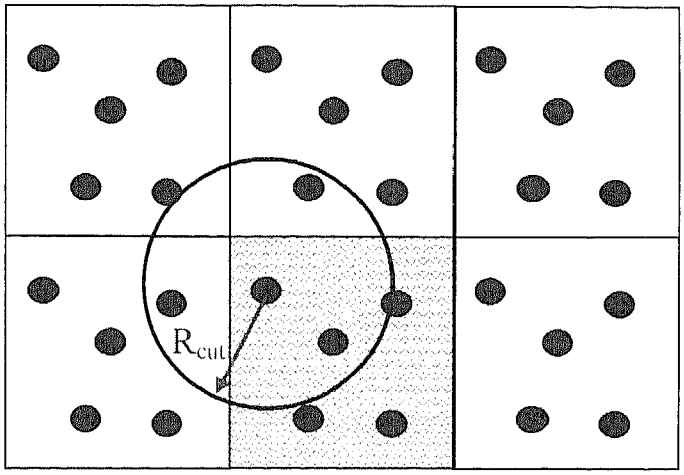

Figure 3.3 - Cut-off radius R_{cut}.
The particle under study is interacting with neighbours through box boundaries.

In the case where the simulation box size, L, is at least equal to $2R_{cut}$, one can see that a particle of the central cell is potentially able to interact with a neighbour of the central cell or with one of the images of this neighbour. The minimum image criterion simply says that among particle *j* and all the possible images, it should be considered as a neighbour of particle *i* the closest representation of particle *j* (Haile, 1992).

3.3.3. Algorithms to solve equations of motion

The "engine" behind a Molecular Dynamics code is its time integration algorithm. This algorithm is required to integrate the equations of motion of interacting particles and also to follow their trajectory. In order to solve numerically these equations, finite-differential methods are commonly used.

The time is discretized on a finite grid, where the time step, Δt, is the distance between two consecutive points on the grid. Knowing the positions and some of their time derivatives at time t (velocities, accelerations...), the integration scheme gives the same quantities at a latter time ($t + \Delta t$). By iterating the procedure, the time evolution of the system can be followed for long times.

The first step is then to solve the equations of motion (for N atoms, Newton's second law represents $3N$ second order ordinary differential equations to solve in a cartesian frame). The algorithm basic idea is to write some Taylor's expansion for positions, velocities and higher position time derivatives. For example, the position at time $t + \Delta t$, by applying Taylor's expansions at time t, is defined by (Haile, 1992):

$$q_i(t+\Delta t) = q_i(t) + \dot{q}_i(t)\Delta t + \ddot{q}_i(t)\frac{(\Delta t)^2}{2!} + q_i^{(3)}(t)\frac{(\Delta t)^3}{3!} + q_i^{(4)}(t)\frac{(\Delta t)^4}{4!} + \ldots \qquad (12)$$

In general, the most widely used finite-differential methods are Runge-Kutta's. With the first order Runge-Kutta's method, we obtain Euler's method, i.e (Haile, 1992):

$$q(t+\Delta t) = q(t) + \dot{q}\,\Delta t \qquad (13)$$

The precision of Runge-Kutta methods differs from one to another depending on how the slope $\dot{q}$ is estimated. For example, for the ordinary fourth-order Runge-Kutta method, it is necessary to make four estimates of the slope for each step forward in the solution procedure. Thus, high precision Runge-Kutta methods are very time consuming because they require several evaluations of intermolecular forces for

each atom and at each step. In order to reduce the calculation time, some other methods available in the literature (Verlet algorithm, Gear predictor-corrector) (Haile, 1992) propose to increase the precision of the scheme by using positions and velocities from several points in time, rather than from just the current time.

It has to be underlined that these schemes are not exact. They approximate the true solution by means of the truncation of Taylor's expansions (truncation errors) and by the generation of errors associated to a particular implementation of the algorithm (round-off errors). Both of these errors have to be minimized in order to ensure the production of high quality results. The former by the choice of an adequate time step (not too large, but not too small also), the later by avoiding writing redundant codes.

3.4 PROPERTIES OBTAINED FROM SIMULATION

With the ensemble of tools and tricks detailed in sections 3.2 and 3.3 of the present chapter, it is possible to begin the simulation work, i.e. to sample the phase space in order to generate sets of atomic positions and *momenta*.

If the conditions to respect in order to carry out reliable simulations have to be thought over, one has also to wonder what kind of relations exist between molecular trajectories and macroscopic properties (thermodynamic and transport properties).

3.4.1.Simulation conditions

Such as it was said before, simulations in Molecular Dynamics are performed on systems with a finite number of particles. The simulation time range goes generally from a few picoseconds to hundreds of nanoseconds. While these numbers are certainly respectable, it may happen to run into conditions where time and/or size limitations become important.

A simulation is considered to be safe, from the point of view of its duration, when the simulation time is much longer than the relaxation time (i.e., the time necessary to obtain uncorrelated data) of the quantities of interest. However, different properties have different relaxation time (Haile, 1992).

3.4.2 Time averages of simple thermodynamic quantities

For the modelling of observable quantities, in order to avoid dealing with very large systems, simulations usually take into account a few hundreds of particles and the results are extended from microscopic to macroscopic scale by means of statistical treatments.

The algorithms are charged to generate, at each time step Δt of the simulation, a basic set of data (essentially, *momenta* and positions of the *N* particles under study). Physical properties are usually functions of particle coordinates and momenta. Thus, one can define the instantaneous value of a generic physical property *A* at time *t*:

$$A(t) = A\left[\mathbf{q}^N(t), \mathbf{p}^N(t)\right] \tag{14}$$

The code is then cumulating instantaneous values of $A(t)$ during the time length τ of the run in order to determine, at the end, the average value of the property under study:

$$\langle A \rangle = \frac{1}{\tau}\int_{t_0}^{t_0+\tau} A\left[\mathbf{q}^N(t), \mathbf{p}^N(t)\right]dt \approx \frac{1}{N_{Timesteps}}\sum_{k=1}^{N_{Timesteps}} A\left[\mathbf{q}^N(k.\Delta t), \mathbf{p}^N(k.\Delta t)\right] \tag{15}$$

Due to the necessary finiteness of the run, we assume that observable quantities are defined as the limit of the simulated averages at infinite time:

$$A_{obs} = \lim_{\tau\to\infty}\frac{1}{\tau}\int_{t_0}^{t_0+\tau} A\left[\mathbf{q}^N(t), \mathbf{p}^N(t)\right]dt \tag{16}$$

For example, from the set of configurations and *momenta*, it is possible to define the following simple instantaneous statistical quantities:

Potential energy: $$U(t) = \sum_{i=1}^{N}\sum_{j>i}^{N}\phi_{LJ}\left(\left|\mathbf{q}_i(t) - \mathbf{q}_j(t)\right|\right) \tag{17}$$

Kinetic energy: $$K(t) = \frac{1}{2}\sum_{i=1}^{N}\frac{\mathbf{p}_i^2(t)}{m_i} \tag{18}$$

Temperature: $$T(t) = \frac{2}{3Nk_B}K(t) \tag{19}$$

If the total energy $H(t)$, defined as the sum of potential and kinetic energies, has to be a constant (conservation of total energy), the other quantities are fluctuating about their average (Figure 3.4). For practical reasons, the properties used in the codes are often converted into dimensionless quantities with the Lennard-Jones potential parameters. In this text, we differentiate unitless from absolute quantities by the use of a superscript asterisk on the symbol of the reduced unit values.

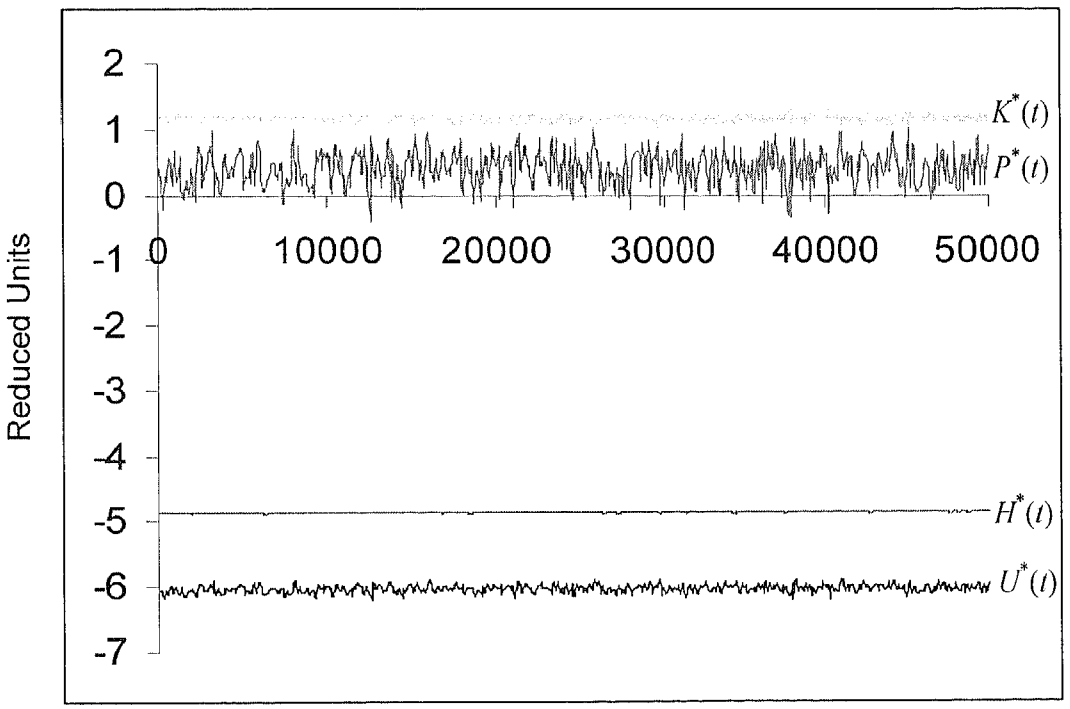

Figure 3.4 - Simulation of 50 000 time steps for a 108 Lennard-Jones system.

Quantity time evolution has been followed for reduced kinetic energy $K^*(t)$, reduced pressure $P^*(t)$, reduced total energy $H^*(t)$ and reduced potential energy $U^*(t)$ (Conditions: $R_{cut} = 2.5\sigma$, reduced time step $\Delta t^* = 0.002$, reduced density $\rho^* = 0.8442$ and reduced temperature $T^* = 0.722$).

In reality, even total energy $H^*(t)$ (see Figure 3) shows some little fluctuations along time evolution. These are due to the errors made during the time integration process and could be reduced in magnitude by increasing the number of molecules of the system or reducing the value of the time step.

The determination of pressure is a little trickier. First, the Clausius virial function of the total force acting on particle i has to be considered (Haile, 1992)

$$\left\langle W^{Tot} \right\rangle = \left\langle \sum_{i=1}^{N} \mathbf{q}_i \mathbf{F}_i^{Tot} \right\rangle = \lim_{\tau \to \infty} \frac{1}{\tau} \int_0^t \left(\sum_{i=1}^{N} \mathbf{q}_i(t) \cdot \dot{\mathbf{p}}_i(t) \right) dt = -3Nk_B \langle T \rangle \tag{20}$$

Now, one may think of the total force acting on a particle as composed of the two contributions:

$$\mathbf{F}_i^{Tot} = \mathbf{F}_i + \mathbf{F}_i^{Ext} \tag{21}$$

where $\mathbf{F}_i$ is the internal force contribution due to particle interactions and $\mathbf{F}_i^{Ext}$ is the contribution of forces exerted by the cell's walls, i.e.,

$$\left\langle W^{Ext} \right\rangle = \left\langle \sum_{i=1}^{N} \mathbf{q}_i \mathbf{F}_i^{Ext} \right\rangle = -3\langle P \rangle V \tag{22}$$

The combination of equations 20 to 22, leads to the following expression for the average pressure:

$$\langle P \rangle = \frac{1}{V} \left(Nk_B \langle T \rangle + \frac{1}{3} \left\langle W^{Int} \right\rangle \right) \tag{23}$$

with $$\left\langle W^{Int} \right\rangle = -\left\langle \sum_{i=1}^{N} \sum_{j>i}^{N} \left| \mathbf{q}_i - \mathbf{q}_j \right| \cdot \left. \frac{d\phi_{LJ}}{d\mathbf{q}} \right|_{|\mathbf{q}_i - \mathbf{q}_j|} \right\rangle \tag{24}$$

It is possible to define in a similar way, as it is suggested in expression 23, an instantaneous pressure function:

$$P(t) = \frac{1}{V} \left(Nk_B T(t) + \frac{1}{3} W^{Int}(t) \right) \tag{25}$$

In fact, this way to obtain the pressure expression from virial theorem appears to be incompatible with the use of periodic boundary conditions (where it is supposed there is no external force acting on the basic cell). Nevertheless, if some other formulations of pressure are proposed in the literature, all of them are leading to the same final expression.

It should be noted that using the laws of classical mechanics (where underlies the idea of the total energy conservation) is equivalent to do sampling in the micro-canonical ensemble (*NVE*). This ensemble is in fact not very compatible with real experimental conditions (for example, constant temperature or constant pressure). In order to consider more adequate states, one can simulate and sample in different ensembles (*NVT*, *NPT*...). Since the ensembles are artificial constructions, they produce average quantities that are consistent with one another when they represent the same state of the system. However, some of the fluctuations vary in different ensembles.

3.4.3 Statistical errors and sampling techniques

The quantity fluctuations presented in Figure 3.4 are in fact natural processes that can also be observed experimentally. They are the consequences of the constraints placed on the system and the continuously varying strength of interactions among atoms. Their nature is thus essentially a random one.
Such as with experiments, simulations are exposed to problems of reproducibility and of statistical error. An important phase of the process, closely linked with the simulation itself, is the result quality analysis. The assessment of the statistical uncertainty associated with an average quantity $\langle A \rangle$ is generally obtained by means of the variance calculation $\sigma^2(A)$ defined by:

$$\sigma^2(A) = \langle \delta A^2 \rangle = \langle A^2 \rangle - \langle A \rangle^2 \quad \text{where} \quad \delta A = A(t) - \langle A \rangle \tag{26}$$

where $\sigma(A)$ is defined as the Root Mean Square (RMS) deviation or standard deviation.

Due to the frequent time correlations of quantity measurements, it should be noticed that it is necessary to be careful about the way averages and fluctuations are determined. For example, if relation (26) is perfectly correct and very handy because $\langle A^2 \rangle$ and $\langle A \rangle^2$ are directly estimated along the run (i.e., it avoids the reanalysis of the data at the end of the run), it is not recommended to use it, from a computing point of view. In fact, the difference of two large numbers, such as $\langle A^2 \rangle$ and $\langle A \rangle^2$, is often associated with important round-off errors. We must also emphasize that the sampling technique choice is a significant point to focus on since it can influence partly the results of a simulation. Among the different type of sampling methods that can be used, the following two have been considered.

With stratified systematic sampling method, one is sampling regularly the run for *M* values (but not too often in order to avoid considering correlated data). The calculation of the global average is then obtained by a simple average over the *M* selected values:

$$\langle A \rangle = \frac{1}{M} \sum_{i=1}^{M} A_i(t) \tag{27}$$

and the RMS deviation in this case is defined as:

$$\sigma(A) = \frac{1}{\sqrt{M}} \sqrt{\frac{1}{M-1} \sum_{i=1}^{M} [A_i(t) - \langle A \rangle]^2} \tag{28}$$

With coarse-graining sampling, the total run is subdivided in *d* equal segments of *n* time steps, calculating over these *n* time steps the property average $\overline{A}_k$ for each segment and finally determining the global average $\langle A \rangle$ as the average over all the segment property averages, i.e. (Haile, 1992):

$$\overline{A}_k = \frac{1}{n} \sum_{i=1}^{n} A_i(t) \tag{29}$$

$$\langle A \rangle = \frac{1}{d} \sum_{k=1}^{d} \overline{A}_k \tag{30}$$

The standard deviation for coarse graining method is defined as:

$$\sigma(A) = \frac{1}{\sqrt{d}} \sqrt{\frac{1}{d-1} \sum_{k=1}^{d} \left[\overline{A}_k - \langle A \rangle \right]^2} \tag{31}$$

Coarse graining method seems in general better adapted to the calculation of simple thermodynamic properties but it is often better to calculate averages and standard deviations with both methods and to choose the one that is giving the smallest RMS deviation.

It should be emphasized that the variance determination of simple thermodynamic values (such as total energy, potential energy, pressure...) is also useful for the calculation of a great number of secondary thermodynamic properties (constant volume specific heat is thus linked with isothermal compressibility factor and thermal expansion coefficient).

3.4.4 Time correlation functions and transport properties

The interest of Molecular Dynamics, compared to other simulation methods such as Monte Carlo, is that they are not restricted to static properties and they can follow dynamic properties such as time correlation functions, thermal transport coefficients or spatial correlations.

Time correlation functions are introduced to quantify the degree of correlation of two points of the phase space with respect to the time. To be more explicit, these functions are giving us a way to know what is the time influence, via algorithm, of a certain system state over the future following system states.

The time correlation function $C_{AB}(t)$ of two time dependent quantities *A* and *B* is defined by the following expression:

$$C_{AB}(t) = \lim_{\tau \to \infty} \frac{1}{\tau} \int_0^{\tau} A(t_0) B(t_0 + t)\, dt_0 = \langle A(t_0) B(t_0 + t) \rangle \tag{32}$$

which means that to determine the time correlation function $C_{AB}(t)$, one is sampling *A* at a time origin t_0 and *B* is measured after a time delay *t*. In order to improve the time correlation function statistics, this operation is repeated over a great number of time origins by the mean of the integration over dt_0. At long time, the behaviour of $C_{AB}(t)$ depends on whether *A* or *B* are periodic functions. If none of them is periodic, one can expect the following properties for $C_{AB}(t)$:

- At zero time, the correlation is given by the static limit, i.e.

$$C_{AB}(0) = \langle A(t_0) B\langle t_0 \rangle \rangle \tag{33}$$

- After long delay times, *A* and *B* become totally uncorrelated, that is:

$$\lim_{t \to \text{large}} C_{AB}(t) = \langle A(t_0) \rangle \langle B\langle t_0 \rangle \rangle \tag{34}$$

From Schwartz inequality (Haile, 1992), it is straightforward to check that the magnitude of any correlation function cannot exceed its static limit. This means that the correlation is maximum at zero time (equation 33) and decreases with time to reach the value given by equation 34 at long time delays. Time correlation functions can be defined for the same property *A* (autocorrelation functions) or for different properties *A* and *B* (cross correlation functions). One can also distinguish between the correlation functions that are referring to each particle (single particle correlation functions) and those determined for all the system (collective correlation functions).

One useful application of time correlation functions holds in the analysis of the results of a simulation. In fact, the examination of the time correlation function of a quantity *A*

gives us the opportunity to assess the time necessary to obtain uncorrelated values of A (that is relaxation time). This research is often required in order to check if the sampling procedure is statistically unbiased.

A second application of time correlation functions is given by the calculation of transport coefficients. When mass, energy or momentum is transferred through a system, the transport of this quantity is described, to first order (first order approximation is available when forces initiated by the gradient are small enough to limit the Taylor's expansion to the first term), by an empirical relation of the form:

$$\text{Flux} = -\text{coefficient} \times \text{gradient} \tag{35}$$

With such an empirical equation, one can obtain directly the Fourier law (thermal conduction), the Newton law (friction) or the Fick law (diffusion). We normally think that the presence of a gradient imposes the system to be in a non-equilibrium state but these equations can be applied to microscopic fluctuations that appear in a system at equilibrium (Onsager's linear regression hypothesis).
From a theoretical point of view, there are two ways to formulate the transport coefficient (TC) of a quantity A:

$$\text{Einstein formulation:} \qquad \mathrm{TC} = \lim_{t\to\infty} \frac{\left\langle [A(t) - A(0)]^2 \right\rangle}{2t} \tag{36}$$

$$\text{or Green-Kubo expression:} \quad \mathrm{TC} = \int_0^\infty \left\langle \dot{A}(\tau) \cdot \dot{A}(0) \right\rangle d\tau \tag{37}$$

where Einstein formulae refer to mean square displacement and Green-Kubo ones to time correlation function.

The two expressions, 36 and 37, are totally equivalent and moreover general in that they do not depend explicitly on intermolecular forces, i.e. they are applied to systems without considering the nature of the potential function (Lennard-Jones or more complex function). In practice, the use of boundary conditions makes mean square displacement calculation harder than time correlation approach. In this work, only Green-Kubo formulae has been considered and defined as (Haile, 1992):

Self-diffusion coefficient: $$D_i = \frac{1}{3}\int_0^\infty \langle \dot{\mathbf{q}}_i(t)\dot{\mathbf{q}}_i(0)\rangle dt \tag{38}$$

Shear viscosity: $$\eta_{xy} = \frac{1}{Vk_BT}\int_0^\infty \langle \mathsf{P}_{xy}(t)\mathsf{P}_{xy}(0)\rangle dt \tag{39}$$

where $\mathsf{P}_{xy}(t)$ are defined as the off-diagonal elements of the instantaneous stress tensor $\mathsf{P}(t)$ given by:

$$\mathsf{P}(t) = \begin{pmatrix} \mathsf{P}_{xx}(t) & \mathsf{P}_{xy}(t) & \mathsf{P}_{xz}(t) \\ \mathsf{P}_{yx}(t) & \mathsf{P}_{yy}(t) & \mathsf{P}_{yz}(t) \\ \mathsf{P}_{zx}(t) & \mathsf{P}_{zy}(t) & \mathsf{P}_{zz}(t) \end{pmatrix} \tag{40}$$

In the case of the property of interest - viscosity, the instantaneous stress tensor elements are composed of a kinetic and a potential part:

$$\mathsf{P}_{\alpha\beta}(t) = \sum_{i=1}^{N}\left(\frac{1}{m}p_{i\alpha}p_{i\beta} - \sum_{j>i}^{N}\frac{\left|q_i - q_j\right|_\alpha \left|q_i - q_j\right|_\beta}{\left|\mathbf{q}_i - \mathbf{q}_j\right|}\cdot\left.\frac{d\phi_{i,j}}{d\mathbf{q}}\right|_{|\mathbf{q}_i - \mathbf{q}_j|}\right) \tag{41}$$

where $p_{i\alpha}$ is the α Cartesian component of particle *i* momentum and $\left|q_i - q_j\right|_\alpha$ is the scalar distance between two particle centres *i* and *j* with respect to α Cartesian component of the vector $(\mathbf{q}_i - \mathbf{q}_j)$.

As a remarkable property of the stress tensor, it can be underlined that for homogeneous isotropic substances (Lennard-Jones fluids, for example), the matrix represented by equation 40 is symmetric and that its trace, according to virial theorem, is equivalent to the instantaneous pressure given by expression 25:

$$P(t) = \frac{1}{3V} \sum_{\alpha=x,y,z} P_{\alpha\alpha}(t) \tag{42}$$

The statistical precision, in the case of single particle correlations such as diffusion coefficients (relation 38), is generally better than with collective correlations (e.g., viscosity), because it can be improved by averaging over all the system particles. Thus, the more particles the system contains, the smaller the statistical uncertainties are. In the case of viscosity coefficient, the statistics can only be enhanced by averaging over the three cyclic permutations of the indices $\alpha\beta$ = (*xy*, *yz*, *zx*) (Haile, 1992),

$$\eta = \frac{1}{3}\left(\eta_{xy} + \eta_{yz} + \eta_{zx}\right) \tag{43}$$

As a drawback of single particle correlation functions, compared to collective correlation functions, one can indicate that they are very time consuming to compute.

In order to give a broader idea of the potential of Molecular Dynamics, one has to underline that it is also possible, during a simulation run, to follow the spatial repartition of molecules in the system. This analysis appears to be very useful to obtain information about the structure of the matter. For example, one can expect with these space correlation functions to observe phase transitions.

3.5 SIMULATION AND RESULTS

The first step, before starting a simulation, is to initiate the trajectory at a certain point of the phase space $\{\mathbf{q}^N, \mathbf{p}^N\}$. For this purpose, some classical "tricks" are used in order to avoid having problems with initial conditions. In the case of the particle configuration, there is a risk if the particle distribution is randomly executed to place a particle within the potential distance σ of a neighbour, situation that could bring problems to the simulator.

A current solution to avoid this troubleshooting situation is to achieve the disposition of particles in the simulation cell with respect to a crystal lattice structure (in our case, Lennard-Jones fluid particle positions were located in a face-centered cubic, that is a fcc structure). Concerning the velocities, in order to reach the equilibrium as quickly as possible, it is usual to sample them from a Maxwellian distribution. As an alternative to these tricks, one can notice that it is very handy to reuse the particle positions and *momenta* generated from a previous run.

At the beginning of a simulation, the system is, in most of the cases, out of equilibrium. The second step for a simulator is then to run the programs in order to reach an equilibrium state. We know that the system could be in a state characterized by a certain density, temperature or pressure. So, if the density is fixed by the choice of the simulation box volume ($V = L^3$), how can one control simulation parameters to go to the desired equilibrium state?

The problem, such as it was defined previously, is that by nature the equations of classical mechanics are conserving, neither the temperature nor the pressure, but the system total energy. With this feature in mind, one used a common device to apply constraints on the algorithm, by means of a velocity scaling, in order to reach for our case the requested temperature (Haile, 1992).

It should be noted that with such a device, we are no longer following Newton's equations and the system total energy is no longer conserved. During the equilibrium phase, we have paid attention, on one hand to the destruction of the initial lattice structure (this step is important due to the eventual presence of metastable states that could lead to erroneous results) and on the other hand to obtain at the end of this step a gaussian distribution of velocities. When all these conditions are checked, it is possible to begin the production run, that is the stage along which the data are collected.

3.5.1 Simulation conditions

The algorithm used to solve the equations of motion is the Gear Predictor-Corrector of fifth order. In fact, this device is one of the more accurate of the algorithms proposed in the literature (Berendsen, 1986) when, such as it is in this case, the reduced time step Δt^* is short. The later parameter was chosen, in all our runs, to be $\Delta t^* = 0.002$.

The size of the simulation box L^* is fixed in fact by the choice of a cubic simulation cell that is,

$$V^* = \left(L^*\right)^3 \quad \text{where} \quad V^* = \frac{N}{\rho^*} \tag{44}$$

and also by the initial conditions imposed to the number of particles that can be placed in a fcc lattice basic cell:

$$N = 4I^3 \tag{45}$$

where I is an integer. Conditions 44 and 45 explain why simulations of simple fluids are mostly done with 32, 108, 256, 500, 864... particles.

In the present work the simulation with 32 particles was not considered due to some classical problems observed when the potential cut-off distance becomes comparable to the size of the simulation cell. Beyond 864 particles, simulation times are extremely long (around 4 days) and runs require a huge storage of data.

For this study, the behaviour of the code was evaluated in some conditions where extensive studies were already available in the literature. The state chosen ($\rho^* = 0.8442$ and $T^* = 0.722$, close to the triple point of Lennard-Jones fluid), although very far from the conditions of the present work (HPHT), it has the advantage, from the evaluation point of view, to be a difficult case to simulate because of the presence of *equilibria* between solid, liquid and gas within a very restricted zone of the *PVT* diagram. The danger with such conditions is to see the system trapped in an ordered region of the phase space $\{\mathbf{q}^N, \mathbf{p}^N\}$. Some care is then required in order to assess the presence of such effects.

A Lennard-Jones potential function combined with a potential cut-off placed at 2.5σ was used in these runs. All the runs were performed for numbers of time steps from 200 000 to 600 000. The simulation conditions are reported in Table 3.1.

Table 3.1 - Conditions of simulation in the case of a Lennard-Jones fluid with $R_{cut} = 2.5\sigma$, reduced time step $\Delta t^* = 0.002$, reduced density $\rho^* = 0.8442$, reduced temperature approx. equal to $T^* = 0.722$.

"Run"	Number of particles: *N*	Length of the run (in time steps)	Length of the time correlation function (in time steps)
1	108	200000	500
2	108	600000	500
3	256	200000	600
4	256	200000	600
5	500	200000	800
6	500	200000	800
7	864	200000	1000

Note: For runs 3 and 4, but also 5 and 6, different initial conditions were used in order to evaluate the results quality.

3.5.2 Results

3.5.2.1 Equilibrium properties:

For the determination of equilibrium properties, averages and uncertainties were estimated by means of a coarse graining sampling method with segments of a hundred time steps. The values obtained are reported in Table 3.2.

Table 3.2 - Results of simulation for simple quantities in the case of a Lennard-Jones fluid with R_{cut} = 2.5σ, reduced time step $\Delta t^* = 0.002$, reduced density $\rho^* = 0.8442$.

"Run"	$\langle K^* \rangle$	$\langle U^* \rangle$	$\langle P^* \rangle$	$\langle T^* \rangle$
1	1.16202(73)	-6.03674(74)	0.41428(395)	0.77468(49)
2	1.08539(41)	-6.09427(42)	0.08541(227)	0.72359(27)
3	1.09617(46)	-6.08096(46)	0.19072(251)	0.73078(31)
4	1.04202(44)	-6.12352(44)	-0.03959(246)	0.69468(29)
5	1.07774(33)	-6.09377(33)	0.12563(182)	0.71849(22)
6	1.04603(33)	-6.11812(33)	-0.01312(179)	0.69739(22)
7	1.07047(25)	-6.10002(25)	0.09061(136)	0.71365(17)

Each statistical uncertainty, given in parentheses in units of the low-order digit of the mean value, is one standard deviation of the mean value.

As a first remark, one can see from Table 3.2 that with the (*NVE*) ensemble, it is quite difficult to reach the target temperature value (T^* = 0.722). It should be interesting in the future to assess the results obtained with other types of ensembles and mainly the (*NVT*) ensemble. If one can see that the values of kinetic and potential contributions are quite similar from one run to the other, this is not the case for pressure.

These results are somewhat problematic (especially for runs 4 and 6) because, such as it was mentioned before, it may mean that the system is "locked" into a certain region of the phase space and that we are not sampling it correctly. In order to evaluate the quality of these results, it should be necessary to accomplish some series of runs with different initializations.

Such as previously suggested, it is possible to increase the statistical precision of simple thermodynamic values in a simulation by increasing the number of particles (see runs 1 and 7) or the length of the run (see, runs 1 and 2).

3.5.2.2 Time correlation functions

The choice of the length of the time correlation function was done with respect to the effects of periodic boundary conditions. In fact, the imposed periodicity in space (PBC) gives rise indirectly to a finite periodicity in time. Thus, one could expect undesired behaviour on time correlation functions when the delay time of sampling exceeds the time necessary for an acoustic-wave to traverse the simulation cell, i.e. the traversal time t^*_{trav}. In the desired conditions of simulation, Levesque and Verlet (Berendsen, 1986) have reported the following expression for t^*_{trav}:

$$t^*_{trav} = \frac{L^*}{5.8} \tag{46}$$

Such as it was stated earlier, it can be observed from Figure 3.5 that the time autocorrelation function is maximum at zero time and decreases with increasing time to reach values almost equal to zero after the relaxation time (data uncorrelated). After 400 time steps, for the example of Figure 3.5, the fluctuations observed could be related to the use of the cut-off potential or to the influence of the periodic boundary conditions.

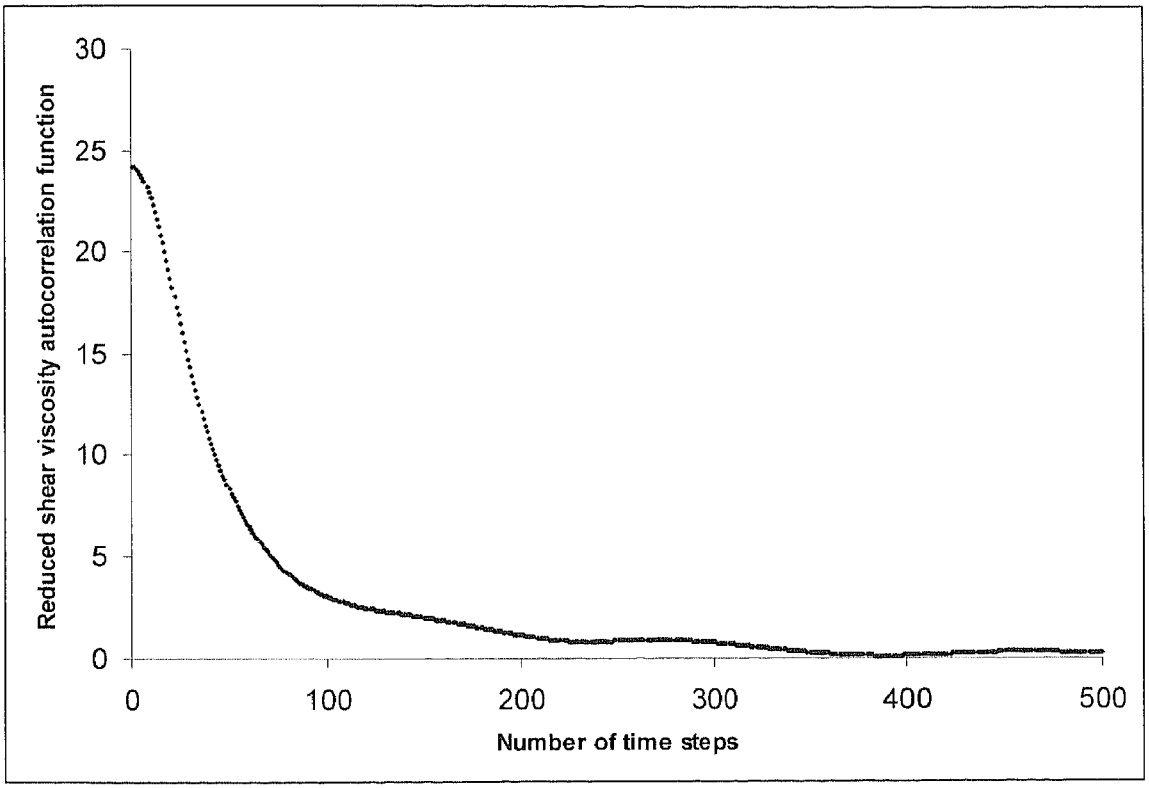

Figure 3.5 - Reduced shear viscosity autocorrelation function as a function of the number of time steps for a 108 Lennard-Jones system - Conditions of Run number 1.

For shear viscosity, averages and uncertainties were estimated by means of a systematic sampling method. For the calculation of the time correlation function, sampled values were obtained each seventh time steps for all runs except the run 2 where values were sampled each twentieth time steps. Time correlation functions were computed over 25 000 time origins.

The values obtained for the reduced shear viscosity are reported in Table 3.3 and compared with the values presented by Erpenbeck (1988) with classical truncated Lennard-Jones potential. In order to avoid the effects of the discontinuity introduced by the potential cut-off R_{cut} (Erpenbeck, 1988) we also used a cubic spline Lennard-Jones function. The values obtained by Erpenbeck (Erpenbeck, 1988), in the later case, are slightly higher than those given by the classical truncated Lennard-Jones function. It seems then difficult to compare them with the results of our simulations.

Table 3.3 - Results of simulation for reduced shear viscosity in the case of a Lennard-Jones fluid with $R_{cut} = 2.5\sigma$, reduced time step $\Delta t^* = 0.002$, reduced density $\rho^* = 0.8442$.

"Run" number	η^* (This work)	η^* for truncated LJ (Erpenbeck, 1988)
1	2.818(90)	2.912(71)
2	2.882(87)	
3	3.394(108)	--
4	3.246(105)	
5	2.732(140)	--
6	3.235(140)	
7	3.276(179)	3.200(160)

Each statistical uncertainty, given in parentheses in units of the low-order digit of the mean value, is one standard deviation of the mean value.

The software used was developed using on Fortran-based routines for MD simulations programed by Furio Ercolessi from SISSA, Trieste University.

As a primary remark, one can see from Table 3.3, by comparison of runs 3 and 4, but mainly 5 and 6, that the choice of initialization parameters could greatly influence the final results for viscosity coefficient. In order to ensure the quality of the results (i.e., to check if all the phase space $\{\mathbf{q}^N, \mathbf{p}^N\}$ was sampled and not only a reduced zone), it should be important, in future works, to carry out a large number of simulations for each condition with different initialisations. The relative reproducibility of the results could give a criterion to assess the quality of a simulation and its confidence interval.

The values observed in Table 3.3 are in statistical agreement with the data obtained by Erpenbeck (1988) with the truncated Lennard-Jones potential. This tendency is confirmed by the examination of Figures 3.6a and 3.6b, where our results are compared with those presented in the literature (Erpenbeck, 1988; Schoen, 1985; Levesque, 1987). Moreover, in Figure 3.6a, the extrapolation of η^* to an infinite number of molecules (i.e., when 1000/*N* is equal to zero) is leading, not taking into account run n°5, to similar results as Erpenbeck's (1988). Thus, the reduced shear viscosity limit is estimated to be 3.40 by Erpenbeck (1988) when we are evaluating it to 3.43 with our data.

If the average values are quite similar from one source to the other, nevertheless some divergences appear with the estimation of uncertainties. Figure 3.6a shows, for our case, that uncertainties (the error bars are statistical uncertainties reported at ± 1 standard deviations of each average) are increasing with the system size. On the contrary, with Figure 3.6b, it is very difficult to give, for literature data, a general tendency for the variation of uncertainties.

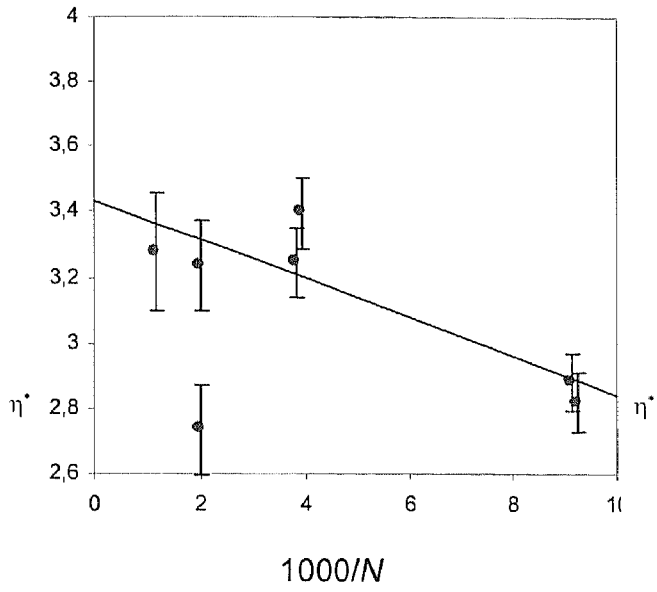

Figure 3.6a - Effect of system size on the reduced shear viscosity η^* of Lennard-Jones fluids at reduced density $\rho^* = 0.8442$ and reduced temperature approximately equal to $T^* = 0.722$. Simulations from this work.

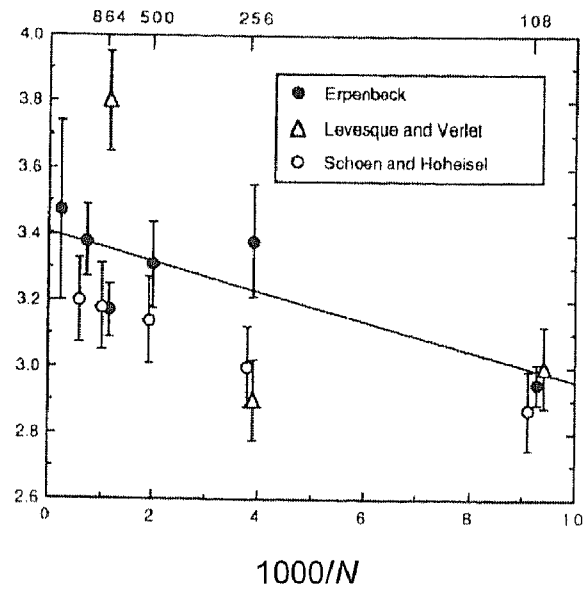

Figure 3.6b - Effect of system size on the reduced shear viscosity η^* of Lennard-Jones fluids at reduced density $\rho^* = 0.8442$ and reduced temperature approximately equal to $T^* = 0.722$. Data from Erpenbeck (1988), Schoen (1985) and Levesque (1987).

3.5.3 General remarks

If these results seem in accordance with those collected from the literature, a general problem remains. Alder and Wainwright (1970) have pointed out that some differences existed between theory and molecular dynamics simulated values.

In fact, according to the Boltzmann-Enskog equation of kinetic theory, the tail of the velocity autocorrelation function should decay exponentially; however, molecular dynamics results show that the velocity autocorrelation function decays as a power of law, $t^{-3/2}$. This long-lived correlation of the velocity of one particle *i* is attributed by Alder and Wainwright (Alder, 1970) to collective effects involving the many atoms that surround particle *i*. As particle *i* moves through a fluid, it creates a vortex motion in neighbouring particles. Some authors (Erpenbeck, 1988) suggest the application to simulated values of a hydrodynamic correction in order to account for these effects.

3.6 CONCLUSIONS

Our goal in the EVIDENT project is to model viscosity phenomena of liquid hydrocarbons with a molecular based approach. By comparison with classical thermodynamics, despite the great complexity introduced by the description of microscopic behaviour (mainly, to take into account the multiple freedom degrees existing in long chain molecules), one can hope a better prediction of macroscopic quantities. As an aim of this study, we believe that simulations can produce a more accurate knowledge of the petroleum fluid viscous behaviour in order to improve the petroleum well productivity in high temperature-high pressure conditions.

This first stage of the work consisted of the evaluation and the validation of computer codes used for the simulation of viscosity phenomena. If the potential model that we have considered is extremely simple (i.e., Lennard-Jones potential), this simulation step was necessary in order to compare our results with those already published in the literature.

From a global point of view, the results obtained seem in agreement with those published by Erpenbeck (1988) and Schoen and Hoheisel (1985). For a few cases, we have observed some problems of results reproducibility due to different initializations. Before introducing a more complex potential function to account for the behaviour of non-spherical molecules, it should be necessary to check the reliability of Lennard-Jones fluid simulations.

Nevertheless, and spite the simplicity of the model fluid studied, it became clear from the simulation runs performed, that the computation time (of the order of tenths of hours and even days) required by the MD simulation process is far from acceptable for use in real petroleum reservoir simulation.

Even with the use of today's fast computers it is not feasible to introduce in the "already-heavy reservoir simulators" a package for simulating viscosity that requires "hours" of calculations for attaining a result for a single point for only one property of the many required in the general reservoir simulator.

For this reason, the research team aimed its efforts to develop a solution that would keep the good "theoretical" background of the MD simulations, but could perform viscosity calculation, with a calculation time of the order of a few seconds.

The work presented in the next chapters shows the results of such effort.

3.7 LIST OF SYMBOLS

$A(t)$	Instantaneous value of A	P	System pressure
$\langle A \rangle$	mean value of A	$P^* = \frac{P\sigma^3}{\varepsilon}$	Reduced pressure
$\dot{A}(t), \ddot{A}(t), \ldots$	First, second and so on... time derivatives of quantity $A(t)$	$P_{xy}(t)$	Element of the instantaneous stress tensor
$C_{AB}(t)$	Time correlation function between quantities A and B after a time delay t	PBC	Periodic Boundary Conditions
D_i	Self-diffusion coefficient	$\mathbf{q}_i$	Position vector of particle i
E_{tot}	Total energy	$\mathbf{q}_k$	Position vector of electron k
$\mathbf{F}_i$	Internal force vector acting on particle i	R_{cut}	Cut-off radius
fcc	Face-centered cubic	t	Time
H	System Hamiltonian	$t^* = \frac{t}{\sigma\sqrt{m/\varepsilon}}$	Reduced time
H^*	Reduced Hamiltonian, i.e. $H^* = \frac{H}{N\,\varepsilon}$	t^*_{trav}	Reduced traversal time
$\hat{H}$	Hamiltonian operator of the system	T	System temperature
k_B	Boltzmann constant	$T^* = \frac{k_B T}{\varepsilon}$	Reduced temperature
K	System kinetic energy	TC	Transport coefficient
$K^* = \frac{K}{N\,\varepsilon}$	Reduced kinetic energy	U	System potential energy
L	Simulation box size	$U^* = \frac{U}{N\,\varepsilon}$	Reduced potential energy
$L^* = \frac{L}{\sigma}$	Reduced simulation box size	V	System volume
m	Mass of a particle	W	Clausius virial function
N	Number of particles of the system	Z_i	Charge of nucleus i
$\mathbf{p}_i$	Momentum vector of particle i	$\{\mathbf{q}^N, \mathbf{p}^N\}$	Phase space for a N-particle system

Greek letters

ε	Potential function energy at the minimum
ϕ	Pairwise potential function
η	Shear viscosity coefficient
η^*	Reduced shear viscosity coefficient, i.e. $\eta^* = \frac{\eta\sigma^2}{\sqrt{m\varepsilon}}$
Λ	de Broglie thermal wavelength
ρ	System density, i.e. $\rho = \frac{N}{V}$
ρ^*	Reduced density, i.e. $\rho^* = \rho\sigma^3$
σ	Potential function distance to the zero
$\sigma(A)$	Root mean square deviation or standard deviation
ψ	Spatial wave function in Schrödinger equation

3.8 REFERENCES

- Alder,B.J., Wainwright,T.E. Phys. Rev. A, 1, 18, 1970.
- Atkins, P., de Paula, J., Elements of Physical Chemistry, 4th Edition (website resources), Oxford University Press, 2005.
- Berendsen,H.J.C., Van Gunsteren,W.F. in Molecular-dynamics simulation of statistical-mechanical systems, Eds. G. Ciccotti and W.G. Hoover, Italian Physical Society, North Holland, Amsterdam, 1986.
- Erpenbeck,J.J. Phys. Rev. A, 38, 6255, 1987.
- Haile, J. M., Molecular Dynamics Simulation, John Wiley&Sons, 1992.
- Levesque,D., Verlet,L. Mol. Phys., 61 , 143, 1987.
- Schoen,M., Hoheisel,C. Mol. Phys., 56, 653, 1985.

3.9 TABLE OF CONTENTS

3.9.1 List of Tables

3.9.2 List of Figures

4. Model Based on Molecular Theory

4.1 INTRODUCTION

As shown in the previous chapter, the use of "pure" Molecular Dynamics (MD) viscosity simulation presents a number of important and limiting operative problems associated to MD computations:

- Extremely high computer calculation time (in the order of 2 to 7 days per state point),
- Difficult algorithm initialization,
- High sensitivity of simulation results to the initial configuration, and difficult automation of the reliability assessment of the simulation results.

With the knowledge of these limitations, the work presented in this chapter is dedicated to the development of a new model that, while based on MD, would be compatible with the computing time constraints required by industrial needs, i.e., a model that could overcome the limits of straight MD simulations but still be based on a microscopic picture of matter behaviour. The model should also be free from the limitations identified in the previous chapters (§2 and §3), hence being applicable to any kind of phase type such as saturated and subcooled liquids, saturated and superheated vapors and supercritical fluids.

Bearing in mind that the "engineering objective" is to analytically calculate the LJ viscosity η^+ at a given temperature T^+ and pressure P^+, we based our work on two analytical relations that represent well MD data obtained for the Lennard-Jones Fluid: the Kolafa-Nezbeda equation of State (1994) (EoS) and the Rowley-Painter Viscosity EoS (1997).

4.2 BASIC CONCEPTS

Model fluids are imaginary substances that have a well-defined expression for the intermolecular potential. The values of the properties of model fluids, at given input conditions, are obtained through computer experiments using methods such as molecular dynamics (MD) (Haile, 1997). Once good quality computer simulation data are available, for a chosen model-fluid, in a wide enough range of conditions, they can be summarized in the form of Equivalent Analytical Relationships (EARs). The EARs are analytical functions that, from the same input information used to run a computer experiment, provide values for the model-fluid properties which agree well with those of the actual computer experiment.

Simulated data correspond to substances which strictly obey a prescribed intermolecular potential model. Therefore, simulated data of a chosen model fluid are conventionally used for studying fundamental issues such as the extension of measurements to regions not accessible to experiments or the correct form for mixing rules (Murad, 1986).

Real fluids behave according to the complex intermolecular interactions of real molecules, whatever their mathematical form may be, rather than according to the relatively crude intermolecular potential forms of well-known model fluids. In spite of this fact, simulated data or their corresponding EARs, have also been used as the basis for engineering models applicable to real fluids. For instance, Sun and Teja (1998) have modeled the vapor-liquid equilibria of systems containing polar or elongated molecules using a Lennard-Jones (LJ) equation of State (EoS) with temperature-dependent effective LJ parameters. In this case, all the complex interactions taking place between real non-spherical molecules, often in the presence of polar or specific intermolecular forces, are lumped into a single pseudo Lennard-Jones intermolecular potential.

This approach is acceptable for engineering calculations and we somehow adopt it in the present work. Sun and Teja (1998) applied their LJ-EoS for mixtures using the van der Waals (VW) one-fluid mixing rules. These researchers (Sun and Teja, 1998) found that the their LJ+VW EoS could be used to correlate as well as extrapolate mixture data over considerable ranges of temperature and pressure, and also found, on the other hand, that commonly used purely empirical equation of state models were inadequate when extrapolated.

The systems studied (Sun and Teja, 1998) contained molecules of considerable complexity (e.g, water, ethanol, methane, n-decane), and the pure-compound LJ parameters were made temperature-dependent. In spite of the "non-Lennard-Jonnescity" of the studied complex molecules, Sun and Teja (1998) concluded that the predictive power is higher for LJ-based EoSs than for cubic EoSs.

The most probable explanation for these conclusions is that LJ equations of state acknowledge the existence of discrete molecules through forced agreement with results from molecular level computer experiments, rather than assuming that fluids have a continuous nature. Results such as those of Sun and Teja (1998) indicate that engineering models based on computer experiments have a higher potential than purely empirical correlations to represent accurately the properties of real fluids, as long as the chosen model-fluid is realistic.

A purely empirical correlation is, on the other hand, a model that does not specify an intermolecular potential function (macroscopic approach) (Gubbins, 1994). The techniques of reference (Sun and Teja, 1998) show how the Lennard-Jones fluid can encapsulate not only the behaviour of simple substances but also the behaviour of complex real fluids, if proper corrections are introduced.

To generate a model applicable to engineering calculations, the choice of a suitable model-fluid should be guided by the following requirements:

a) ability to represent well the essential behaviour of real fluids with good predictive capabilities,
b) availability of computer simulation data in wide ranges of pressure and temperature to build proper EARs, and
c) relative simplicity of the intermolecular potential function.

With respect to the first requirement, the intermolecular potential function u and its derivatives with respect to the intermolecular distance r should preferably be continuous functions of r. The well-known Lennard-Jones (LJ) model-fluid fulfills, in principle, all these prerequisites.

The physical property of focus in the present work is the Newtonian shear viscosity. Our goal is to develop a model applicable in wide ranges of temperature and pressure, with special emphasis on the dense region. However, the model should also provide reasonable viscosity values for low-density fluids. Hence, a unified treatment of all possible fluid phase states, such as liquid, vapor and supercritical fluid, is required. This is also a precondition for the description of asymmetric mixtures.

The model must be based on molecular theory, and should take advantage of recent EARs and/or computer simulation data. Besides, the computation time should be compatible with engineering needs. Hence, a good balance between accuracy and simplicity should be reached. Additionally, the required experimental input information should be kept to a minimum.

Towards those goals, the purpose of the work presented in this chapter is to evaluate the potential of combining existing LJ-EARs for representing the viscosities of real fluids. We review the relevant literature and test the consistency between previous works of different authors. In view of our objectives, some simplifications are proposed. Afterwards, the potential of the new modeling approach is assessed by looking at the qualitative trends for viscosity in wide ranges of temperature and pressure, and through the quantitative comparison of predicted and experimental viscosities.

4.2 THE LENNARD-JONES (LJ) FLUID

The expression for the Lennard-Jones intermolecular potential is the following:

$$u(r) = 4\varepsilon\left[\left(\frac{\sigma}{r}\right)^{12} - \left(\frac{\sigma}{r}\right)^{6}\right] \qquad (1)$$

where r is the intermolecular distance, u is the potential energy, ε is the depth of the LJ potential well and σ is the LJ separation distance at zero energy.

The LJ reduced temperature T^+, reduced pressure P^+, reduced density ρ^+ and reduced viscosity η^+ are conventionally defined as follows:

$$T^+ = \frac{kT}{\varepsilon} \qquad (2)$$

$$P^+ = \frac{P\sigma^3}{\varepsilon} \qquad (3)$$

$$\rho^+ = \frac{N}{V}\sigma^3 = N_A\,\rho\sigma^3 \qquad (4)$$

$$\eta^+ = \eta\frac{\sigma^2}{\sqrt{m\varepsilon}} \qquad (5)$$

where k is the Boltzmann constant, T is the absolute temperature, P is the absolute pressure, N is the number of molecules, V is the system volume, N_A is Avogadro's number, ρ is the amount-of-substance density, η is the Newtonian shear viscosity, and m is the molecular mass. The variable ρ^+ is not necessarily limited to values smaller than unity.

Rowley and Painter (RP) (1997) computed LJ shear viscosities and self-diffusion coefficients at 171 different conditions covering a wide range of density and temperature, using the method of molecular dynamics. They fitted EARs to the simulation data, which makes it possible to calculate viscosities and self-diffusion coefficients from the values of T^+ and ρ^+. For the case of viscosity, the RP-EAR is the following:

$$\eta^+ = \eta_0^+ \exp\left[\sum_{i=1}^{4}\sum_{j=1}^{6} b_{ji}\frac{\left(\rho^+\right)^i}{\left(T^+\right)^{(j-1)}}\right] \qquad (6)$$

with

$$\eta_0^+ = \frac{5}{16}\sqrt{\frac{T^+}{\pi}}\left(\sum_{j=1}^{5}\omega_j\left(T^+\right)^{(j-1)}\right)^{-1} \qquad (7)$$

where η_0^+ is the LJ reduced viscosity limit at zero density. The coefficients b_{ji} and ω_j (Rowley and Painter, 1997) are tabulated in Appendix 4A.

The RP viscosity equation of state, i.e., equation 6, has the temperature range of application $0.8 \le T_+ \le 4$. The range for ρ^+ is from 0 (zero) to the minimum between 1 (unity) and the density of the dense LJ fluid in equilibrium with the LJ solid ($\rho^+_{\text{fluid},SFE}$). Throughout the present chapter, any reference to solid-fluid equilibrium excludes the equilibrium between the solid and a low-density vapor (i.e., the sublimation equilibrium is excluded).

Viscosity diverges at the critical point (Vogel *et al.*,1998). equation 6 does not account for the critical enhancement of viscosity that takes place in the neighborhood of the critical point.

In contrast with the case of the thermal conductivity, the critical enhancement in viscosity is small and becomes important only within a narrow region around the critical point (Vogel *et al.*,1998; Watson *et al.*, 1980) presented a clear illustration of the critical enhancement effect.

They also argued in favor of the viscosity factorization of equation 6, as opposite to an additive representation expressing the dense fluid viscosity as the summation of the zero-density viscosity plus a residual term.

The usual engineering need is to calculate viscosities at a given temperature and pressure. Hence, we need a LJ EAR, connecting the temperature, the pressure and the density, which could be combined with equation 6. Kolafa and Nezbeda (1994) proposed one such analytical EoS for the Lennard-Jones Fluid: The Perturbed-Virial-Expantion / hybrid Barker-Henderson equation of State (PVE/hBH LJ-EoS). This EoS is based on a perturbed virial expansion with a theoretically defined temperature-dependent reference hard sphere term. The PVE/hBH LJ-EoS is based on critically assessed computer simulation data from several sources. The good quality of this LJ-EoS was confirmed by Mecke *et al.* (1998)

The PVE/hBH LJ-EoS is the following:

$$z = \frac{P^+}{\rho^+ T^+} = f_{KN}\left(\rho^+, T^+\right) \qquad (8)$$

Were z is the compressibility factor and f_{KN} is a function of ρ^+ and T^+ defined in Appendix 4B

The temperature range of application of equation 8 is $0.68 \leq T^+ \leq 10$. The range for ρ^+ is from 0 (zero) to the density of the dense LJ fluid in equilibrium with the LJ solid ($\rho^+_{\text{fluid},SFE}$).

According to Kolafa and Nezbeda (1994), equation 8 was built without imposing constraints related to the location of the critical point. Hence, the PVE/hBH EoS is a classical Lennard-Jones EoS. Kolafa and Nezbeda (1994) discussed the problems associated to the generation of a LJ-EoS accurate at the close neighborhood of the critical point.

The critical coordinates corresponding to equation 8 are the following (Kolafa and Nezbeda, 1994):

$$T_c^+ = 1.3396 \tag{9}$$

$$P_c^+ = 0.1405 \tag{10}$$

$$\rho_c^+ = 0.3108 \tag{11}$$

$$z_c = 0.3375 \tag{12}$$

It can be shown that, in spite of the non-cubic nature of the PVE/hBH LJ-EoS, equation 8, the number of ρ^+ values compatible with given physically meaningful values of T^+ and P^+ never exceeds the number of three, as in the case of semi-empirical cubic EoSs (e.g., Zabaloy and Vera (1996), as long as equation 8 is used within its range of applicability. At subcritical temperatures, the number of ρ^+ values compatible with a given value P^+ can be quickly established using the techniques of reference (Topliss *et al.*, 1988).

The availability of a procedure to compute $\rho^+_{\text{fluid},SFE}$ is required to properly use equations 6 and 8. Agrawal and Kofke (1995) reported properties of the LJ fluid at solid-fluid coexistence from the LJ triple point temperature up to temperatures much higher than the vapor-liquid LJ critical temperature. Agrawal and Kofke (1995) provided the following semiempirical fit of the melting line:

$$P^+_{SFE} = \beta^{-\frac{5}{4}}\left(A + B\beta + C\beta^2\right)\exp\left(-D\beta^{\frac{1}{2}}\right) \tag{13}$$

where P^+_{SFE} is the melting pressure P^+ and

$$\beta = \frac{1}{T^+} \qquad (14)$$

The parameters of equation 13 are given in Table 4.1 (Agrawal and Kofke,1995).

Table 4.1 - Parameters in equation 13

A	16.89
B	-7.19
C	-3.028
D	0.4759

equation 13 is an EAR that corresponds both to the solid-liquid equilibrium and to the solid-supercritical fluid equilibrium. equation 13 is not valid for the LJ solid-vapor equilibrium that takes place at temperatures lower than the LJ triple point temperature. The applicability range of equation 13 is $0.00365 \leq \beta \leq 1.456$, which corresponds to the (wide) T^+ range $0.686813 \leq T^+ \leq 273.973$.

At a given value of T^+ the pressure of LJ solid/dense-fluid equilibrium can be computed using equation 13 . The resulting value of P^+ can then be introduced into equation 8 to calculate the dense fluid ρ^+ value. The ρ^+ values obtained in this way, for a range of values of T^+, should be equal to the values of $\rho^+_{\text{fluid},SFE}$ reported by Agrawal and Kofke (1995). Figure. 4.1 shows such a comparison.

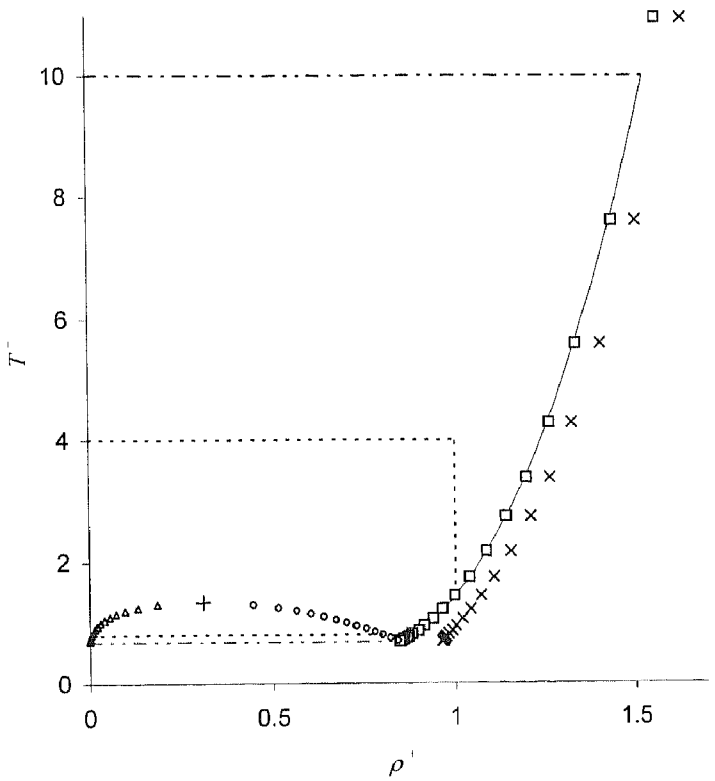

Figure 4.1 - Temperature-density phase diagram for the Lennard-Jones (LJ) Fluid.

Solid line: highest ρ^+ given by the PVE/hBH Lennard-Jones equation of State, equation 8, at solid-fluid equilibrium P^+ (equation 13). Symbols: × LJ Solid density data at solid-fluid equilibrium Agrawal and Kofke (1995) □ LJ fluid density data at solid-fluid equilibrium Agrawal and Kofke (1995) ○ PVE/hBH LJ-EoS VLE liquid density calculated by Mecke *et al.* (1998) | | PVE/hBH LJ-EoS VLE vapor density calculated by Mecke *et al.* (1998), + Lennard-Jones critical point according to equations 9 and 11. VLE means vapor-liquid equilibrium

The solid line corresponds to calculated values of $\rho^+_{\text{fluid},SVE}$, while the squares correspond to the LJ fluid density data of Agrawal and Kofke (1995). From this figure it is clear that there is a very good agreement between different reference data: Kolafa and Nezbeda (1994) and Agrawal and Kofke (1995). Figure 4.1 also shows the LJ data for the saturated solid, and for the LJ fluid at conditions of vapor-liquid equilibrium.

The horizontal and vertical simple dashed lines and the solid line define the limits of applicability of equation 6. The two horizontal compound dashed lines and the solid line define the limits of applicability of equation 8. The range of the PVE/hBH LJ-EoS completely contains the range of the RP viscosity EAR.

4.3 NEW LENNARD-JONES VISCOSITY PARAMETERS

The development of the present work requires the calculation of properties of real fluids based on LJ properties. Real fluid conditions of temperature and pressure can make the required LJ computations fall outside the range of applicability of equations 6 and 8. Hence, for such cases, proper extrapolation schemes will be set for computing LJ densities and viscosities, which will be presented in the next chapter.

Equation 6, coupled to the original coefficients b_{ji} and ω_i tabulated in Appendix 4A, shows a relatively complex viscous behaviour at low density and low temperature: a minimum appears for viscosity as a function of density. Such behaviour complicates the setting of robust extrapolation schemes, to be used at low temperatures. On the other hand, the effect is not quantitatively important. Hence, we modified slightly the model set by equations 6 and 7 by setting an additional equation and by refitting the parameters of equation 6, forcing the absence of minima for viscosity as a function of density and forcing the fulfillment of some suitable restrictions. This is acceptable for engineering purposes. We provide the details in Appendix 4C.

The additional equation is the following:

$$b_{11} = (-1)\sum_{j=2}^{6} \frac{b_{j1}}{\left(T^{+}\right)^{j-1}} = (-1)\left[\frac{b_{21}}{\left(T^{+}\right)} + \frac{b_{31}}{\left(T^{+}\right)^{2}} + \frac{b_{41}}{\left(T^{+}\right)^{3}} + \frac{b_{51}}{\left(T^{+}\right)^{4}} + \frac{b_{61}}{\left(T^{+}\right)^{5}}\right] \qquad (15)$$

which sets the value of the coefficient b_{11} as a function of temperature T^{+} and of the parameters b_{21} to b_{61}. Equation 15 imposes the flatness of the η^{+} vs. ρ^{+} curve at $\rho^{+} = 0$.

Table 4.2 presents the new set of parameters. When using equation 6 with the parameters of Table 4.2, the required η_0^+ value comes from equation 7 used with the constants of Table A-II of Appendix 4A, i.e., we only refitted the constants of equation 6. We have not refitted the constants of equation 7. Appendix 4C provides information on the quantitative performance of the coupled equations 6, 7 and 15, used with the parameters reported in Table 4.2 and Table A-II (Appendix 4A).

Now, our LJ viscosity EAR is defined by equations 6, 7 and 15, with the parameters reported in Table 4.2 and Table A-II. The temperature range of applicability is $0.8 \leq T_+ \leq 4$. The range for ρ^+ is from 0 (zero) to the minimum between 1 (unity) and the density of the dense LJ fluid in equilibrium with the LJ solid ($\rho^+_{\text{fluid},SFE}$), computed as described in the previous section. The new set of equations and parameters constitute our basic model for the results presented on the coming sections.

4.4 RESULTS: QUALITATIVE ASSESSEMENT

Figure 4.2 shows, on the viscosity-pressure plane, the effect of combining the viscosity-temperature-density EAR equation 6, with the pressure-temperature-density EAR equation 8, for the Lennard-Jones Fluid. The parameters used in equation 6 are those from Table 4.2.

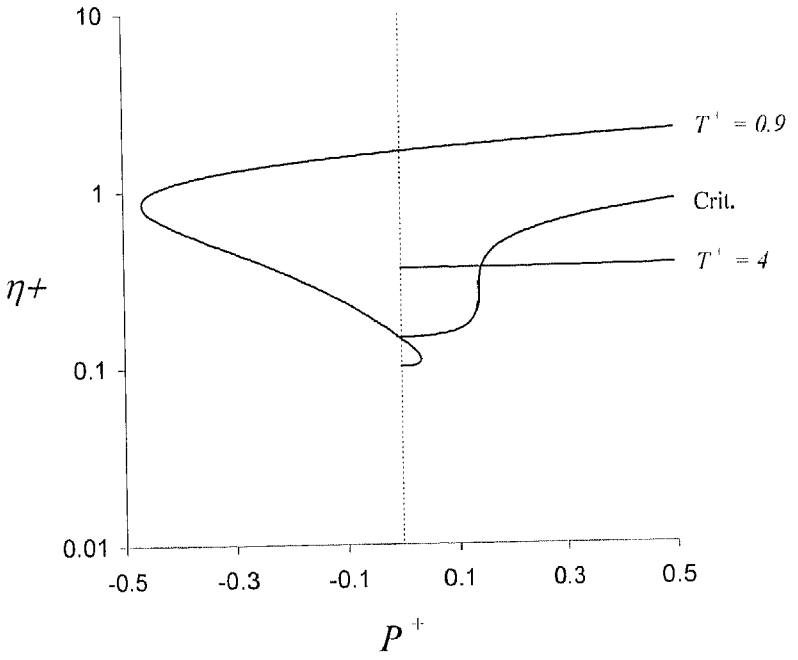

Figure 4.2 – Viscosity-pressure diagram for the Lennard-Jones Fluid, as represented by equations 6 , 7 and 15 coupled with equation 8.

The values of the coefficients of equation 6 are those reported in Table 4.2.

Table 4.2 – New values for equation 6 parameters (obtained in this work)

j	i	b_{ji}	j	i	b_{ji}	J	i	b_{ji}	j	i	b_{ji}
1	1	equation 15	1	2	0.7607120	1	3	0.4221662	1	4	-0.6411574
2	1	62.382722	2	2	8.1770068	2	3	1.7296571	2	4	0.2811374
3	1	2282.3282	3	2	2.5445750	3	3	-14.372592	3	4	-5.1536547
4	1	-6.5634819	4	2	-0.0532996	4	3	-9.3141867	4	4	26.873939
5	1	-22.117548	5	2	1.6436829	5	3	5.2107990	5	4	-15.182439
6	1	3.7696134	6	2	-1.2500496	6	3	0.9588608	6	4	1.7614285

For chosen values of temperature and density the viscosity and the pressure are obtained respectively from equations 6 and 8, and plotted. For a given isotherm the computations are performed from zero density up to a high enough density (which is at most equal to the fluid density at solid-fluid-equilibrium $\rho^{+}_{\text{fluid},SFE}$). Figure 4.2 shows three isotherms: a subcritical one, the critical isotherm, and a supercritical isotherm.

A region of negative pressure for the subcritical isotherm is the consequence of having used equation 8, which, in this respect, behaves as simpler analytical PVT EoSs. The critical isotherm shows a flat region where small changes in pressure produce important changes in viscosity. On the other hand, at very high temperature, the LJ viscosity is much less sensitive to pressure. From Figure 4.2 it is clear that the set of equations 6-8 can basically represent the viscosity of subcritical vapors and liquids, and of near-critical or supercritical fluids in the whole pressure (density) range.

The shape of the subcritical isotherm is in part a consequence of the restrictions described in Appendix 4C. If viscosity would have been allowed to have a minimum with respect to density in the low density region, a more complicated shape for subcritical isotherms would have been obtained.

From equation 5 it can be shown that

$$\eta^{+} = \eta_0^{+} \frac{\eta}{\eta_0} \qquad (16)$$

where η_0 is the value of η at zero density.

Also, from equation 3 we write

$$P^{+} = P_r \, P_c^{+} \qquad (17)$$

where P_c^{+} is a constant (equation 10) and P_r is the practical reduced pressure, defined as

$$P_r = \frac{P}{P_c} \qquad (18)$$

A chosen value of P_r sets a value for P^+ through equation 17. Using equations C-1, 17, 6, 7 and 15, with the parameters of Table 4.2, and equation 8, the plot of Figure 4.3 can be generated, according to the calculation procedure reported in Appendix 4D.

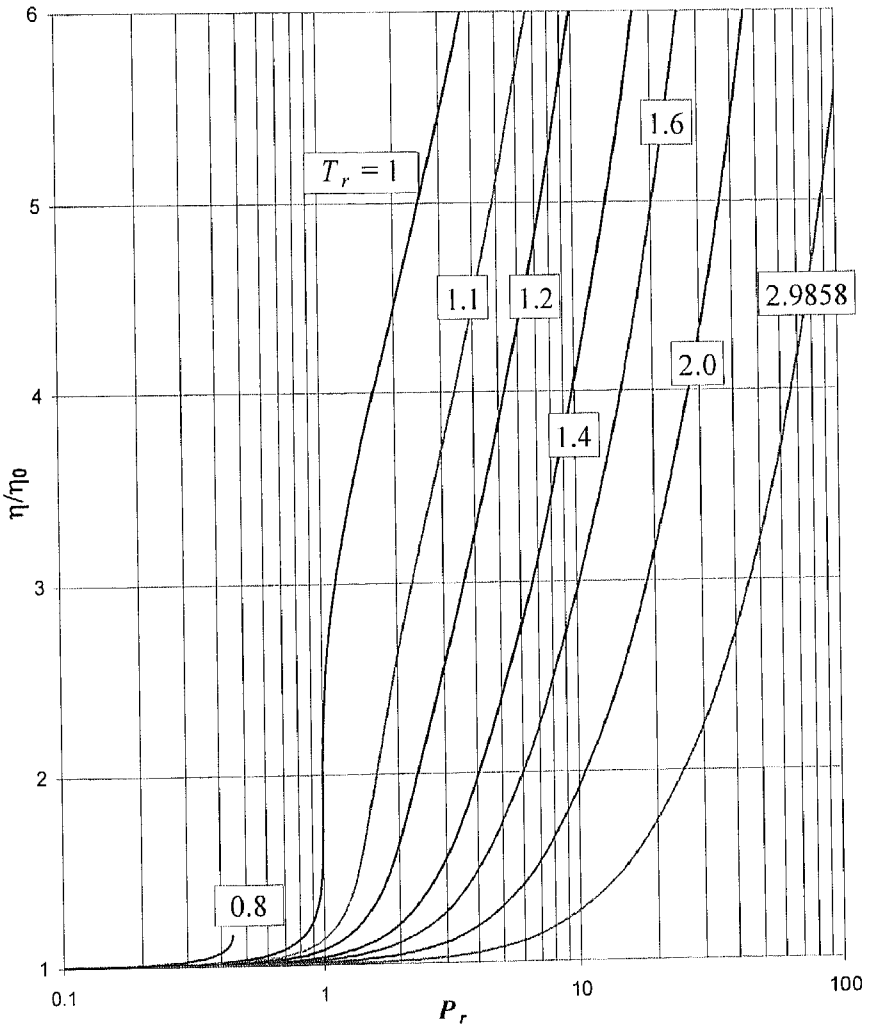

Figure 4.3 - Ratio of viscosity over zero-density viscosity (η/η_0) as a function of the reduced pressure P_r for the Lennard-Jones Fluid.
The parameters of Table 4.2 were used for equation 6.

Figure 4.3 depicts the ratio of viscosity over zero-density viscosity (η/η_0) as a function of the reduced pressure P_r for the Lennard-Jones fluid for different isotherms. Figure 4.3 agrees well with figure 1.3.2 available in the classical book of Bird *et al.* (1960).

From equation 5, for a Lennard-Jones fluid having ε and σ independent of temperature, it can be shown that

$$\eta^+ = \eta_c^+ \frac{\eta}{\eta_c} \qquad (19)$$

where η_c is the viscosity at the critical point, and the ratio η/η_c is the practical reduced viscosity. η_c^+ is the critical value of η^+, calculated from equations 9, 11 and 6 with the parameters reported in Table 4.2.
The result is

$$\eta_c^+ = 0.269409 \qquad (20)$$

It should be mentioned that viscosity models which, as the present one, do not account for any critical enhancement effect give a finite value for the critical viscosity. Actually, viscosity diverges at the critical point (e.g., Table C2 of reference (Watson *et al.*, 1980)), and the incorporation of such effect requires a special modeling treatment (Watson *et al.*, 1980). Watson *et al.* (1980) discriminated the normal viscosity from the actual viscosity.

The normal viscosity is equal to the actual viscosity at any condition except within a small region around the critical point. Reported 'experimental' finite values for the critical viscosity should be regarded as values 'defined empirically by extrapolating the behaviour of the normal viscosity outside the critical region smoothly into the critical region (Watson *et al.*, 1980).

Figure 4.4 shows the reduced viscosity η/η_c as a function of the reduced temperature T_r at a number of values for the reduced pressure P_r. This figure is in good agreement with fig 1.3.1 of Bird *et al.* (1960). Figure 4.4 was generated according to the calculation procedure outlined in Appendix 4D. The density values corresponding to Figures 4.3 and 4.4 never exceeded the limits of applicability of equation 6.

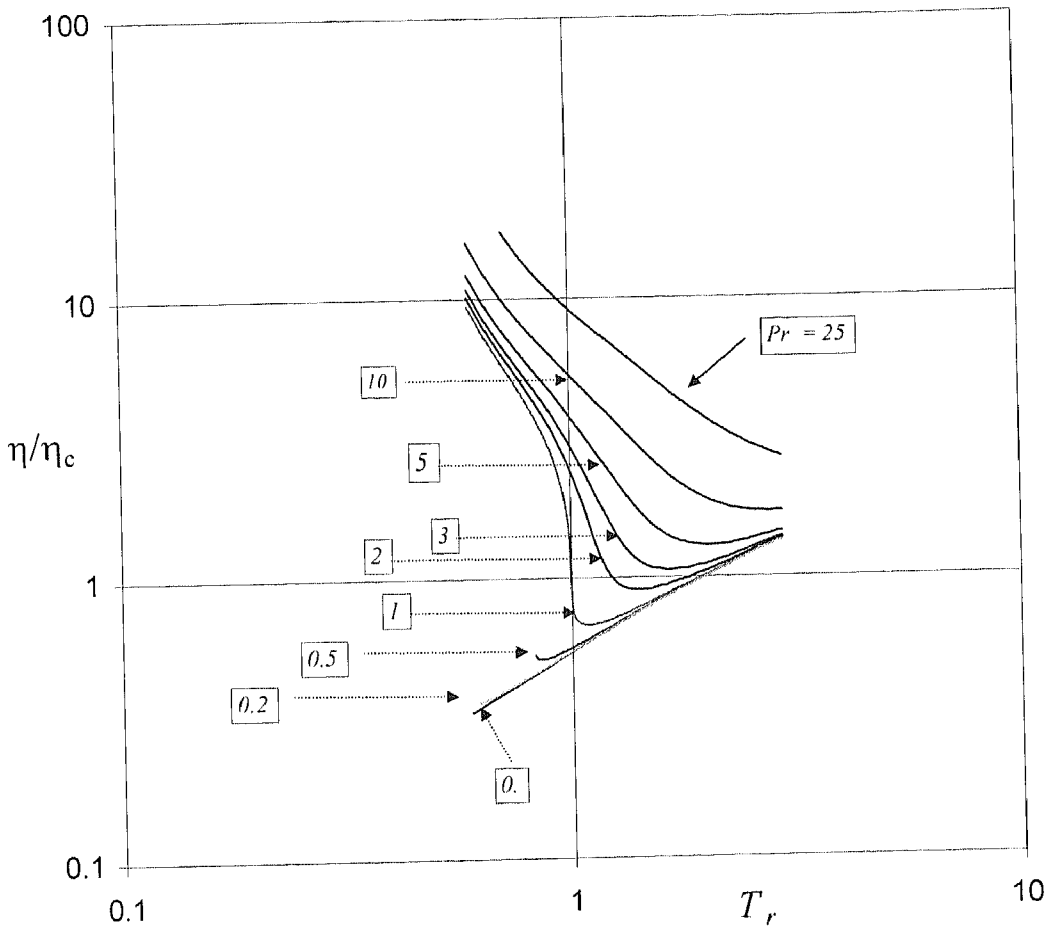

Figure 4.4 - Practical reduced viscosity as a function of the reduced temperature T_r for the Lennard-Jones Fluid. The parameters of Table 4.2 were used for equation 6.

Figures 1.3.1 and 1.3.2 of Bird *et al.* (1960) represent two independent analyses of a large number of experimental data. On the other hand, no single real fluid viscosity data point was used to generate the wide-ranging Figures 4.3 and 4.4. The remarkable agreement between these figures and the figures of reference (Bird *et al.*, 1960) is a proof of the realism of the Lennard-Jones fluid.

4.5 RESULTS: QUANTITATIVE ASSESSEMENT

To assess more completely the potential of using the LJ analytical representation studied here as a basis for describing the viscosities of real fluids, we now concentrate on the quantitative performance of the model, through comparing model predictions against viscosity data for simple real fluids. To this end, we first need to set a criterion to assign numerical values to ε and σ for a given real fluid.

The choice we made in this work is as follows: we write equations 2 and 3 at the critical point. For that, we have to introduce the critical values of the dimensionless LJ variables given by equations 9 and 10. Hence,

$$T_c^+ = 1.3396 = \frac{\kappa T_c}{\varepsilon} \tag{21}$$

$$P_c^+ = 0.1405 = \frac{P_c \sigma^3}{\varepsilon} \tag{22}$$

We compute the values of ε and σ from the values of the experimental critical temperature T_c and of the experimental critical pressure P_c, by solving the system of equations 21 and 22. In this way, the experimental critical temperature and pressure will be exactly reproduced by the LJ PVE/hBH model (Kolafa and Nezbeda, 1994), equation 8.

The advantage of this choice is that the unique behaviour that takes place at the critical point, i.e, a high density sensitivity with small changes in pressure, will be recovered by the model at a temperature equal to the experimental critical temperature.

Since even for simple fluids the true intermolecular potential can be much more complicated than the LJ function, the computed values of ε and σ have the meaning of effective LJ parameters compatible with the experimental values of critical temperature and pressure.

We compared predicted viscosities of simple pure fluids against the data available in the compilation of Stephan and Lucas (1979). The only input experimental information used was the critical temperature, critical pressure and the molecular weight, which were also taken from Stephan and Lucas (1979). The parameters used in equation 6 were those given Table 4.2. Appendix 4E provides a numerical calculation example.

Table 4.3 shows the viscosity prediction results discriminated according to compounds and phase type (liquid, vapor or supercritical fluid). In the calculations, the range of applicability of equation 6 was never exceeded neither for density nor for temperature. For around 2 000 datapoints presented by Stephan and Lucas (1979), presented in Table 4.3, it was not possible to compute viscosities due to range limitations. This referred range limitation will be the subject of the work presented in chapter 5. Results are shown for a total number of 12 182 within-range points.

Table 4.3 - Comparison between predicted Lennard-Jones and experimental viscosities, for pure compounds[1]

NAME	Phase Type[2]	AAD%[3]	NDP	Max AD%[4]	Min T_r	Max T_r	Min P_r	Max P_r
Ethylene	SCF	9	420	19	1.06	2.47	0.02	15.81
Propylene	LIQ	18	147	39	0.79	0.99	0.43	19.57
Propylene	SCF	11	420	43	1.04	1.78	0.02	19.57
Propylene	VAP	3	8	4	0.79	0.99	0.02	0.02
n-Hexene	LIQ	22	105	35	0.62	0.74	0.03	14.66
n-Heptene	LIQ	19	141	39	0.61	0.91	0.04	17.61
n-Octene	LIQ	28	123	47	0.60	0.86	0.04	19.08
ChloroDiFluoroMethane	LIQ	25	200	58	0.68	0.99	0.20	12.05
DiChloroDiFluoroMethane	VAP	16	15	83	0.65	0.99	0.02	0.49
DiChloroDiFluoroMethane	SCF	11	140	72	1.01	1.49	0.02	14.56
DiChloroDiFluoroMethane	LIQ	25	151	46	0.65	0.99	0.49	14.56
BromoTriFluoroMethane	LIQ	23	172	183	0.85	0.99	0.50	15.11
BromoTriFluoroMethane	VAP	3	28	8	0.85	0.99	0.03	0.76
BromoTriFluoroMethane	SCF	6	380	25	1.01	1.28	0.03	15.11
TriChloroTriFluoroEthane	LIQ	47	182	63	0.62	0.99	0.03	17.60
Hydrogen	VAP	19	6	20	0.64	0.91	0.08	0.08
Hydrogen	LIQ	38	43	68	0.61	0.91	0.08	23.08
Hydrogen	SCF	13	66	28	1.00	2.42	0.08	76.92
Neon	VAP	5	4	6	0.68	0.91	0.04	0.36
Neon	LIQ	26	74	31	0.68	0.91	0.36	7.27
Neon	SCF	12	390	50	1.02	2.95	0.04	7.27
Nitrogen	LIQ	14	182	29	0.63	0.99	0.29	14.71
Nitrogen	VAP	9	18	15	0.63	0.99	0.03	0.88
Nitrogen	SCF	7	574	27	1.03	2.78	0.03	29.41
Oxygen	SCF	9	612	19	1.00	2.90	0.02	19.84
Oxygen	LIQ	7	226	21	0.61	0.97	0.20	9.92
Oxygen	VAP	11	26	17	0.61	0.97	0.02	0.79
Fluorine	SCF	7	294	14	1.08	2.08	0.02	3.83
Fluorine	LIQ	15	72	27	0.63	0.97	0.38	3.83
Fluorine	VAP	4	6	4	0.63	0.97	0.02	0.02
Argon	LIQ	19	101	26	0.73	0.93	0.41	6.16
Argon	VAP	4	7	4	0.73	0.93	0.02	0.02
Argon	SCF	11	342	17	1.13	2.98	0.02	10.27
Krypton	SCF	12	284	19	1.20	2.87	0.02	9.09
Krypton	VAP	2	2	3	0.72	0.96	0.02	0.02
Xenon	SCF	13	460	22	1.03	1.48	0.02	8.56

Table 4.3 (Continued): Comparison between predicted Lennard-Jones and experimental viscosities, for pure compounds[1]

NAME	Phase Type[2]	AAD%[3]	NDP	Max AD%[4]	Min T_r	Max T_r	Min P_r	Max P_r
Carbon Monoxide	SCF	8	124	18	1.64	2.99	0.03	22.86
Carbon Dioxide	SCF	5	495	20	1.02	2.96	0.01	13.53
i-Butane	SCF	7	544	27	1.03	2.08	0.03	13.70
i-Butane	LIQ	31	105	39	0.76	0.98	0.55	13.70
i-Butane	VAP	4	9	10	0.76	0.98	0.03	0.82
i-Pentane	LIQ	26	199	40	0.61	0.99	0.03	17.80
i-Pentane	SCF	16	264	32	1.00	1.63	0.03	17.80
i-Pentane	VAP	5	9	6	0.70	0.99	0.03	0.03
Methane	SCF	10	416	16	1.05	2.74	0.02	15.18
Methane	LIQ	5	117	23	0.61	0.95	0.43	6.51
Methane	VAP	12	11	18	0.61	0.95	0.02	0.65
Ethane	SCF	8	650	16	1.05	2.46	0.02	14.34
Ethane	LIQ	14	15	31	0.98	0.98	1.00	14.34
Propane	SCF	6	326	13	1.08	2.03	0.02	8.24
Propane	LIQ	24	185	34	0.62	0.98	0.02	8.24
Propane	VAP	4	13	9	0.65	0.98	0.02	0.71
n-Butane	SCF	6	440	21	1.06	2.00	0.03	18.42
n-Butane	LIQ	23	128	34	0.66	0.94	0.53	18.42
n-Butane	VAP	6	8	8	0.66	0.94	0.03	0.53
n-Pentane	LIQ	25	118	35	0.68	0.94	0.59	14.79
n-Pentane	VAP	4	8	12	0.68	0.94	0.03	0.59
n-Pentane	SCF	10	312	22	1.04	1.91	0.03	14.79
n-Hexane	SCF	13	280	26	1.02	1.97	0.03	16.61
n-Hexane	LIQ	28	104	44	0.75	0.98	0.66	16.61
n-Hexane	VAP	9	9	24	0.75	0.98	0.03	0.83
n-Heptane	SCF	11	170	31	1.02	1.15	0.04	18.25
n-Heptane	VAP	7	18	22	0.70	0.99	0.04	0.73
n-Heptane	LIQ	28	184	46	0.63	0.99	0.04	18.25
n-Octane	LIQ	32	160	52	0.60	0.99	0.04	20.08
n-Octane	SCF	10	134	24	1.01	1.18	0.04	20.08
n-Octane	VAP	5	16	21	0.70	0.99	0.04	0.80
i-Octane	LIQ	33	190	56	0.61	0.96	0.04	20.16

[1] The general LJ parameters used are those of Table 4.2. The parameters ε and σ were computed from the experimental critical temperature and pressure, being this the only experimental input information used.

[2] LIQ = liquid, VAP = vapor, SCF = supercritical fluid.

[3] Average absolute-value percent relative deviation

$$= AAD\% = (100/NDP)\sum_{i=1}^{NDP}\left|\eta_{pred} - \eta_{\exp}\right|/\eta_{\exp}$$

[4] Maximum absolute-value percent relative deviation

$$= Max\ AD\% = \max_{i=1}^{NDP}\left\{100\left|\eta_{pred} - \eta_{\exp}\right|/\eta_{\exp}\right\}.$$

NDP = Number of data points. η_{pred} = predicted viscosity. $\eta_{\exp}$ = experimental viscosity.

Table 4.3 results are true predictions, i.e., the model does not use as input any single experimental real-fluid viscosity datapoint or any adjustable parameter obtained from experimental viscosities. The only input experimental information was the critical temperature and the critical pressure, as previously mentioned. An average error of the order of 10 % should be considered low for a true prediction of viscosities in a wide range of conditions. According to such criterion, it can be seen that for simple fluids such as N_2, O_2, F_2, Ar, Kr and Xe the average errors are low.

Average errors are also low for more complex fluids such as Ethylene, Propylene, Carbon Monoxide, Carbon Dioxide, Methane and Ethane. For even more complex compounds errors are often low for vapors and supercritical fluids. For instance for supercritical BromoTriFluoroMethane the average error is only 6 % for 380 points, and for supercritical n-Octane the error is 10 % for 134 points.

For long-shaped molecules, such as *n*-Octane and *n*-Octene, in the liquid-state, the average error is high and often in the order of magnitude around 30 %. In spite of this last figure we conclude, from Table 4.3, that it is promising to use the present approach as a basis for the viscosity modeling of real fluids, due to the low average errors obtained for simple fluids and for relatively complex fluids in supercritical and vapor condition, in a purely predictive way. We stress that, at the stage of development reported here, the model is not intended to be used for quantitative modeling of viscosities of complex real fluids.

The reader should bear in mind that Table 4.3 results are in principle identical to the results that would be obtained from LJ Molecular Dynamics runs, with input values of ε and σ consistent with the pure compound critical *T,P* coordinates.

The differentiation between components with regard to model performance is more evident for the liquid state. From Table 4.3, the average error for liquid viscosity is minimum for Methane, Oxygen, Nitrogen, Ethane and Fluorine, in that order. These are the type of molecules for which the best results are expected by a LJ representation.

Liquid Propylene, n-Heptene and Argon come next with practically the same average error but with a smaller maximum error for Argon. Argon is normally regarded as a LJ-like fluid. The higher error for liquid Argon viscosity with respect to, e.g., liquid Methane, may be due to several reasons. Some of them may be the effect of high-density many body forces which are not accounted for by the LJ intermolecular potential, accuracy differences between both viscosity databases or between the critical coordinates used to set the values of ε and σ, and fortuitous cancellations of errors.

Table 4.3 shows bigger errors for the liquid viscosities of H_2 and Neon. This is not surprising, since H_2 and Neon are quantum fluids for which the classical mechanics approach of Molecular Dynamics breaks down at high enough densities and low enough temperatures (hansen and MacDonald, 1976). Table 4.3 also shows that, roughly, the liquid viscosity error increases with molecular complexity for the aliphatic hydrocarbons.

For comparison purposes, we repeated the calculations corresponding to Table 4.3 using the original Rowley and Painter (1997) values for the constants of equation 6 (Appendix 4A). The results were very similar to those presented in Table 4.3. This is not surprising since, as reported in Appendix 4C, the error with respect to MD LJ viscosities is similar for both sets of constants (Table 4.2 and Table A-I); being their main difference only the way in which equation 7 zero-density viscosity limit is approached (mainly at low temperatures). For the reasons we stated in the first paragraph of section 3 of this chapter, and because of the tight control on the viscous qualitative behaviour associated to Table 4.2, we will use the parameters of Table 4.2 for future developments of the present model.

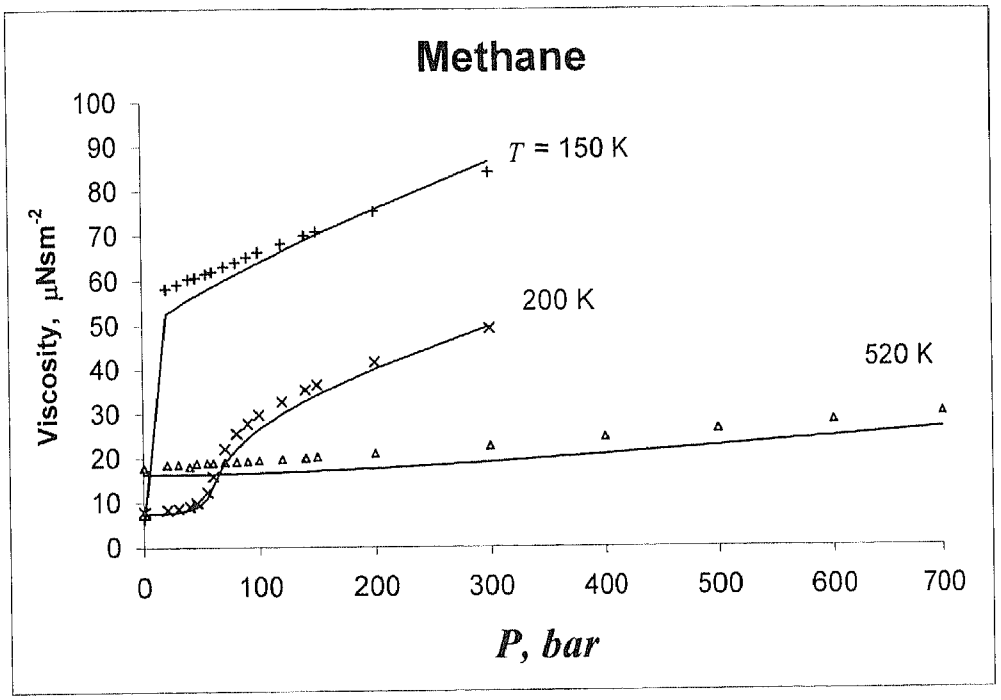

Figure 4.5 - Viscosity versus pressure for Methane for different isotherms. Solid lines: Lennard-Jones model predictions using the parameters of Table 4.2.
Experimental Data (Stephan and Lucas, 1979).

Figure 4.5 illustrates the model performance for Methane, showing predicted and experimental viscosities as a function of pressure, at different temperatures. It can be seen that the predictions match very well the experimental data. The intersection pressure between the 200 K isotherm and the 520 K isotherm is also properly described.

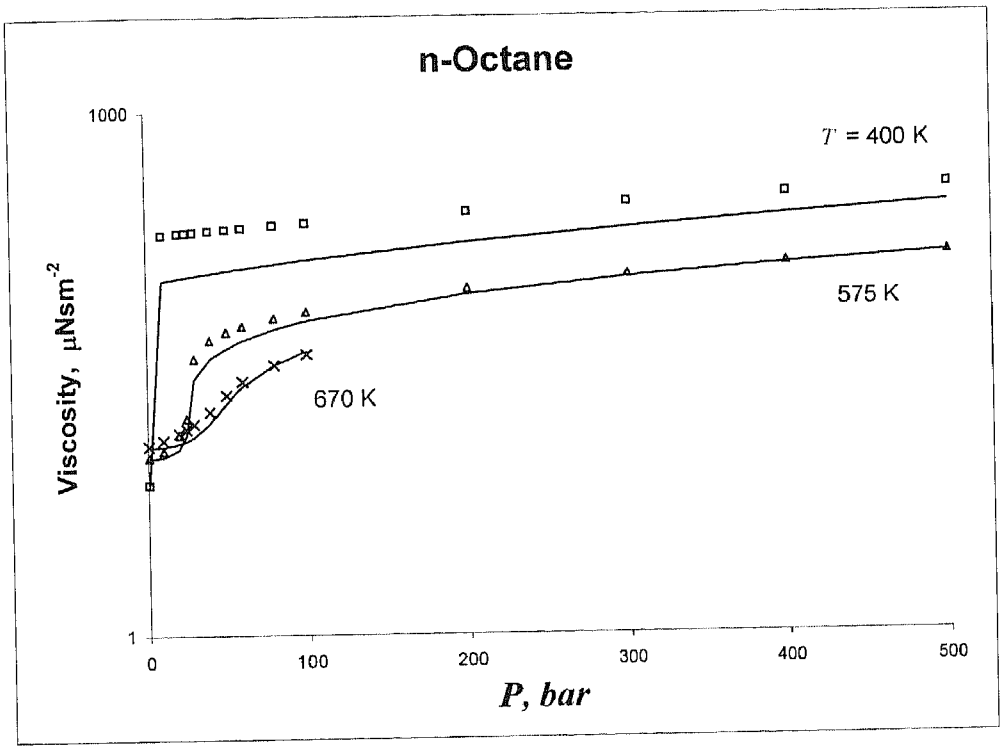

Figure 4.6 - Viscosity versus pressure for n-Octane for different isotherms.
Solid lines: Lennard-Jones model predictions using the parameters of Table 4.2.
Experimental Data (Stephan and Lucas, 1979).

Figure 4.6 shows viscosities as a function of pressure for n-Octane. Here, the model predictions give relatively high errors for the liquid viscosity. In spite of this fact, the model properly follows the experimentally observed qualitative trends keeping track of the order-of-magnitude changes in viscosity. It is worth noting that the pressure and temperature ranges of Figures 4.5 and 4.6 are wide. In spite of the fact that neither Methane nor n-Octane are Lennard-Jones fluids, Figures 4.5 and 4.6 suggest that it would be reasonable to base the modeling of the viscosities of these fluids on the viscosities of the Lennard-Jones fluid, with LJ parameters consistent with the experimental pure-compound critical temperature and critical pressure.

As it is clear from equations 6, 7, 8 and 15 and as it is illustrated by Figures 4.3 and 4.4, the Lennard-Jones fluid is itself a corresponding states fluid. This means, for instance, that two LJ fluids differing in their values of ε and σ will behave according to the curves of Figures 4.3 and 4.4. On the other hand, the calculations leading to

Table 4.3 assumed that real fluids behave as LJ fluids. Therefore, the values of viscosity calculated to generate Table 4.3 match the curves of Figures 4.3 and 4.4.

Hence, Table 4.3 can be seen as the result of the application of a corresponding states model where the reference fluid is the Lennard-Jones fluid. The definition of the model is completed with a specific recipe to compute the values of ε and σ. According to that recipe, the only input information required to calculate viscosities are the critical temperature, critical pressure and molecular weight. From Table 4.3, the present LJ-based corresponding states model has obvious limitations. The work presented in the next chapter will concentrate on removing those limitations.

4.6 CONCLUSIONS

In the present chapter we presented an analytical representation of the relation among pressure, temperature, density and viscosity for the Lennard-Jones (LJ) fluid. We clearly identified its range of applicability and set convenient restrictions for its parameterization.

The resulting qualitative trends, in a wide range of conditions, agreed well with those of real fluids. Predictions for pure compounds were performed. Considering that they used only the experimental critical temperature and pressure as input information, error values, that should be regarded as low, were obtained for compounds such as N_2, O_2, F_2, Ar, Kr, Xe, Ethylene, Propylene, Carbon Monoxide, Carbon Dioxide, Methane and Ethane, in the gaseous and dense states.

For more complex compounds errors were often low for vapors and supercritical fluids. For complex liquids errors were relatively high but the qualitative trends were properly described. The model was used in a truly predictive way, i.e., no adjustable parameters coming from experimental viscosity data were used, and not a single viscosity data point was used as model input. Hence, we conclude that using the viscosity of the Lennard-Jones fluid, in wide ranges of pressure and temperature, as a basis for the viscosity modeling of real fluids, is very promising. In the next chapter,

suitable modifications are introduced to describe better the viscous behaviour of complex fluids.

4.7 REFERENCES

- Agrawal, R., Kofke, D.A., Mol. Phys. 85, 43,1995.
- Bird, R.B., Stewart, W.E. , Lightfoot, E.N., Transport Phenomena, John Wiley & Sons., New York, pp. 16-17, 1960.
- DIPPR 801. Evaluated Process Design Data. Public Release. American Institute of Chemical Engineers. Design Institute for Physical Property Data. BYU-DIPPR. Thermophysical Properties Laboratory. Provo, Utah, 1998
- Fenghour, A., Wakeham, W.A., Vesovic, V., Watson, J.T.R., Millat, J. , Vogel E., J. Phys. Chem. Ref. Data 24, 1649 , 1995.
- Gubbins, K.E., Application of molecular theory to phase equilibrium predictions, In Models for Thermodynamic and Phase Equilibria Calculations (Editor: Stanley I. Sandler, Marcel Dekker, Inc. New York, 1994.
- Haile, J.M., Molecular Dynamics Simulation. Elementary Methods (John Wiley & Sons., New York, 1997.
- Hansen, J.P. , McDonald, I.R., Theory of Simple Liquids, Academic Press, London, p. 1, 1976.
- Hendl, S., Vogel, E., Fluid Phase Equilib. 76, 259, 1992.
- Kolafa, J., Nezbeda, I., Fluid Phase Equilib. 100, 1 ,1994.
- Mecke, M., Müller, A., Winkelmann, J., Vrabec, J., Fischer, J., Span, R. , Wagner, W., Int. J. of Thermophys. 17: 391 1996. Also Erratum 1 in Int. J. of Thermophys. 19, 1493, 1998.
- Murad, S., AIChE J., 32, 513, 1986
- Rowley, R.L, Painter, M.M., Int. J. of Thermophys. 18, 1109, 1997.
- Rowley, R.L, Personal communication, May 19, 1999
- Stephan, K. , Lucas, K., Viscosity of Dense Fluids, Plenum Press, New York and London, 1979
- Sun, T. , Teja, A.S., Ind. Eng. Chem. Res., 37, 3151-3158, 1998
- Takahashi, M., Yokoyama, C. , Takahashi, S., J. Chem. Eng. Data 32, 98 1987.
- Takahashi, M., Shibasaki-Kitakawa, N., Yokoyama, C. andTakahashi, S., J. Chem. Eng. Data 40, 900, 1995.
- Topliss, R.J., Dimitrelis, D. , Prausnitz, J.M., Computers & Chemical Engineering 12, 483, 1988.
- Vesovic, V., Assael, M.J. , Gallis, Z.A., Int. J. of Thermophys. 19, 1297, 1998.
- Vogel, E., Bich, E., Nimz, R., Physica 139 A, 188, 1986.
- Vogel, E. , Hendl, S., Fluid Phase Equilib. 79, 313, 1992.
- Vogel, E., Kuchenmeister, C., Bich, E., Laesecke, A., J. Phys. Chem. Ref. Data 27, 947, 1998.
- Watson, J.T.R., Basu, R.S. , Sengers, J.V., J. Phys. Chem. Ref. Data 9, 1255 1980.
- Younglove, B.A. , Ely, J.F., J. Phys. Chem. Ref. Data 16, 577, 1987.
- Zabaloy, M.S., Vera, J.H., Ind. Eng. Chem. Res. 35, 829, 1996.

4.8 LIST OF SYMBOLS

AAD%	average absolute-value percent relative deviation
B_η	second viscosity virial coefficient
EoS	equation of state
EAR	equivalent analytical relationship
k	Boltzmann constant
LIQ	liquid
LJ	Lennard-Jones
m	molecular mass
Max AD %	maximum absolute-value percent relative deviation
MD	Molecular Dynamics
N	number of molecules
N_A	Avogadro's number
NDP	number of data points
P	absolute pressure
P_c	critical pressure
P_r	practical reduced pressure
P^+_{SFE}	LJ melting P^+
PVT	Pressure-Volume-Temperature
r	intermolecular distance
RP	Rowley and Painter
SCF	supercritical fluid
SFE	solid-fluid equilibrium
T	absolute temperature
T_c	critical temperature
T_r	practical reduced temperature
u	potential energy
V	system volume
VAP	Vapor
VLE	vapor-liquid equilibrium
z	compressibility factor

Greek letters

ε	depth of the LJ potential well
η	(Newtonian shear) viscosity
η_0	viscosity at zero density
η_c	(normal) critical viscosity
$\eta_{\exp}$	experimental viscosity
η_{pred}	predicted viscosity
$\rho^+_{\text{fluid},SFE}$	dimensionless density of the dense LJ fluid in equilibrium with the LJ solid.
ρ	amount-of-substance density (in, e.g., mole cm^{-3} units)
ρ_c	critical amount-of-substance density (in, e.g., mole cm^{-3} units)
σ	LJ separation distance at zero energy

4.9 TABLE OF CONTENTS

4.9.1 List of Tables

4.9.2 List of Figures

APPENDIX 4A: ORIGINAL CONSTANTS FOR EQUATIONS 6 AND 7

The tables in this Appendix contain the constants fitted by Rowley and Painter (1997) for equations 6 and 7.

Table A-I: Constants for equation 6 fitted by Rowley and Painter (1997)

j	i	b_{ji}	j	i	b_{ji}	j	i	b_{ji}	j	l	b_{ji}
1	1	-7.53814	1	2	36.0319	1	3	-47.0432	1	4	19.7791
2	1	66.0342	2	2	-299.373	2	3	430.291	2	4	-191.670
3	1	-220.881	3	2	1067.97	3	3	-1575.25	3	4	725.006
4	1	334.883	4	2	-1638.92	4	3	2445.08	4	4	-1140.09
5	1	-226.756	5	2	1112.30	5	3	-1669.43	5	4	783.084
6	1	52.4394	6	2	-255.199	6	3	380.704	6	4	-176.589

Note: There is a typographical error in the original paper of Rowley and Painter (1997) in which the value of b_{32} appears with two decimal points (10.67.97) . The proper value is b_{32} = 1067.97 (Rowley, 1999).

Table A-II: Constants for equation 7 fitted by Rowley and Painter (1997)

ω_1	ω_2	ω_3	ω_4	ω_5
2.8745	-2.0265	0.9158	-0.1960	0.0160

Note: There is a typographical error in the original paper of Rowley and Painter (1997) in which the value assigned to ω_2 was -2.2065 . The proper value is ω_2 = -2.0265 (Rowley, 1999).

APPENDIX 4B: THE KOLAFA-NEZBEDA LJ-EOS

The PVE/hBH LJ-EoS of Kolafa and Nezbeda (1994) is the following:

$$z = \frac{P^+}{\rho^+ T^+} = f_{KN}\left(\rho^+, T^+\right) \tag{8}$$

where

$$f_{KN}\left(\rho^+, T^+\right) = z_{HS} + z_{VIR} + z_{RES} \tag{B-1}$$

With

$$z_{HS} = \frac{1+\tau+\tau^2-\frac{2}{3}\tau^3(1+\tau)}{(1-\tau)^3} \tag{B-2}$$

$$\tau = \frac{\pi \rho^+ d_{hBH}^3}{6} \tag{B-3}$$

$$d_{hBH} = \sum_i C_{d,i}\left(T^+\right)^{\frac{i}{2}} + C_{d,\ln}\ln\left(T^+\right) \tag{B-4}$$

$$z_{VIR} = \Delta B_{2,hBH}\rho^+\left[1-2\gamma\left(\rho^+\right)^2\right]\exp\left[-\gamma\left(\rho^+\right)^2\right] \tag{B-5}$$

$$\Delta B_{2,hBH} = \sum_i C_{VIR,i}\left(T^+\right)^{\frac{i}{2}} \tag{B-6}$$

$$z_{RES} = \sum_i \sum_j j\, C_{ij}\left(T^+\right)^{\left(\frac{i}{2}-1\right)}\left(\rho^+\right)^j \tag{B-7}$$

The values of the constants for equations B-4 to B-7 are given in Tables B-I and B-II.

Table B-I: Coefficients for equations B-4 to B-6

i	$C_{d,i}$	i	$C_{VIR,i}$
-2	0.011117524	-7	-0.58544978
-1	-0.076383859	-6	0.43102052
0	1.080142248	-5	0.87361369
1	0.000693129	-4	-4.13749995
ln	-0.063920968	-3	2.90616279
		-2	-7.02181962
equation B-5		0	0.02459877
γ	1.92907278		

Table B-II: Coefficients for equation B-7

i	j	C_{ij}	i	j	C_{ij}
0	2	2.01546797	-2	2	29.34470520
0	3	-28.17881636	-2	3	-112.35356937
0	4	28.28313847	-2	4	170.64908980
0	5	-10.42402873	-2	5	-123.06669187
			-2	6	34.42288969
-1	2	-19.58371655	-4	2	-13.37031968
-1	3	75.62340289	-4	3	65.38059570
-1	4	-120.70586598	-4	4	-115.09233113
-1	5	93.92740328	-4	5	88.91973082
-1	6	-27.37737354	-4	6	-25.62099890

APPENXIX 4C: MODIFICATION OF LENNARD-JONES VISCOSITY EARS

Figure C-1 shows two Lennard-Jones supercritical isotherms computed using equation 6 of the text coupled to the original Rowley and Painter (1997) values for the constants (Appendix 4A).

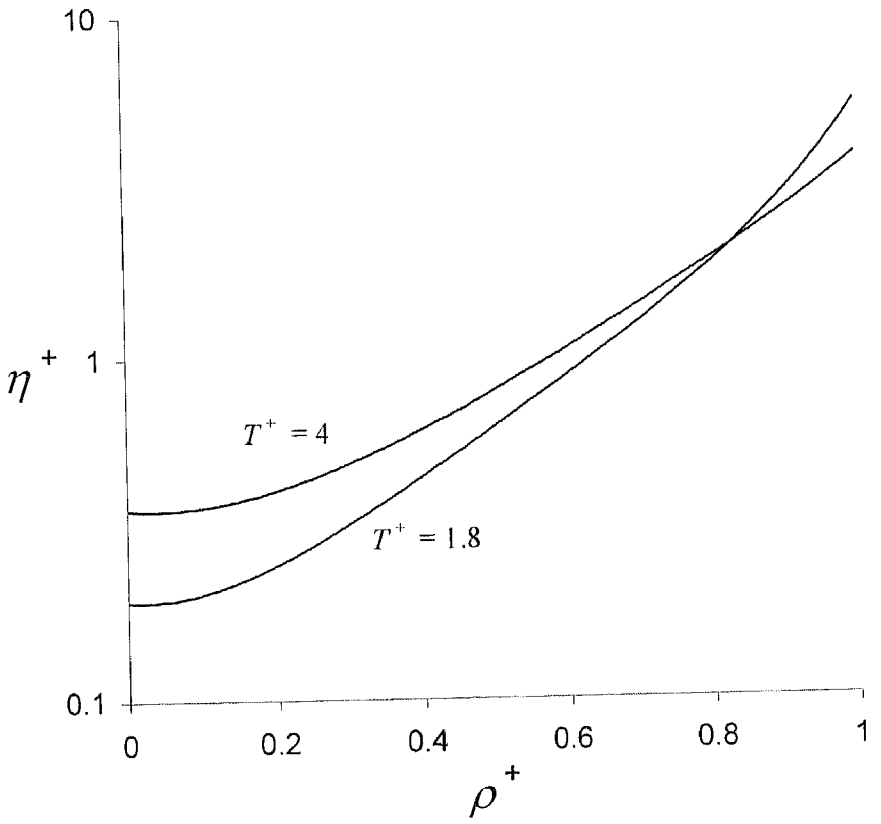

Figure C-1 - Lennard-Jones viscosity η^+ as a function of density ρ^+ for two supercritical isotherms.
The isotherms were computed using equation 6 coupled to the original Rowley and Painter (1997) values for the constants, reported in Appendix 4A

Figure C-1 depicts the following viscous behaviour:

(a) At constant temperature, viscosity increases with density.

(b) At zero density, viscosity increases with temperature. In contrast, at high densities, viscosity decreases with temperature.

(c) At zero-density, viscosity is smaller at T^+=1.8 than at T^+=4. At T^+=1.8, viscosity increases with density faster than at T^+=4. Hence, the isotherms intersect each other at high enough density value.

(d) At constant temperature, the viscosity curves are flat at low density and steeper at high densities, i.e., the slope of η^+ vs. ρ^+, at constant temperature increases with density.

The viscous behaviour of Fig. C-1 is in essential agreement with that of real fluids. However, the previous list of statements is to some extent biased by the scale of Fig. C-1, and by the chosen temperature values.

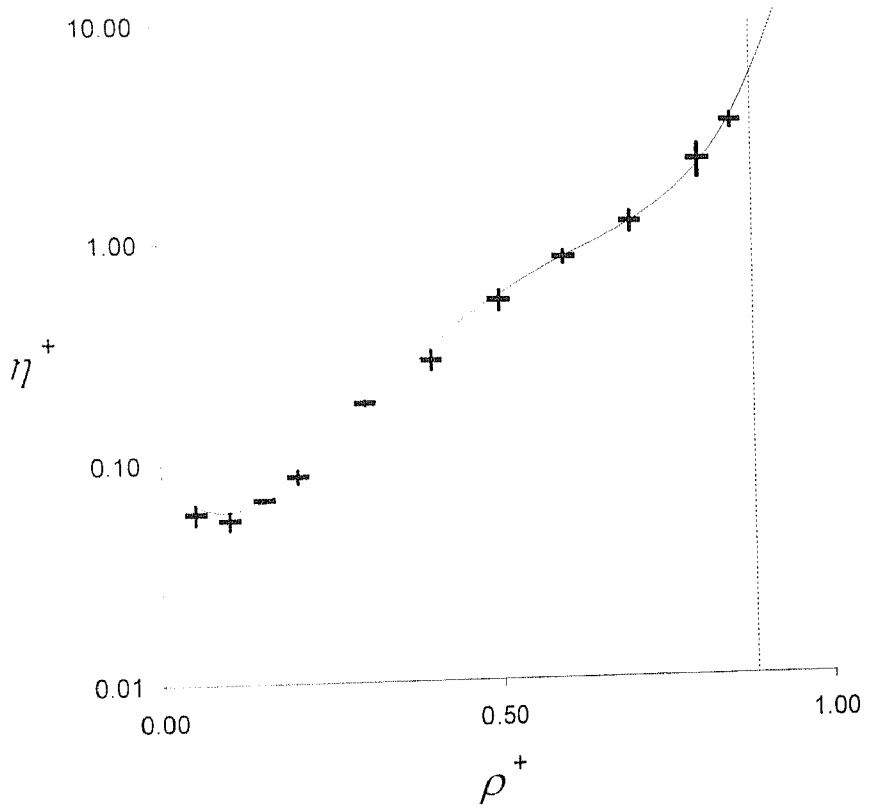

Figure C-2 - Lennard-Jones viscosity η^+ as a function of density ρ^+ at $T^+ = 0.8$.
Solid line: computed using equation 6 coupled to the original Rowley and Painter (1997) values for the constants, reported in Appendix 4A.
Dashed line: Fluid density at solid-fluid equilibrium. + MD RP LJ data (Rowley and Painter, 1997). The height of the plus (+) signs corresponds to the uncertainties reported by Rowley and Painter (1997).

Let us look at a lower temperature isotherm. Figure C-2 shows the original MD RP LJ viscosity data for $T^+ = 0.8$, together with the corresponding η^+ vs. ρ^+ curve computed at $T^+ = 0.8$ using equation 6 with the original constants of Appendix 4A.

It can be observed, for both the data and the curve, that there is a minimum at viscosity in the low-density region. It can also be seen that the zero-density limit is approached with a notably negative η^+ vs. ρ^+ slope. Most of the MD data shown in Fig. C-2 actually fall within the two phase region, and hence they correspond to a metastable Lennard-Jones fluid.

According to Rowley and Painter (1997) *'Simulations were performed in the two-phase region only to provide continuity of states between vapor and liquid densities in anticipation of correlating the data into polynomial equations. Values in the two-phase region have no other significance.'* Hence, the justification for the minimum of Fig. C-2 is weak.

By producing viscosity values in the metastable region the authors probably intended to avoid unphysical oscillations in the polynomial fitting function (equation 6). It should be noted that equation 6 represents the LJ viscosity as a continuous function of density, at any given temperature. This means that within the (subcritical) two-phase region equation 6 provides viscosity values of an hypothetically homogeneous equilibrium LJ fluid or of a metastable homogeneous LJ fluid.

This has clear advantages as discussed by Vesovic *et al.* (1998). In spite of the weak justification for the minimum of Fig. C-2, homogeneous real fluids can have a viscous behaviour qualitatively similar to that presented in Fig. C-2. For real fluids, the viscosity-vs.-density slope at zero density is in general different from zero. It can change sign from positive to negative as the temperature is reduced Fenghour *et al.*, 1995). At subcritical temperatures the sign is usually negative. In such a case "the viscosity along an isotherm should first decrease in the vapor phase and subsequently increase with increasing density." (Vogel *et al.*, 1998). A minimum may or not occur, depending on the location of the two-phase boundary (Vogel *et al.*, 1998).

For a Lennard-Jones fluid having ε and σ independent of temperature, it can be shown, from equation 2 of the text that

$$T^+ = T_r\, T_c^+ \qquad \text{(C-1)}$$

where T_c^+ is a constant [equation 9 of the text] and T_r is the practical reduced temperature, defined as

$$T_r = \frac{T}{T_c} \qquad \text{(C-2)}$$

where T_c is the critical temperature. A chosen value of T_r automatically sets a value for T^+ through equation C-1.

Consider the product $(\rho_c/\eta_0)(\partial\eta/\partial\rho)_0$ where ρ_c is the critical density and where subscript "0 " stands for the zero-density limit. $(\partial\eta/\partial\rho)_0$ is the derivative of viscosity with respect to density at zero density, i.e., the initial slope for the viscosity dependence with respect to density. For a chosen value of T_r , the product $(\rho_c/\eta_0)(\partial\eta/\partial\rho)_0$ can be computed using equations C-1, 6, 7 and 11. The dimensionless product $(\rho_c/\eta_0)(\partial\eta/\partial\rho)_0$ can be calculated with the model without having to specify values for ε and σ .

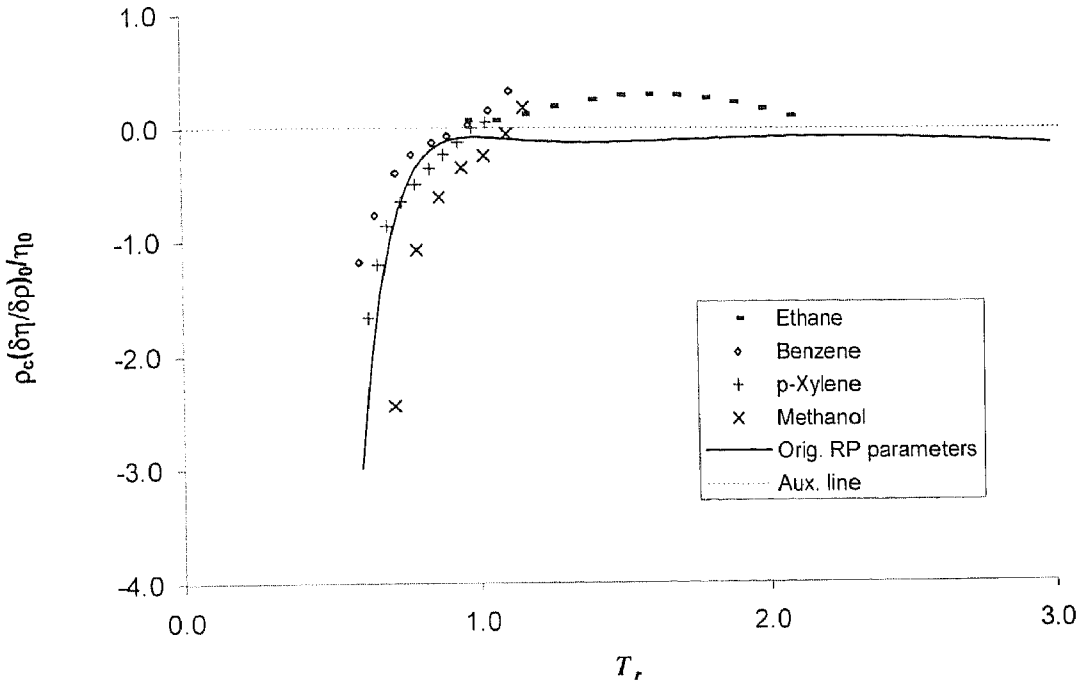

Figure C-3 - Dimensionless zero-density viscosity-vs.-density slope as a function of practical reduced temperature.
Solid line: equation 6 with Appendix 4A constants, at zero density, coupled to equations 7 and 11. Experimental data: Ethane (Hendl and Vogel, 1992), Benzene and Methanol (Vogel *et al.*, 1986), p-Xylene (Hendl and Vogel, 1992). Experimental critical densities were obtained from (DIPPR 801, 1998).

Figure C-3 shows the product $(\rho_c/\eta_0)(\partial\eta/\partial\rho)_0$ as a function of reduced temperature for both, the LJ model corresponding to equation 6 with the original constants of Appendix 4A and for real fluids (experimental values). Figure C-3 shows that the model always gives a negative zero-density viscosity-vs.-density slope throughout the temperature range of equation 6. For reduced temperatures higher than unity the model slope value is very close to zero. For real fluids, it can be seen from Fig. C-3 that the initial slope can be negative or positive depending on the temperature range.

The non-zero viscosity-vs.-density slope observed at zero density for real fluids is a minor effect. For instance, for propane (Vogel *et al.*, 1998) the appearance of low-density minima at subcritical temperatures is at most a 1% effect. This number for some refrigerants is 1.8% (Takahashi *et al.*, 1987; Takahashi *et al.*, 1995), for ammonia 3% (Fenghour *et al.*, 1995), and for water 3 % (Watson *et al.*, 1980).

On the other hand, the minimum in Fig. C-2 corresponds roughly to a 30 % decrease in viscosity with respect to the zero-density value. Such an overestimation of the minimum probably comes from having used MD simulation data corresponding to a metastable Lennard-Jones fluid. Additionally, for real-fluids, the magnitude of the viscosity-vs.-density slope at low densities is in most cases much smaller than the slope values a high density.

As stated in the main text of the present chapter, we foresee the need to set proper extrapolation schemes for computing reference LJ viscosities at conditions falling outside the range of applicability of equations 6 and 8, during the development of the present model. The relatively involved behaviour shown in Fig. C-2 complicates the setting of robust extrapolation schemes. On the other hand, the minimum-viscosity effect is small for real fluids. Hence, we decided to re-fit the parameters of equation 6 forcing the viscosity-vs.-density slope to be zero at zero density and imposing on the general LJ adjustable parameters other restrictions consistent with statements (a) to (d) of the present Appendix.

We screened out from the MD LJ data set used as input for the refitting process the three RP MD LJ viscosity data clearly responsible for the minimum shown in Fig. C-2. The three removed data correspond to T^+ = 0.8 and to the following values of ρ^+: 0.05, 0.1 and 0.15. Note that for the refitting process we considered as valid the η_0^+ values calculated with equation 7.

In the following we present in detail the simplifying restrictions imposed on the refitted parameters of equation 6. The restrictions stem from statements (a) to (d) of the present Appendix, which arose from Fig. C-1.

The flatness of the η^+ vs. ρ^+ curve at $\rho^+ = 0$ corresponds to the following restriction:

$$\left(\frac{\partial \eta^+}{\partial \rho^+}\right)_0 = 0 \qquad \text{(C-3)}$$

where the subscript '0' implies that the partial derivative of equation C-3 is evaluated at zero density. The expression for the slope $\partial\eta^+/\partial\rho^+$ can be readily obtained from equation 6, and from it, it can be shown that equation 15 of the main text guarantees the satisfaction of restriction C-3 is obeyed, at any value of T^+. Equation 15 of the text establishes that the value of parameter b_{11} is determined by the temperature T^+ and by the parameters b_{21} to b_{61}. We used equation 15 in our re-fitting procedure and in all further calculations. Due to equation 15, the number of adjustable parameters is now lower (by one) than the number of parameters of the original Rowley and Painter (1997) fit.

The monotonic increase of viscosity with density at constant temperature, adopted as basic reference behaviour, is expressed by the following restriction:

$$\frac{\partial\eta^+}{\partial\rho^+} > 0 \quad \text{for } \rho^+ > 0 \qquad \text{(C-4)}$$

The increase in the η^+ vs. ρ^+ slope with density is set by the restriction:

$$\frac{\partial\left(\frac{\partial\eta^+}{\partial\rho^+}\right)}{\partial\rho^+} > 0 \qquad \text{for } \rho^+ \geq 0 \qquad \text{(C-5)}$$

The faster increase of viscosity with density that takes place at lower temperatures, implies that at a given density (different from zero) the slope $\partial\eta^+/\partial\rho^+$ has to decrease with temperature, i.e.,

$$\frac{\partial\left(\frac{\partial\eta^+}{\partial\rho^+}\right)}{\partial T^+} < 0 \quad \text{for} \quad \rho^+ > 0 \qquad \text{(C-6)}$$

We used relations 15 and C-4 to C-6 for the refitting of the parameters of equation 6. The objective function was based on the relative errors with respect to the RP MD LJ viscosity data. Rowley and Painter (1997) have not reported any use of restrictions such as C-4 to C-6 for fitting the coefficients of equation 6 of the text (Appendix 4A).

It is worth noting that the temperature dependency of the coefficient b_{11} set by equation 15 has to be taken into account in the computation of the temperature derivative of equation C-6. Note that restriction C-4 is not set at zero density because equation 15 implies a zero slope at zero density. Restriction C-5 has to be met even at zero density. At zero density, restriction C-6 does not apply: since equation 15 implies a zero slope at zero density, and at any temperature, the derivative $\partial\left(\partial\eta^{+}/\partial\rho^{+}\right)/\partial T^{+}$ equals zero at zero density.

Compliance with the previous restrictions ensures the absence of problematic loops in the two-phase region, thus assuring a smooth path from the slowly varying low-density viscosity values to the dramatic viscosity rise in the dense region. This issue has been discussed by Vogel *et al.* (1998). The previous restrictions imply that $\left(\eta^{+}-\eta_{0}^{+}\right)$ vs. ρ^{+} isotherms will all merge at zero density, while at high density, they will be fully stratified.

Table 4.2 in the main text presents the new set of parameters. They produce an average absolute relative deviation of 6.1 % with respect to the RP MD LJ viscosity data (168 accepted points). The bias is -0.77 %. These values are similar to those reported for the original RP parameters (171 points) (Rowley and Painter, 1997).

The parameters of Table 4.2 of the main text are such that restrictions C-4 to C-6 are satisfied at all temperature-density conditions of the MD RP LJ viscosity data. We also tested the absence of violations to restrictions C-4 to C-6 for more than 12 000 regularly spaced points in a section of the temperature-density plane defined by the ranges $0.8 \leq T_{+} \leq 4$ and $0 \leq \rho^{+} \leq 1$.

Equation C-3 sets the low-density viscosity-vs.-density slope to be zero. This is acceptable for our modeling purposes. However, the reader should bear in mind that, in order to get from experimental information the zero-density viscosity η_0, for a real fluid, it is of utmost importance to determine the value of the low-density viscosity-vs.-density slope (Vogel and Nimz, 1986), which is normally different from zero. The real fluid viscosity η_0 is then obtained through extrapolation to the limit of zero density, i.e., η_0 is not an 'experimentally accessible quantity' (Vogel *et al.*, 1998). Forcing the zero-density viscosity-vs.-density slope to be zero, as set by equation C-3, implies that the model will predict a second viscosity virial coefficient B_η (Vogel and Nimz, 1986) equal to zero. This would not be acceptable if the goal was to represent well B_η. Our objectives do not include the description of B_η. A previous work where a zero value of B_η was also set, is that of Younglove and Ely (1987), for the case of propane (Vogel *et al.*, 1998).

The new set of constants (Table 4.2 of the main text) is consistent with the vast majority of the RP LJ viscosity data. With regard to real fluids, such set of constants gives a qualitative behaviour simpler than the observed one. However, it provides a reference viscosity description with well-defined qualitative trends, grasping the essential known viscous behaviour of fluids. In this way the user can keep control on the expected model behaviour. Corrections can potentially be added to this reference model to account for more complex phenomena, such as some real fluid abnormal phenomenological behaviour. For instance, the tabulated values of viscosity for dense water (Watson *et al.*, 1980) show a minimum in viscosity as a function of density, for the metastable liquid at 0° C and at atmospheric pressure.

APPENDIX 4D-CALCULATION PROCEDURES FOR GENERATING FIG. 4.3 AND 4.4

Common block for Figures 4.3 and 4.4

- Set a value of the reduced temperature T_r and a value for the reduced pressure P_r
- Calculate T^+ using equation C-1 and P^+ from equation 17.
- Compute ρ^+ using equation 8.
- Obtain η_0^+ from equation 7 and η^+ from equations 6 and 15 , using the parameters of Table 4.2 of the main text.

For Figure 4.3:

- Calculate the ratio η/η_0 from equation 16.

For Figure 4.4

- Obtain the reduced viscosity η/η_c from equations 19 and 20.

APPENDIX 4E – CALCULATION EXAMPLE - PREDICTING THE VISCOSITY OF OXYGEN AT 100 K AND 10 BAR.

Input data

Compound	Mw in g/mole (Stephan and Lucas, 1979)	T_c in K (Stephan and Lucas, 1979)	P_c in bar (Stephan and Lucas, 1979)	T (K)	P (bar)
Oxygen	31.999	155	50.4	100	10

The values of T_c and P_c are introduced into equations 21 and 22 to compute ε and σ. The resulting values are used in equations 2 and 3, together with the values of T and P to calculate T^+ and P^+.

ε/κ in K	σ (Å)	T^+	P^+
115.71	3.54	0.8642581	0.027877

The value of T^+ is introduced into equation 13 to obtain the dimensionless pressure of solid-fluid equilibrium P^+_{SFE}. At the obtained P^+_{SFE} value equation 8 is solved to compute the density of the dense LJ fluid in equilibrium with the LJ solid $\rho^+_{\text{fluid},SFE}$ at T^+ = 0.8642581. The resulting value is $\rho^+_{\text{fluid},SFE}$ = 0.8966233. Since this number is less than unity it should be taken as the limit of applicability of equation 6 .

The value of ρ^+ is obtained by solving equation 8 used with T^+ = 0.8642581 and P^+ = 0.027877. Two solutions are found, one corresponding to a liquid and the other to a vapor.

$\rho^+_{\text{fluid},SFE}$	Phase A type	ρ^+_A	Phase B type	ρ^+_B
0.8966233	LIQ	0.7727073	VAP	0.0480563

The two density values are smaller than $\rho^{+}_{\text{fluid},SFE}$. Hence, the viscosity can be computed for both of them. The needed zero density viscosity at T^{+} = 0.8642581 is obtained from equation7, and the two viscosity values come from equation 6, used sequentially for the two density values, with the parameters of Table 4.2 of the main text. The dimensionless viscosities are transformed into dimensionful values through equation 5.

η_0^+	η_0 (Nsm^{-2})	η_A^+	η_A (Nsm^{-2})	η_B^+	η_B (Nsm^{-2})
0.0970133	7.1141776	1.9083063	139.9	0.0999625	7.33

The experimental value reported by Stephan and Lucas (1979) is 150.7 Nsm^{-2}. Hence, the LJ model underpredicts this value by 7.2 %.

5. Extrapolation Schemes and Extension to Mixtures

5.1 INTRODUCTION

In the previous chapter, we presented a model, based on Molecular Dynamics (MD), able to accurately compute viscosities for single fluids, in wide ranges of temperature and pressure and with a good predictive capability.

We have also presented the limitations of the model, mainly due to physical constraints (solid-fluid density) and to the range of applicability of MD data used in the original models.

Following the work previously presented, an Extended Lennard-Jonnes equation of State is proposed (EXT-LJ-EoS), along with a complete algorithm for viscosity calculations. A set of extrapolation schemes is also presented, required to overcome range limitations from the previous model, presented in chapter 4. A temperature dependency for the LJ parameters is introduced.
Results for a large database of simple fluids are shown, along with results for mixtures, using mixing rules based on the "One Fluid Approach".

Finally, results for pure compounds, simple mixtures and synthetic petroleum reservoir fluids are presented. A full set of binary interaction parameters K_{ij} is presented, obtained by optimization of a comprehensive 22 binary mixtures database. Finally, model results for a database of mixture viscosities are presented, with good agreement with the experimental data presented. A comparison benchmarking is also done, against a recent alternative methodology (f-theory) proposed in the literature (Quiñones-Cisneros *et al.*, 2000).

5.2 DEVELOPMENT OF THE FINAL MODEL

The current chapter completes the description of the work carried out, aiming to obtain a viscosity model, based on molecular theory (whether Molecular Dynamics or Monte-Carlo). The final model should be capable of depicting the behaviour of this physical property on a wide range of conditions (e.g. temperature, pressure, density) for any kind of phase type, such as saturated and subcooled liquids, saturated and superheated vapors and supercritical fluids, applicable to pure compounds or complex mixtures (Machado *et al.*, 2001).

It should be kept in mind that the main motivation for the research was the unavailability of a unified model, capable of "handling" such a diversified range of physical situations, as can be encountered in petroleum reservoir conditions.

The reasons for choosing a model based on molecular theory lay on the good qualitative behaviour of this technique (based on the microscopic behaviour of fluids). The choice of the Model-Fluid was the next step in our research. Due to its simplicity, but yet good qualitative behaviour, the Lennard-Jones (LJ) fluid was selected. Another reason for selecting LJ was the fact that it is a well known fluid, with a large availability of published simulation data.

5.3 THE LJ VISCOSITY MODEL

The work carried out was based on the model of Rowley and Painter (RP) (1997). This EAR is a viscosity EoS. It correlates high-quality MD simulation data and has good mathematical behaviour (continuous function and first derivatives).

The basic equations of the LJ-EoS for our model are presented in chapter 4, equations 1 to 7.

As can be seen from equations 6 and 7 of chapter 4, RP-EoS gives the viscosity value, when inputting density and temperature.

$$\eta_0^+ = f_{RP}(T^+, \rho^+) \qquad (1)$$

Nevertheless, the usual engineering purpose is to obtain viscosity, at given conditions of temperature and pressure.

Therefore, we coupled the RP-EoS with a suitable EAR, also based on MD, capable of yielding density as a function of temperature and pressure. The choice, due to its quality and relative easy of manipulation was the Kolafa-Nezbeda EoS (Kolafa and Nezbeda, 1994; Machado *et al.*, 2001).

$$\rho^+ = f_{KN}(T^+, P^+) \qquad (2)$$

For our engineering purposes, we devised a direct calculation method, similar to the one applied by Soave (1986), in order to be able to use pressure as an input parameter in the final model (Machado *et al.*, 2001).

The final coupled viscosity EoS a combined function able to calculate viscosity as function of pressure and temperature:

$$\eta^+ = F(T^+, P^+) \qquad (3)$$

5.4 THE MODEL PARAMETERS

In the proposed model, each compound is characterized by its "LJ parameters" ε and σ. A LJ model fluid is based on a concept of "soft spheres", with a potential field characterized by these parameters. This approach consists on determining an "equivalent sphere" for each compound, characterized by their set of ε and σ parameters. As a first approach (presented in chapter 4), the compound parameters were calculated based on their critical pressure and temperature (Zabaloy *et al.*, 2001).

The application of these "critical" LJ parameters to the model yielded predictive viscosity results with an average error of 10%, for a large viscosity database (Zabaloy *et al.*, 2001). For "sphere-like" compounds such as N_2, O_2, F_2, Ar, Kr and Xe, average errors for the data sub-set are lower, while for more complex-shaped molecules (e.g. compounds with less LJ-like geometry) average errors increased as molecule geometry distanced from the spherical shape.

To cope with the "non-Lennard-Jonnescity" nature of complex-shaped molecules, namely long chain alkanes abundant in petroleum reservoir fluids, the solution adopted was to make the model parameters temperature dependent.
In the present work, we opted for a linear dependency with temperature.

From equation «Tdef» and 3 of the previous chapter, the following equations can be derived:

$$T^+/T_c^+ = T_r/\alpha_\varepsilon \qquad (4) \qquad T_r = T/T_c \qquad (5) \qquad \alpha_\varepsilon = \varepsilon/\varepsilon_c \qquad (6)$$

$$P^+/P_c^+ = P_r/\alpha_\varepsilon \qquad (7) \qquad P_r = P/P_c \qquad (8)$$

where α_ε and α_σ were made linearly dependent with temperature.

$$\alpha_\varepsilon = m_\varepsilon\left(\frac{T}{T_C}-1\right)+1 \quad (9) \qquad \alpha_\sigma = m_\sigma\left(\frac{T}{T_C}-1\right)+1 \quad (10)$$

In addition, and to cope with the sub-estimation of the critical value by the LJ fluid - the critical point in the LJ fluid is lower than the "natural" critical point – a correction factor F was introduced as a "shifting factor", able to correct the critical point displacement.

$$\eta^+ = \frac{\eta_0^+ \sigma^2}{F\sqrt{\varepsilon}} \quad (11)$$

5.5 RESULTS FOR PURE COMPOUNDS

As above-mentioned, the LJ parameters ε and σ were made temperature-dependent in order to compensate for the molecular geometry deviation from the LJ model. Results for alkanes are presented in Table 5.1 using equations 9 and 10 and F optimized using equation 11.

The slopes m_ε and m_σ , as well as the shifting factor F, were then obtained by optimization using a 6441 experimental points database, including 39 pure compounds, kindly provided by DTU .

A full table with slope values for equations 9,10 and F values referred to equation 11 is given in Appendix 5 - Table A1, obtained for 39 typical petroleum reservoir pure compounds.

As can be observed, the relative errors are higher for long chain alkanes, increasing with the chain length. Deviations are quite acceptable for the temperature dependency proposed.

Table 5.1 - Lennard-Jones based representation of n-alkane viscosities with ε and σ depending linearly on temperature and F shifting factor optimized.

Temperature and pressure limits of the dataset are also presented. (Database: DTU recommended viscosity data for n-alkanes – 6441exp. points).

Compound	T_r^{min}	T_r^{max}	P_r^{min}	P_r^{max}	AAD% in Viscosity	Max AD%	NDP
Ethylene	1.13	2.48	1.00	15.87	2.6	13	255
Propylene	0.88	1.78	0.99	19.29	3.7	32	442
1-Hexene	0.63	0.74	1.59	14.33	2.8	11	63
1-Heptene	0.60	0.91	1.77	17.67	3.7	16	143
1-Octene	0.56	0.86	1.95	19.47	4.3	23	143
Methylcyclohexane	0.56	0.93	1.44	28.77	2.3	10	165
Ethylcyclohexane	0.53	0.87	1.65	16.50	2.9	16	156
Cyclohexane	0.58	0.94	1.47	12.28	4.1	19	194
iso-Pentane	0.70	1.63	1.48	17.75	5.0	21	250
2,2-Dimethylpropane (Neopentane)	0.72	1.02	1.72	17.23	1.0	4	36
Nitrogen	2.54	3.57	1.47	29.41	0.8	2	120
Hydrogen Sulfide	1.04	1.11	1.12	5.58	3.3	21	33
Carbon Dioxide	1.05	2.96	0.68	13.54	1.0	7	390
iso-Butane	0.78	2.08	1.37	13.71	5.9	22	273
Methane	1.68	2.73	1.20	15.22	1.1	7	165
Ethane	1.05	2.29	1.00	14.37	1.6	6	170
Propane	0.87	2.03	1.18	8.24	2.2	11	198
n-Butane	0.75	1.88	1.32	18.44	4.7	24	222
n-Pentane	0.68	1.81	1.48	14.84	3.9	25	208
n-Hexane	0.64	1.97	1.65	16.75	5.3	35	194
n-Heptane	0.59	1.15	1.82	36.50	6.0	34	210
n-Octane	0.56	1.18	2.01	20.08	5.9	20	126
n-Nonane	0.54	0.79	2.62	21.83	2.7	11	214
n-Decane	0.50	0.83	2.61	26.13	3.1	12	105
Undecane	0.50	0.81	3.05	25.44	2.0	11	144
n-Dodecane	0.49	0.79	3.29	27.41	1.9	9	144
n-C14	0.45	0.54	12.34	61.68	4.4	13	20
n-C15	0.44	0.53	13.16	65.79	6.4	25	20
n-C16	0.44	0.52	14.10	70.49	8.5	35	20
n-C18	0.42	0.50	16.59	82.93	11.1	32	18
Benzene	0.57	0.98	1.00	8.17	2.1	8	185
Toluene	0.54	0.93	1.46	9.74	2.6	10	187
Ethylbenzene	0.52	0.91	1.66	11.09	3.3	14	143
Butylbenzene	0.47	0.57	6.93	34.63	2.5	9	20
Naphthalene	0.50	0.61	8.47	25.01	3.1	11	17
1-Methylnaphthalene	0.39	0.44	5.61	28.04	13.6	30	15
Isooctane	0.59	0.99	1.95	39.05	3.4	13	164
Phenanthrene	0.45	0.66	9.40	27.77	3.3	13	14
Water	0.48	1.50	0.27	3.63	11.5	39	855

As can be observed from Table 5.1, the correlation capability of the model, using the set of parameters, is good in most cases and very good for most compounds.
The importance of a good representation of the individual pure component viscosity lay not only in the results for the pure compounds itself, but mostly on the approach used to model mixtures, when accurate individual pure compound contributions are critical for the accurate representation of the mixture viscosity.

The results for selected compounds of Table 5.1, using a best-worst selection criteria, are presented in Figures 5.1 to 5.7, where viscosity vs. pressure isotherms calculated by the model are plotted against the experimental points.

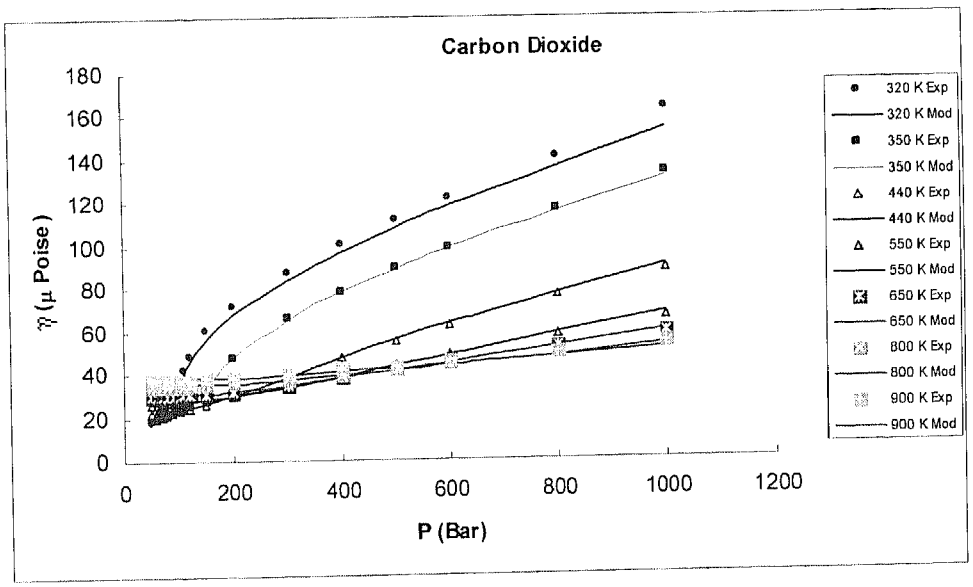

Figure 5.1 – Viscosity - Pressure diagram for Carbon Dioxide for different isotherms.
Solid lines: Lennard-Jones model predictions using the linear temperature dependent parameters and F shifting factor.
Experimental Data (Stephan and Lucas, 1979).

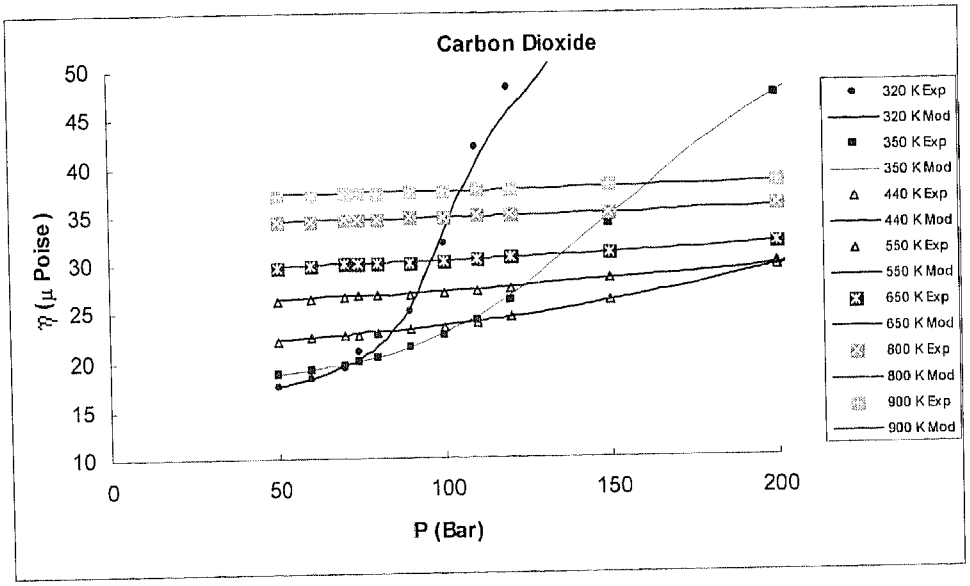

Figure 5.2 – Viscosity - Pressure diagram for Carbon Dioxide for different isotherms. Zoom at the "crossing isotherms" region of the Pressure domain of Figure 5.1

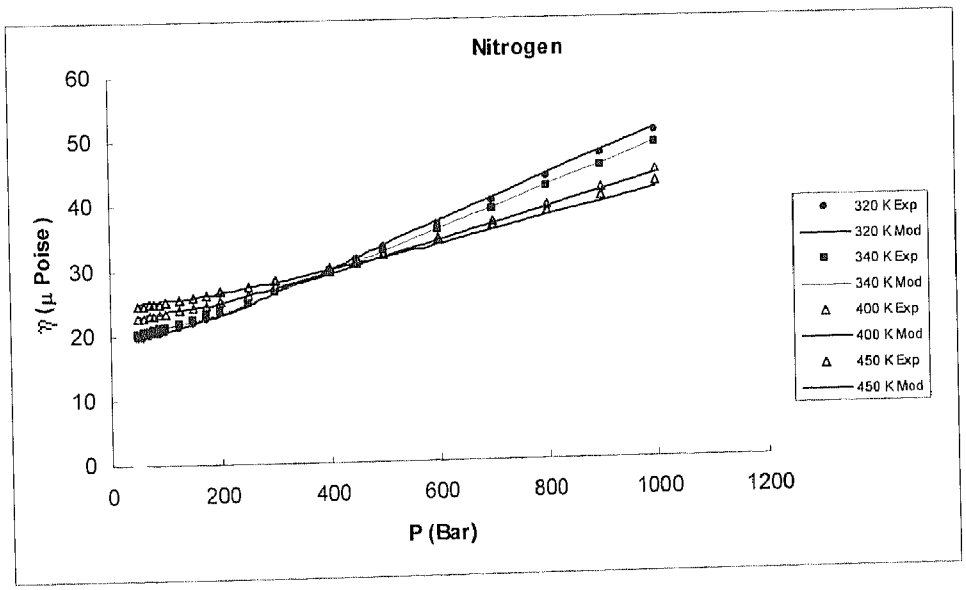

Figure 5.3 – Viscosity - Pressure diagram for Nitrogen for different isotherms. Solid lines: Lennard-Jones model predictions using the linear temperature dependent parameters and F shifting factor.

Experimental Data (Stephan and Lucas, 1979).

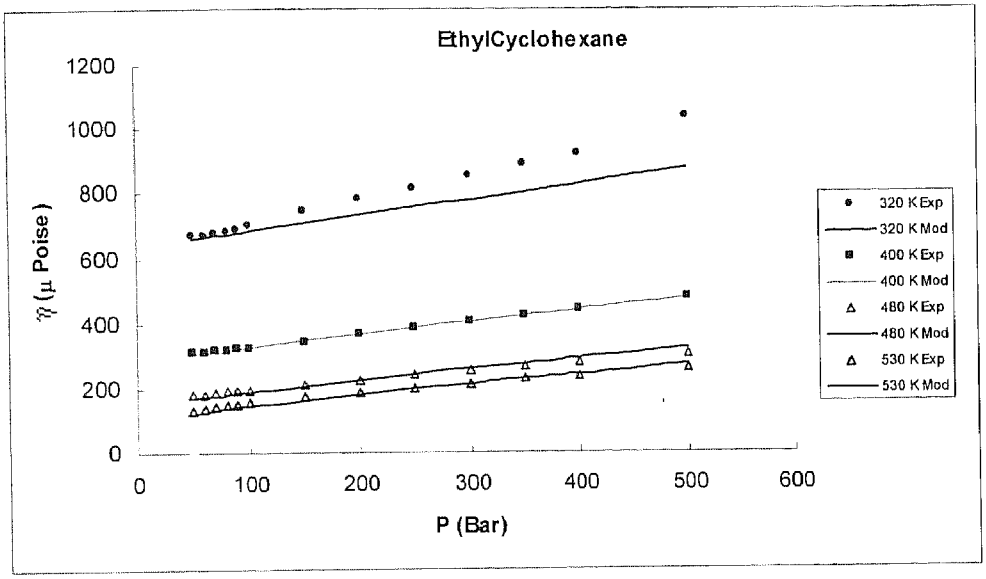

Figure 5.4 – Viscosity - Pressure diagram for Ethylcyclohexane for different isotherms.

Solid lines: Lennard-Jones model predictions using the linear temperature dependent parameters and F shifting factor. Experimental Data (Stephan and Lucas, 1979).

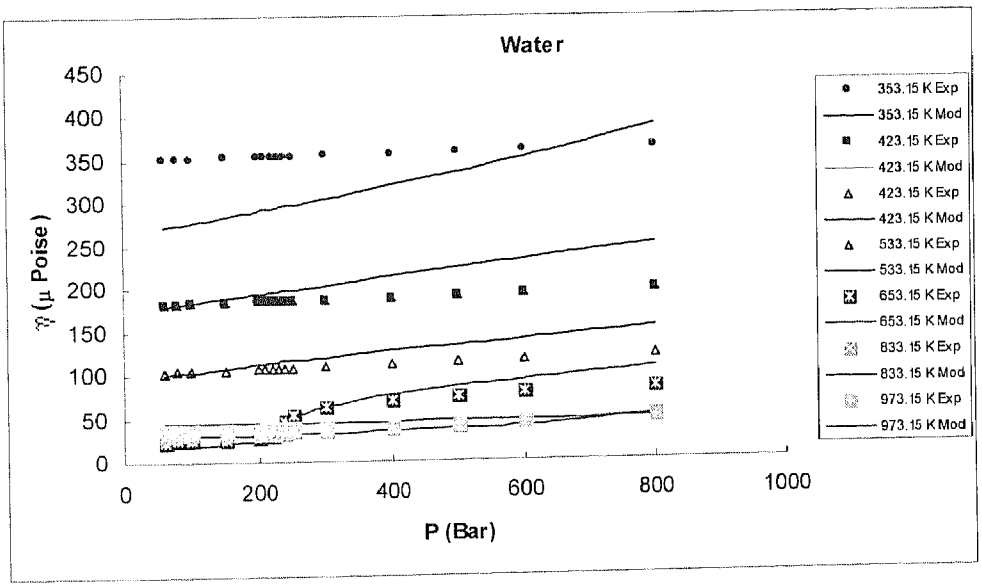

Figure 5.5 - Viscosity - Pressure diagram for water for different isotherms.
Solid lines: Lennard-Jones model predictions using the linear temperature dependent parameters and F shifting factor. Experimental Data (DTU Viscosity Database).

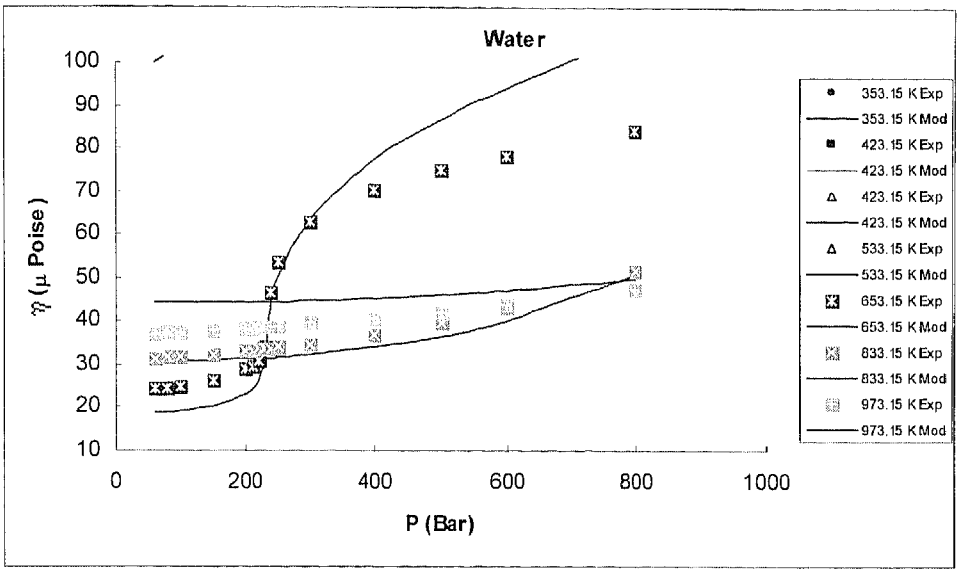

Figure 5.6 – Viscosity - Pressure diagram for Water for different isotherms.
Zoom at the "crossing isotherms" region of the pressure domain of Figure 5.5.

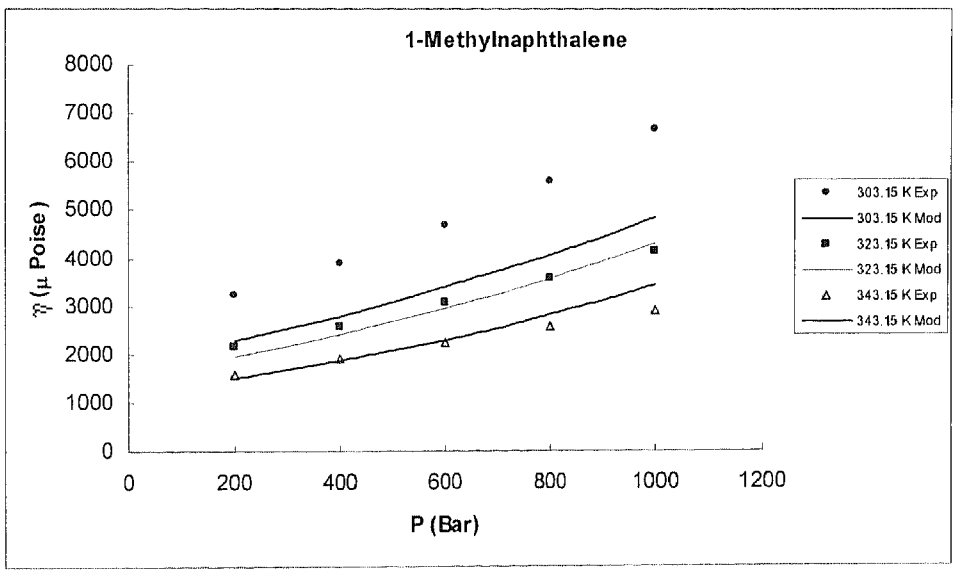

Figure 5.7 – Viscosity - Pressure diagram for 1-Methylnaphthalene for different isotherms. Experimental Data (Baylaucq *et al., 1997).*

Results for the 39 pure compounds, in the form of Average Absolute Deviations (AAD%) for the mentioned database are presented in Table 5.1 and shown in Figures 5.1 to 5.7.

As it can be observed from the above mentioned Table and Figures, AAD% values are generally quite below 10%, even for the longer chain alkanes. Compounds with spherical molecule geometry (like N_2) present AAD% values below 2%. It should be noted that only three adjustable parameters were used for each compound.

The main objective behind using good quality data for parameter fitting and attaining a good match with pure compound viscosity values is the application of the present model to mixtures. This issue will be further addressed in this work.

5.6 EXTRAPOLATION SCHEMES

A clear disadvantage of the original EAR's (RP and KN) was the relatively "limited" range of application (Table 5.2) , with regard to temperature and density, for the use on petroleum reservoir fluids at High Temperature-High Pressure (HP-HT) conditions. The reasons for this limitation does not lie on each EoS by itself, but on the LJ as model fluid.

The limits on the original RP and KN models are as follows:

Table 5.2 - Limits of applicability of original models

	RP (Rowley and Painter, 1997)	KN (Kolafa and Nezbeda, 1994)
T^+	$1 < T^+ < 4$	$0.68 < T^+ < 10$
ρ^+	$0 < \rho^+ < \rho^+_{\text{fluid},SFE}$	$0 < \rho^+ < \rho^+_{\text{fluid},SFE}$

The main "limitation" was the fact that the (engineering) LJ reduced temperature at the triple point $T_{r,LJ,tp}$ is higher than those found for real fluids (Machado *et al.*, 2001). Another important drawback was the LJ solid-fluid equilibrium (SFE) density $\rho^+_{\text{fluid},SFE}$, according to Agrawal and Kofke (1995), as the original RP Model would only allow for computations up to the SFE line.

An illustration of the undesirable results of using EAR's outside their ranges of applicability is presented by Machado *et al.* (2001).

5.6.1 Extrapolation for viscosity EoS in temperature

For the viscosity EoS, extrapolation on temperature is based on the principle of constant residual viscosity, e.g., the residual η^+ is considered to be independent of T^+ as long as the density used at the reference T^+_{ref} is properly transformed.
η^+_0 in the Chapman-Enskog zero density limit according to Reid *et al.* (1987).

$$\eta^+ - \eta^+_0\Big|_{\substack{T \\ \rho^+}} = \eta^+ - \eta^+_0\Big|_{\substack{T_{ref} \\ \rho^+ = \rho^+ \cdot K(T^+)}} \qquad (12)$$

T^+_{ref} can be one of the original limits of KN (T^+_{ref} =1 for T^+<1 or T^+_{ref} =4 for T^+>4).

The multiplying factor, K(T^+), was made proportional to T^+ for T^+>4, and was calculated by adjusting LJ MD data of Heyes (1988) at T^+ = 6 and T^+ = 10.
For T^+<1, a function form was determined using LJ MD data of RP at T^+ = 0.8 and a few data points from Heyes (1988) (only the data having ρ^+ less than the fluid ρ^+ at SFE were used) at T^+= 0.72.

$$T^+ > 4 \qquad K(T) = 1 + \alpha_\rho \left(T^+ - T_{Ref}{}^+\right) \qquad (13)$$

$$T^+ < 1 \qquad K(T) = 1 + \frac{\sum_{i=1}^{3} A_i (T^+ - 1)^i}{1 + \sum_{j=1}^{4} B_j (T^+ - 1)^j} \qquad (14)$$

The parameters for equations 13 and 14 are presented in Table 5.3

Table 5.3 – K(T^+) factor parameters for equations 13 and 14

α_ρ	7.500x10^{-3}	B_1	6.793241
A_1	-0.123796	B_2	15.034009
A_2	-0.767150	B_3	12.093522
A_3	-1.227422	B_4	5.374925

5.6.2 Extrapolation for viscosity EoS in density

For density extrapolations ($\rho^+ > \rho^+_{fluid,SFE}$), the solution proposed is to use a quadratic function, based on the first and second partial derivatives of the viscosity EAR (equation 3) with respect to density, with parameters estimated using the viscosity evaluated at the SFE density (Agrawal and Kofke, 1988).

$$\eta^+ = a\rho^{+2} + b\rho^+ + c \tag{15.0}$$

$$a = \frac{1}{2}\frac{\partial^2 \eta^+}{\partial \rho^{+2}}\bigg|_{\rho^+_{SFE}} \tag{15.1}$$

$$b = \frac{\partial \eta^+}{\partial \rho^+}\bigg|_{\rho^+_{SFE}} - 2a\rho^+_{SFE} \tag{15.2}$$

$$c = \eta_{SFE}{}^+ - a\rho^+_{SFE}{}^2 - b\rho^+_{SFE} \tag{15.3}$$

As a validity procedure and for sake of comparison, a different pure component database was compiled, including most of the pure compounds for which results are presented in Table 5.1. The data was compiled based on the open literature, and, when possible from sources different from the ones used for the optimization of the parameters. Results are presented in Table 5.4.

It should be pointed out that for the results presented, no model parameter optimization was performed using the presented set of data. The temperature dependency coefficients and shifting factor for the pure compounds used on equation 9, 10 and 11 are presented in Table A1 of Appendix A5.

Table 5.4 - Lennard-Jones based representation of n-alkane viscosities with ε and σ linearly dependent on temperature.

Reduced temperature and reduced pressure limits of the dataset are also presented. (DTU recommended Viscosity Data).

Compound	T_r^{min}	T_r^{max}	P_r^{min}	P_r^{max}	AAD% in Viscosity	Max AD%	NDP
1-Heptene	0.56	0.91	0.036	18.14	5.03	26.09	200
1-Hexene	0.56	0.74	0.033	14.71	6.33	18.90	149
1-Octene	0.53	0.86	0.040	19.99	4.94	30.69	202
Carbon-Dioxide	1.02	2.96	0.014	13.91	1.23	12.23	495
Ethane	0.98	2.46	0.021	14.75	2.02	15.63	665
Ethylene	1.06	2.48	0.020	16.30	2.90	13.14	420
i-Butane	0.76	2.08	0.028	14.07	8.36	30.30	658
i-Octane	0.53	0.99	0.040	20.02	5.55	34.62	258
i-Pentane	0.61	1.63	0.030	18.22	5.65	36.41	476
Methane	0.52	2.73	0.022	15.63	8.31	51.61	590
n-Butane	0.66	2.00	0.027	18.93	4.48	33.95	576
n-Heptane	0.56	1.15	0.037	18.73	7.43	45.54	408
n-Hexane	0.75	1.97	0.034	16.97	5.32	20.65	393
Nitrogen	0.52	7.13	0.030	30.20	3.05	89.96	1046
n-Octane	0.56	1.18	0.041	20.62	8.48	54.36	328
n-Pentane	0.68	1.92	0.030	15.23	4.28	24.79	438
Propane	0.47	2.03	0.024	8.46	15.34	95.71	632
Propylene	0.79	1.78	0.022	19.81	4.33	31.64	575

From Table 5.4, the good prediction capability of the model in wide ranges of temperature and pressure, well beyond the parameter optimization range, can be observed.

As an example of the "wideness" of the dataset conditions, one can focus on Nitrogen, where pressure varies from 0.030 to 30 times its critical pressure. Again, no parameter optimization was done over the dataset.

The graphic representation for some of the compounds is presented below, again in a "best-worst" selection criteria.

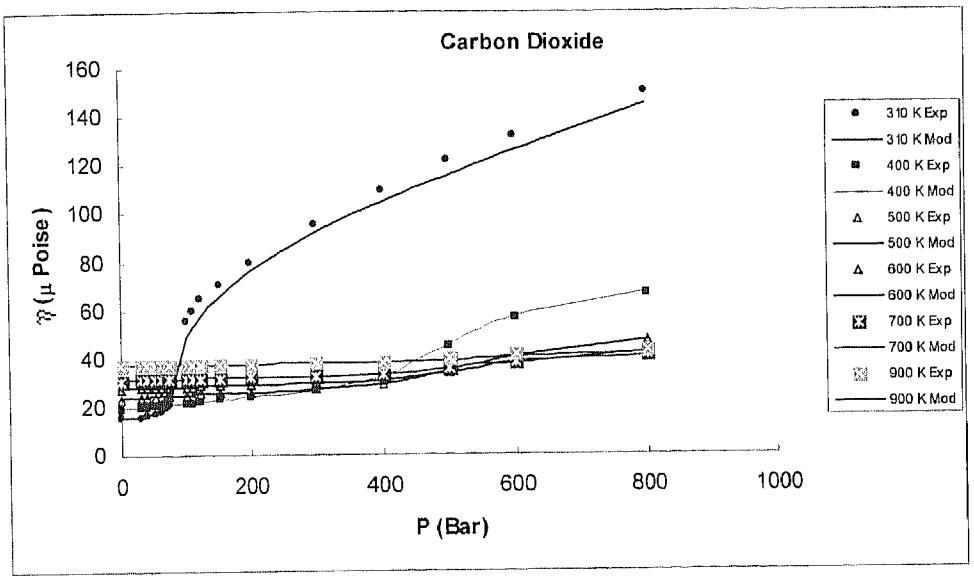

Figure 5.8 - Viscosity - Pressure diagram for Carbon Dioxide for different isotherms.

Solid lines: Lennard-Jones model predictions using the linear temperature dependent parameters and F shifting factor.Experimental Data: DTU Recommended viscosity database

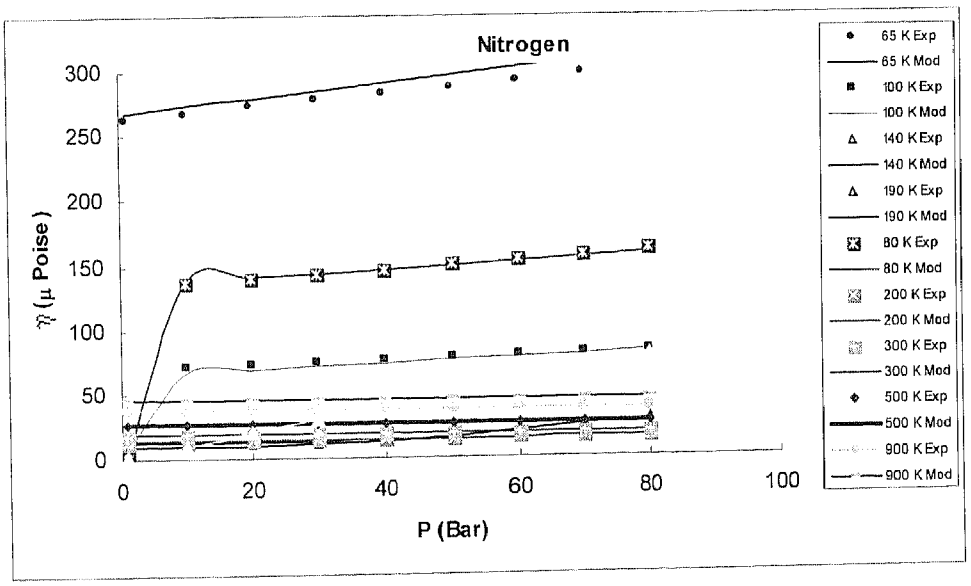

Figure 5.9 – Viscosity - Pressure diagram for Nitrogen for different isotherms.

Solid lines: Lennard-Jones model predictions using the linear temperature dependent and F shifting factor parameters. Experimental Data: DTU Recommended viscosity database

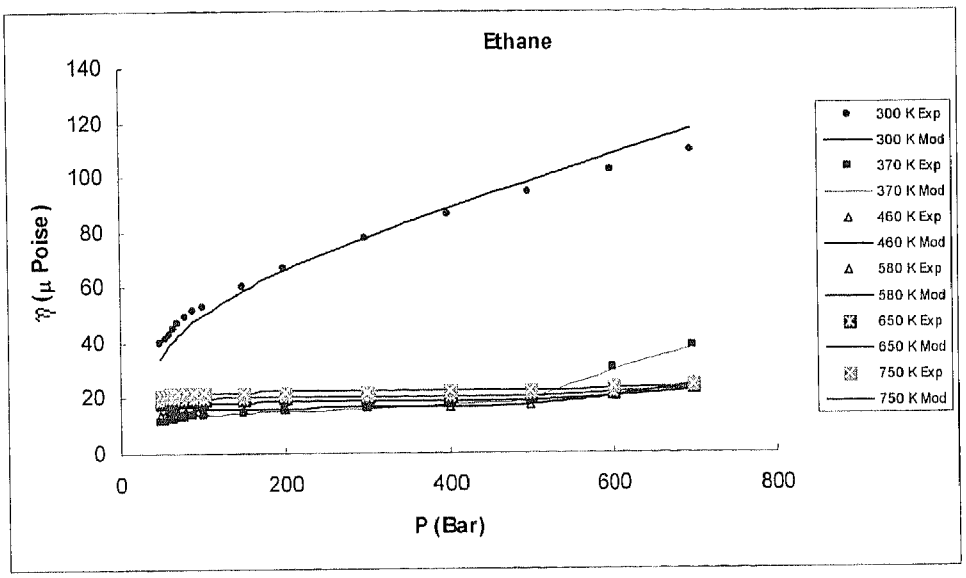

Figure 5.10 – Viscosity - Pressure diagram for Ethane for different isotherms.

Solid lines: Lennard-Jones model predictions using the linear temperature dependent parameters and F shifting factor. Experimental Data: DTU Recommended viscosity database

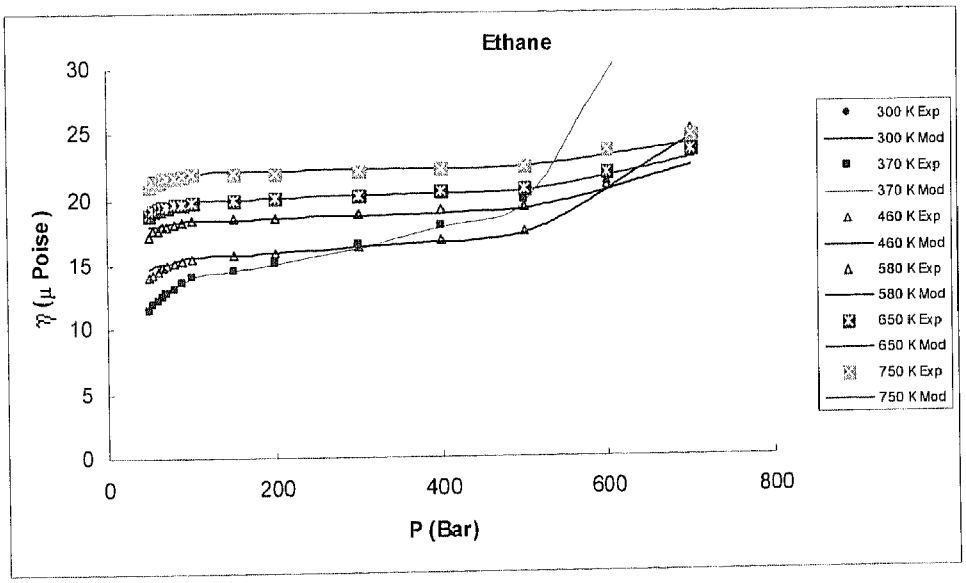

Figure 5.11– Detail of the gas phase on Figure 5.10.

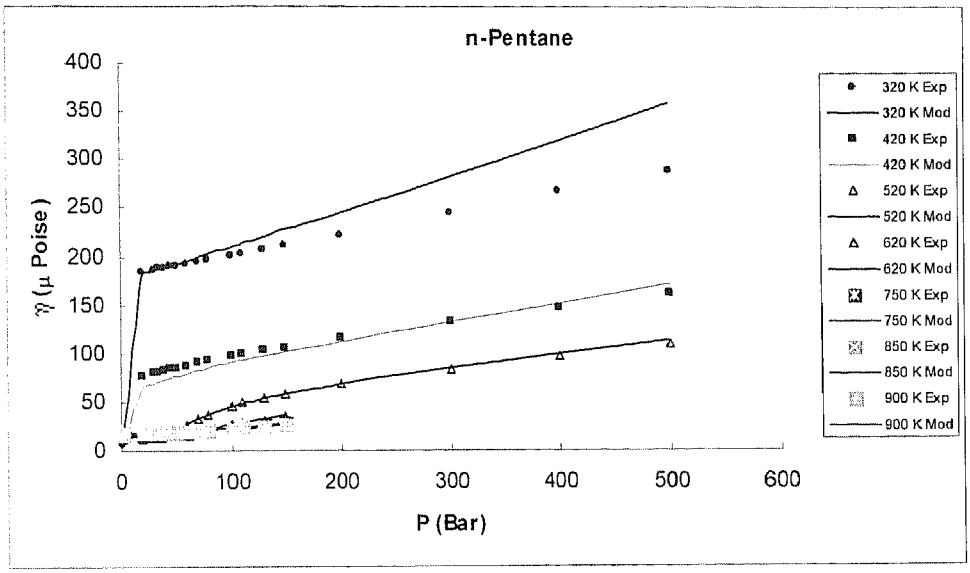

Figure 5.12 – Viscosity - Pressure diagram for n-Pentane for different isotherms.
Solid lines: Lennard-Jones model predictions using the linear temperature dependent parameters and F shifting factor. Experimental Data: DTU Recommended viscosity database

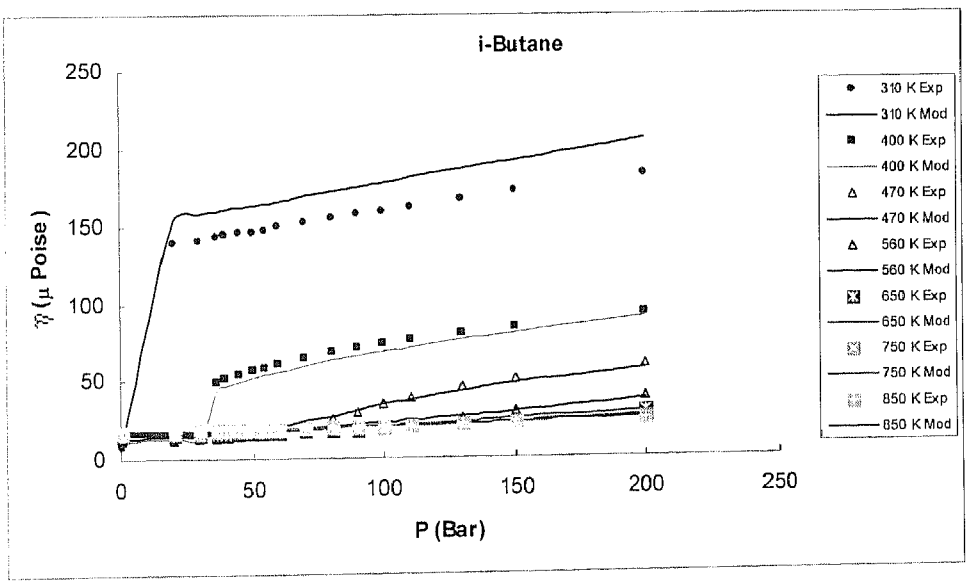

Figure 5.13 – Viscosity - Pressure diagram for iso-Butane for different isotherms.
Solid lines: Lennard-Jones model predictions using the linear temperature dependent parameters and F shifting factor. Experimental Data: DTU Recommended viscosity database

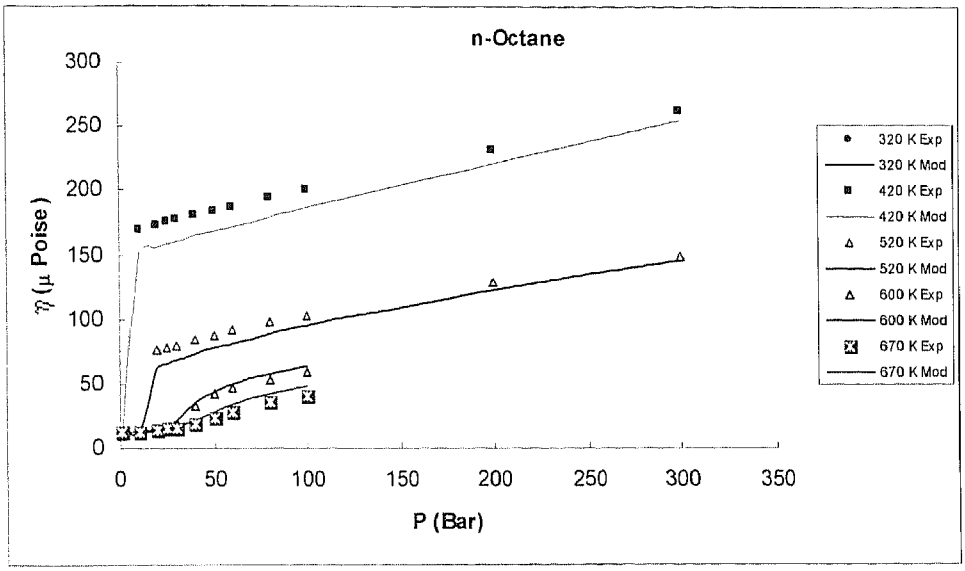

Figure 5.14 – Viscosity - Pressure diagram for n-Octane for different isotherms.
Solid lines: Lennard-Jones model predictions using the linear temperature dependent parameters and F shifting factor. Experimental Data: DTU Recommended viscosity database

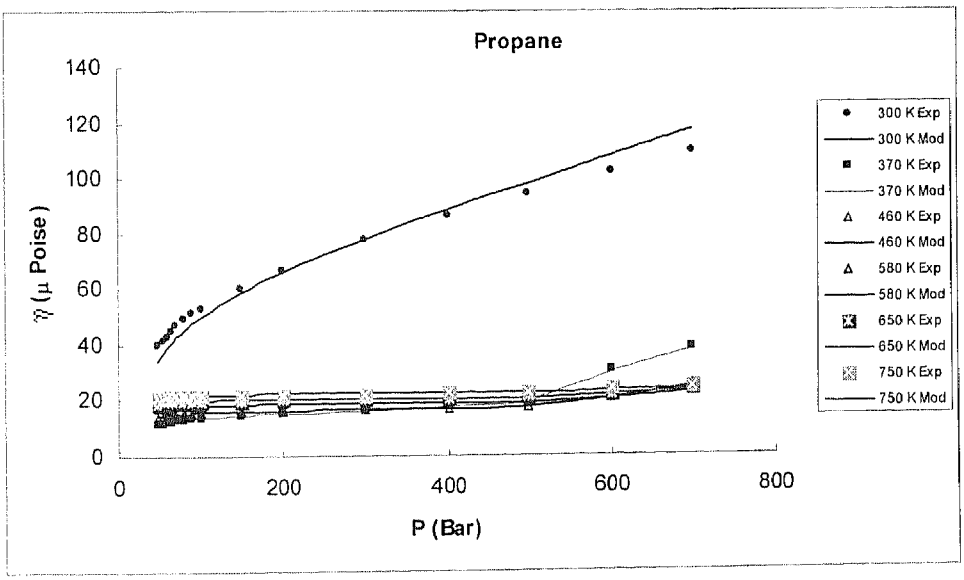

Figure 5.15 – Viscosity - Pressure diagram for Propane for different isotherms.
Solid lines: Lennard-Jones model predictions using the linear temperature dependent parameters and F shifting factor. Experimental Data: DTU Recommended viscosity database

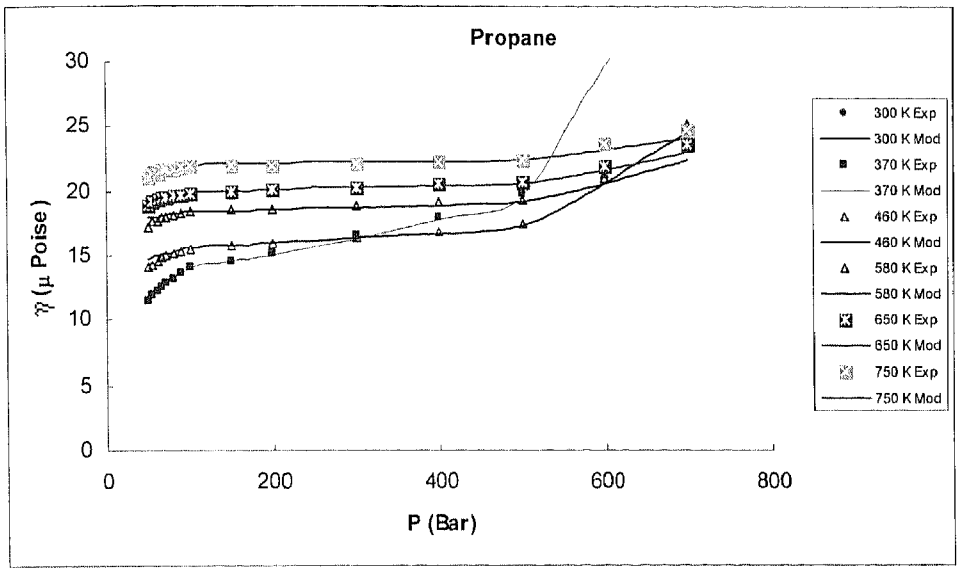

Figure 5.16 – Zoom on Figure 5.15

Solid lines: Lennard-Jones model predictions using the linear temperature dependent parameters. Experimental Data: DTU Recommended viscosity database

From the results shown in Table 5.4 and in Figures 5.8 to 5.16, the extrapolation schemes coupled with the model proposed in this work for viscosity yield good results, in a very wide range of PVρ conditions, enabling the calculation of viscosity values quite far from the initial Rowley and Painter model. The schemes proposed do not seem to affect neither the "physical" behaviour of viscosity, nor the absolute value of the property itself, for the vast majority of the pure compounds present in the database.

If for most of the compounds the AAD% is quite acceptable, some maxAD% values are quite high. We believe that this fact can have two possible explanations: from the model side, deviations from the "LJ-like" shape, i.e., non-sphericity of the compound molecule – as in the case of i-Butane and n-Pentane. Another possible explanation for these deviations is eventual errors in the experimental data. This can be the case of Nitrogen or Propane.

Nevertheless, the model depicts both qualitative and quantitative the viscosity behaviour of the pure compounds, and we decided to move forward into the development of an extension of the model to mixtures.

5.7 EXTENSION OF THE MODEL TO MIXTURES

The next step on our work is to devise an extension of this model to mixtures, in order to cope with the original goal of the project – the calculation of viscosity values in deep-offshore petroleum reservoir conditions.

The temperature dependence and shifting factor solution, using the parameters obtained by optimization (Table A1) are now applied to the mixtures using the One Fluid Approach (Wei and Sadus, 2000).This solution consists in admitting that the mixture is composed of only one type of "pseudo-component", being its LJ parameters determined by the weighted average of the individual components parameters. We tested several solutions for the "weighting" method. The simpler method is to consider either the mole fraction or the mass fraction. Nevertheless, Zéberg-Mikkelsen *et al.*, (2000), proposed the use of an alternative concentration definition, where the exponent factor **p** is allowed to vary between 0 and 1 (equation 16).

$$z_i = \frac{x_i M_i^p}{\sum_{m=1}^{NC} x_m M_m^p} \qquad (16)$$

The p factor allows for the correction of molecular weight asymmetry and takes into account other molecular forces that may affect the linear nature of the mole/mass fractions. This factor can also serve as adjustable parameter for optimization, although it was made constant in the present work.

In equation 16, x_i is the mole fraction and M_i is the molecular weight of component *i*. *NC* is the number of components in the mixture and p is the exponent factor that transforms mole fractions into z_i fractions.

As can be easily observed, mole fraction and mass fraction are two particular cases of equation 16 for p equal to 0 and p equal to 1, respectively.

We applied this methodology to the model for mixtures, defining:

$$z_{\varepsilon,i} = \frac{x_i M_i^{p_\varepsilon}}{\sum_{m=1}^{NC} x_m M_m^{p_\varepsilon}} \quad (17.a)$$

$$z_{\sigma,i} = \frac{x_i M_i^{p_\sigma}}{\sum_{m=1}^{NC} x_m M_m^{p_\sigma}} \quad (17.b)$$

$$z_{F,i} = \frac{x_i M_i^{p_F}}{\sum_{m=1}^{NC} x_m M_m^{p_F}} \quad (17.c)$$

Exponents p_σ, p_ε and p_F are universal but do not need to be equal to each other. Nevertheless, the conclusion was, after trying a wide variety of combinations, that they should be kept equal.

To adopt the One Fluid Approach, a mixing rule has to be used in order to define the mixture fluid parameters.
We applied a quadratic mixing rule as it makes possible to have one adjustable parameter per binary for a given mixture variable, as opposite to linear mixing rules which do not have the possibility of any interaction parameter. This option was made due to the high-quality viscosity database available, containing a large number of binary mixtures datapoints, kindly provided by DTU, partner of the Evident project.

The mixture parameters are defined as according to:

$$\sigma^3 = \sum_{k=1}^{NC}\sum_{n=1}^{NC} z_{\sigma,k} z_{\sigma,n} \sigma_{kn}^3 \quad (18)$$

$$\varepsilon = \sum_{k=1}^{NC}\sum_{n=1}^{NC} z_{\varepsilon,k} z_{\varepsilon,n} \varepsilon_{kn} \quad (19)$$

$$F = \sum_{k=1}^{NC}\sum_{n=1}^{NC} z_{F,k} z_{F,n} F_{kn} \quad (20)$$

The binary combining rules applied are:

$$\sigma_{ij} = \left(\frac{\sigma_i + \sigma_j}{2}\right)\left(1 - k_{\sigma,ij}\right) \quad (21)$$

$$\varepsilon_{ij} = \left(\varepsilon_i\, \varepsilon_j\right)^{1/2}\left(1 - k_{\varepsilon,ij}\right) \quad (22)$$

$$F_{ij} = \left(F_i F_j\right)^{1/2}\left(1 - k_{F,ij}\right) \quad (23)$$

Some restrictions were imposed during the optimization of the interaction parameters:

1. For a pure compound i=j=m and $k_{\sigma,mm} = k_{\varepsilon,mm} = k_{F,mm} = 0$
2. Symmetry $k_{\sigma,ml} = k_{\sigma,lm} < 1$ $k_{\varepsilon,ml} = k_{\varepsilon,lm} < 1$ $k_{F,ml} = k_{F,lm} < 1$

After a few trial calculations with the binary viscosity database, we came to the conclusion that the best results were achieved using exponent factors p_ε ,p_σ and p_F all equal to 0.5.

The interaction parameters were then obtained by optimization using the above-rmentioned database. (k_{ij} values are presented in Appendix 5A – Table A2)

Finally, we compiled a high quality database of viscosity data for mixtures, evaluated in extensive ranges of temperature and pressure. The database includes 3474 datapoints distributed by 22 different mixtures, ranging from binaries to quinary mixtures.

The model was then applied to the mixtures compiled in the database. The overall AAD% was 6.4%, with a maximum value of 25%. Results are presented in Tables 5.5 and 5.6

Table 5.5 – LJ Viscosity EoS applied to mixtures - Database statistics and results.

System Type	AAD%	NDP	N. of systems
Binaries	6.36	3041	28
Ternaries	4.73	393	3
Quaternaries	6.40	32	3
Quinary	10.22	8	1

Table 5.6 – LJ Viscosity EoS applied to mixtures.(Results are expressed in AAD%)

Mixture	AAD%	NDP
Cyclohexane/n-Hexadecane	8.91	70
Ethane/Carbon Dioxide	5.85	94
Ethylbenzene/Ethylene	8.13	65
Isooctane/Ethylene	5.03	73
Methane/Benzene	2.02	102
Methane/Carbon Dioxide	1.39	132
Methane/Cyclohexane	4.68	57
Methane/Ethane	5.29	103
Methane/n-Buthane	7.19	120
Methane/n-Decane	8.81	664
Methane/n-Hexane	13.02	53
Methane/Propane	5.59	282
Methylcyclohexane/1-Methylnaphthalene	4.84	126
n-Decane/Carbon Dioxide	3.70	70
n-Decane/n-Hexadecane	4.85	54
n-Dodecane/Cyclohexane	9.22	93
n-Heptane/1-Methylnaphthalene	4.17	126
n-Heptane/Methylcyclohexane	3.35	126
n-Heptane/n-Decane	1.59	12
n-Heptane/n-Nonane	2.06	57
n-Heptane/n-Undecane	1.32	57
n-Hexane/Benzene	3.45	60
n-Hexane/Cyclohexane	25.07	74
n-Hexane/n-Heptane	1.44	53
n-Hexane/Toluene	20.31	111
n-Octane/Cyclohexane	9.96	112
n-Pentane/n-Decane	1.40	5
Toluene/1-Methylnapthalene	5.35	90
n-Butane/n-Hexane/n-Decane	5.08	5
n-Pentane/n-Decane/Carbon Dioxide	4.22	10
n-Heptane/Methylcyclohexane/1-Methylnaphthalene	4.88	378
n-Butane/n-Hexane/n-Decane/Carbon Dioxide	7.85	10
n-Pentane/n-Hexane/n-Heptane/n-Decane	6.28	4
n-Decane/n-Dodecane/n-C14/n-C16	5.06	18
n-Pentane/n-Hexane/n-Heptane/n-Decane/Carbon Dioxide	10.22	8

Viscosity-pressure and viscosity-temperature diagrams are presented in Figures 5.17 to 5.21 for most representative systems. For the binaries, best-worst systems were selected, while best cases are presented for higher-order mixtures.

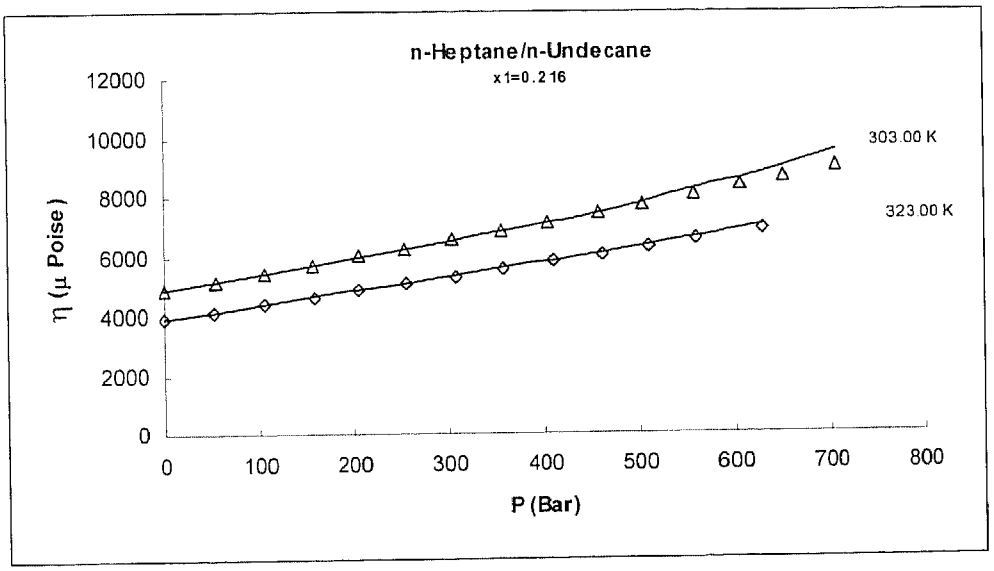

Figure 5.17 - Viscosity – Pressure diagram for n-Heptane/n-Undecane.
Data: Assael *et al.* (1991)

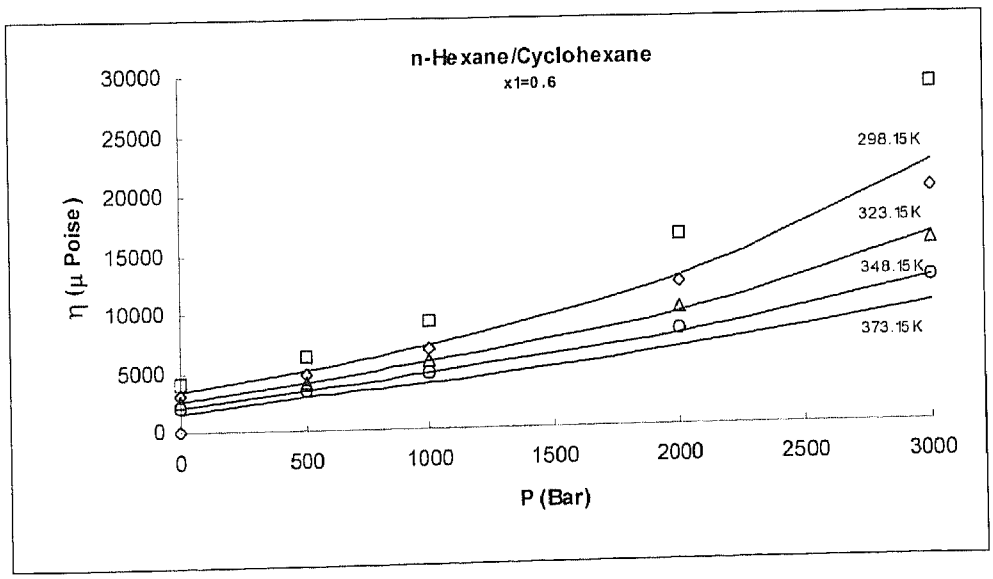

Figure 5.18 – Viscosity – Pressure diagram for n-Hexane/Cyclohexane ("worst case")
Data: Tanaka *et al.* (1991)

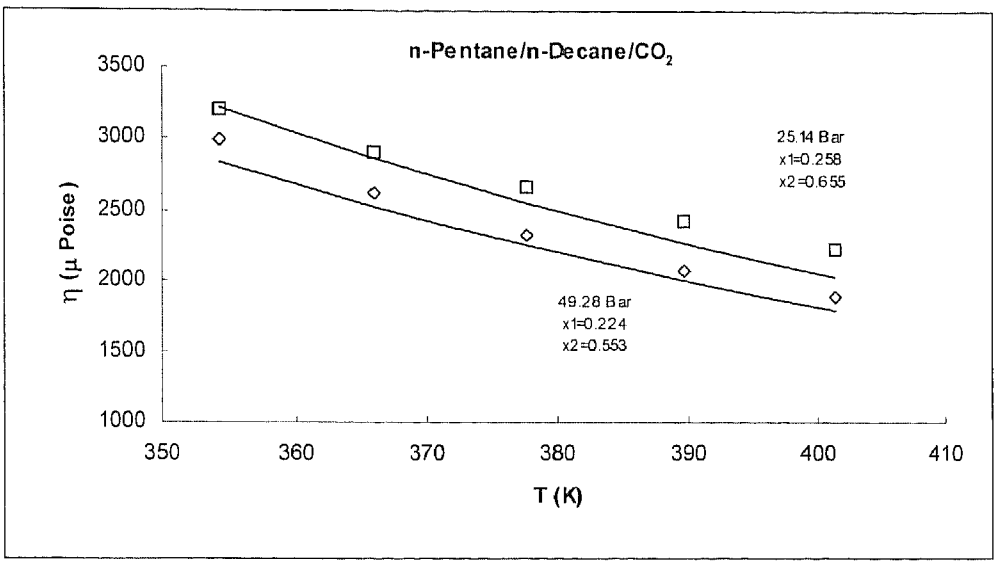

Figure 5.19 – Viscosity – Temperature diagram for n-Pentane/n-Decane/CO_2
Data: Barrufet *et al.* (1996)

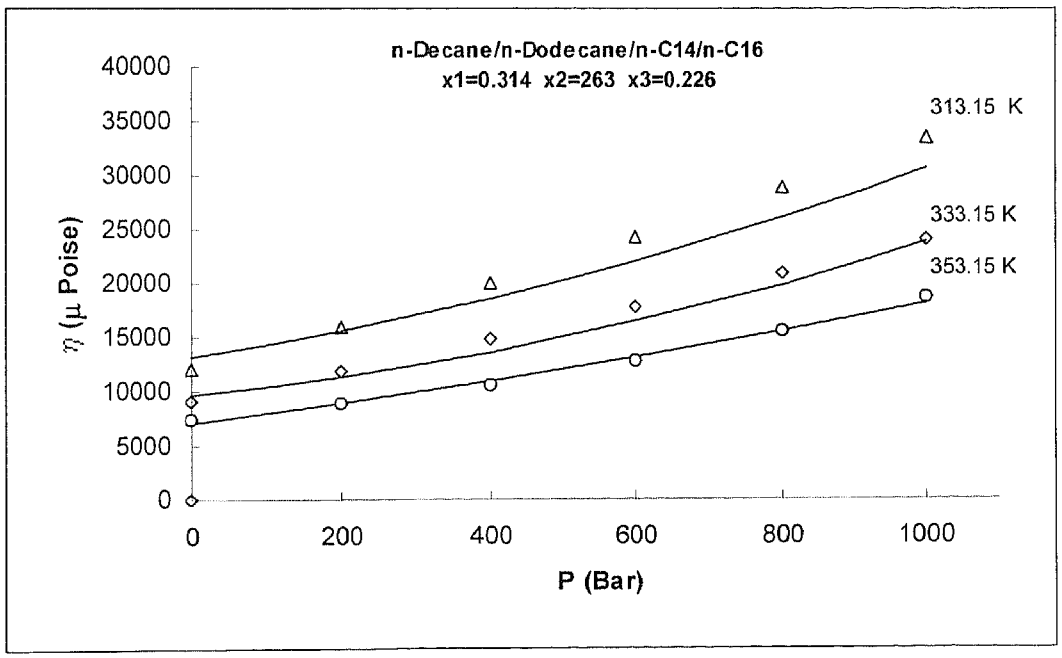

Figure 5.20 – Viscosity – Pressure diagram for the system n-Decane/nC12 / nC14 / nC16.
Data: Ducuolombier *et al.* (1986)

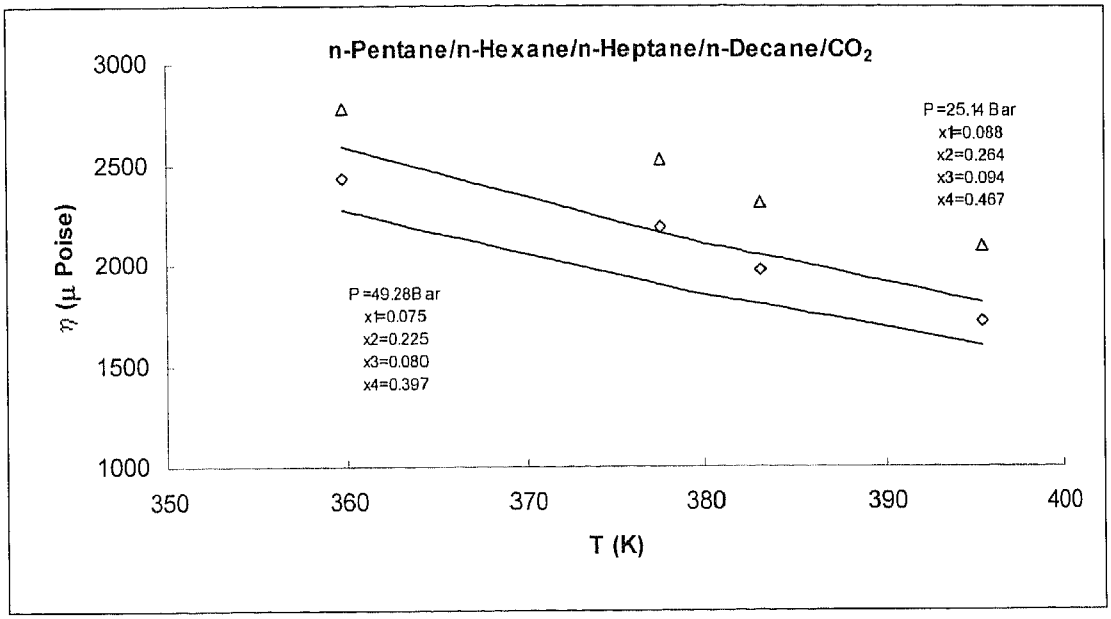

Figure 5. 21– Viscosity – Temperature diagram for n-Pentane/n-Hexane/n-Heptane/n-Decane/CO_2

Data: Barrufet et *al.*(1996)

5.7.1 Application to synthetic reservoir mixtures

As a "final test" for the model, and due the availability of high-quality data on multi-component mixtures, provided by the partner of the EVIDENT project responsible for the experimental viscosity measurements, it was to possible test the model against high quality data on synthetic mixtures simulating real reservoir fluids. The data were kindly provided by ELF (today TOTAL-FINA-ELF) and Harriot-Watt University (HWU). Data from "ELF" were measured using the "falling plug" method, while HWU data was obtained using the capillary tube method. Fluid compositions are presented in Table 5.7, while results of application of the model and database statistics are given in Table 5.8.

Table 5.7 - Composition of synthetic mixtures, expressed in mole %.

Compound	ELF 3-A*	ELF 3-B*	ELF 3-C*	GEC-001**
Ethane	6.43	8.66	8.96	8.79
Propane	2.84	4.51	4.87	4.72
n-Butane	1.11	2.04	2.17	2.07
n-Pentane	0.57	1.08	1.17	1.01
n-Hexane	1.31	2.35	2.47	1.37
n-Heptane	1.42	2.48	2.52	1.64
n-Octane	1.20	2.11	2.04	1.89
n-Nonane	0.81	1.46	1.33	1.50
i-Butane	0.67	1.00	1.06	1.07
i-Pentane	0.64	1.04	1.11	0.94
Methane	74.71	63.68	62.69	63.43
n-Decane	0.70	1.38	1.21	1.07
n-C16	2.28	5.04	5.21	2.49
Carbon Dioxide	3.15	2.47	2.39	2.48
Nitrogen	2.18	0.70	0.80	2.66
Hydrogen Sulfide	0.00	0.00	0.00	0.00
n-Undecane	0.00	0.00	0.00	0.78
n-Dodecane	0.00	0.00	0.00	0.64
n-C14	0.00	0.00	0.00	0.47
n-C15	0.00	0.00	0.00	0.39

* Elf, 2000

** Bell *et al*, 2000

Table 5.8 - LJ Viscosity EoS applied to synthetic mixtures. Database limits are presented, along with results expressed in AAD%

Mixture	T_{min} (K)	T_{max} (K)	P_{min} (bar)	P_{max} (bar)	AAD%	Max AD%	NDP
ELF3A	410.85	469.15	549.11	1200	7.08	18.11	20
ELF3B	410.85	455.15	544.93	1200	17.67	27.69	20
ELF3C	410.85	460.15	544.93	1200	18.00	33.93	20
GCE00-1	323.15	423.15	345.90	1380	9.76	14.67	20

Results for the synthetic mixtures in graphic form are presented in Figures 5.22 to 5.25.

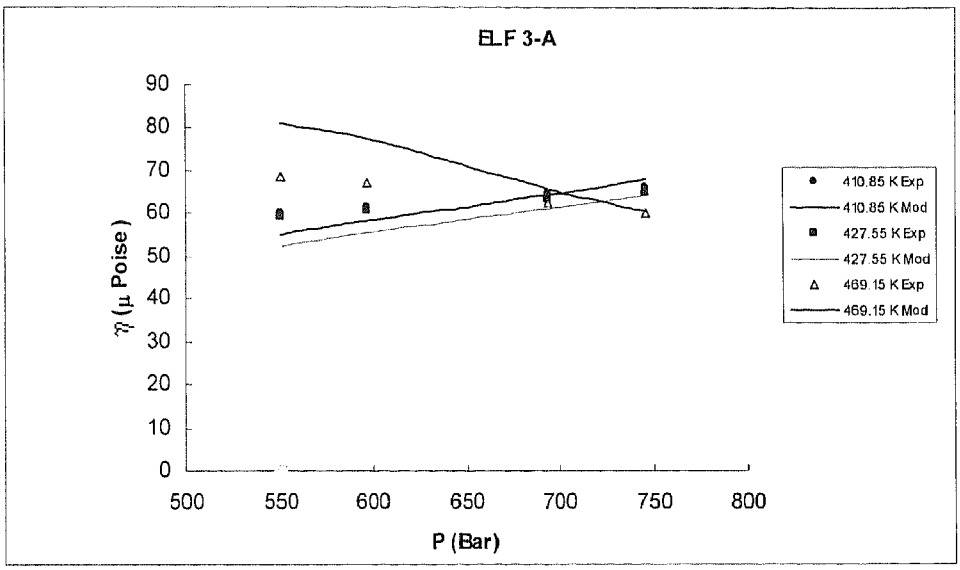

Figure 5.22 – Viscosity – Pressure diagram for ELF 3-A fluid (15 compounds mixture). Solid lines represent LJ model calculation. Experimental data from ELF (2000)

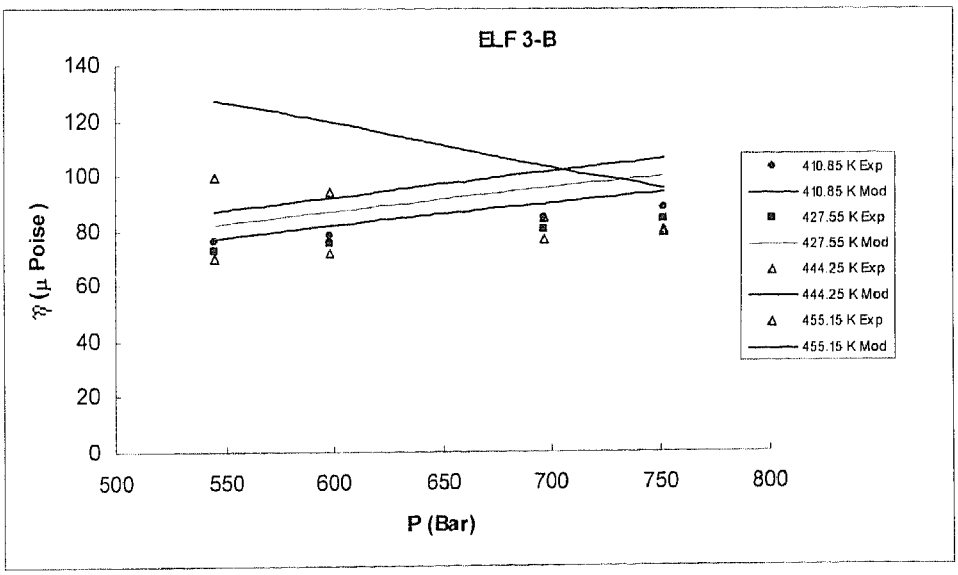

Figure 5.23 - Viscosity – Pressure diagram for ELF 3-B fluid (15 compounds mixture). Solid lines represent LJ model calculation. Experimental data from ELF (2000)

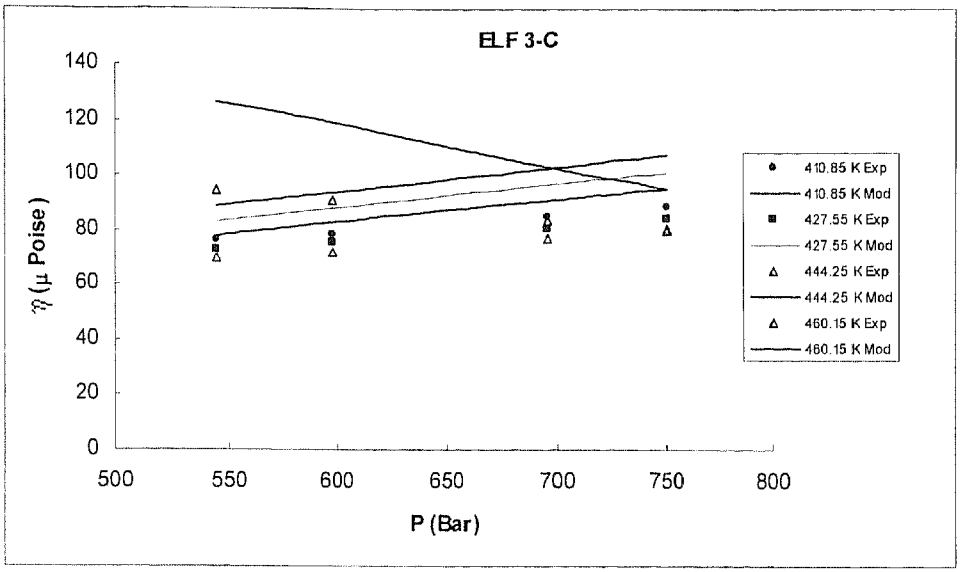

Figure 5.24 – Viscosity – Pressure diagram for ELF 3-C fluid (15 compounds mixture). Solid lines represent LJ model calculation. Experimental data from ELF (2000)

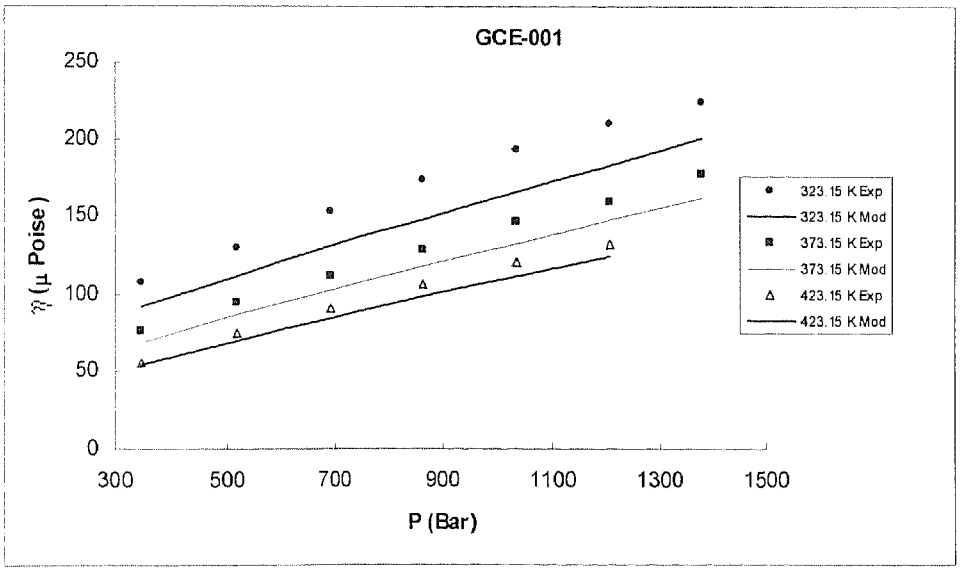

Figure 5.25 - Viscosity – Pressure diagram for GCE-001 fluid (19 compounds mixture) Experimental data from Bell *et al.*(2000)

As can be observed from Table 5.8 and Figures 5.22 to 5.25, the model is able to predict with quite acceptable accuracy both the viscosity values and the "physical" mixture behaviour.

In fact, and as far as "*optimized* parameters" are concerned, only the already available temperature-dependent parameters (slopes of equation 9 and 10), F shifting parameters of pure components present in the mixtures and the available binary mixture interaction parameters (k_{ij} of equation21 to 23) were used for the calculations. No mixture specific parameter was introduced or calculated.

From the analysis of the values of AAD% and maxim AD% on Table 5.8, it is clear that average values of deviations are within acceptable levels, and within the uncertainty of the experimental data. Moreover, the model kept its capability of depicting the "crossing isotherms" behaviour of viscosity, in spite of the deviations shown, especially for the ELF data sets. One explanation for theses deviations may be the experimental method used for obtaining the data points. As above mentioned, the ELF team used the "falling plug" method, while HWU data points were obtained using the capillary tube method. Taking into consideration the technical complexity of obtaining data in experimental equipment working with pressures up to 1 000 bar, capturing data of dynamic nature, the absolute accuracy of the experimental technique can be considered as one possible reason for the lower degree of representation for the ELF data, when compared with the HWU data, of similar composition and TP range.

Nevertheless, and considering that no parameter fitting was carried out using the represented experimental data for the systems presented, it can be concluded that the model has good predictive capabilities and accuracy.

5.8 BENCHMARKING THE MODEL – THE FRICTION THEORY (F-THEORY)

Recently, Quiñones-Cisneros *et al* (2000). proposed the friction theory (f-theory) for viscosity modelling. In the f-theory, the Amontons-Coulomb friction law was linked to the van der Waals repulsive and attractive pressure terms, obtaining a general purpose petroleum fluid viscosity model, with the use of a simple cubic equation of state (EoS).

The f-theory has been applied to the viscosity modelling of pure n-alkanes. This model requires the use of PVT EoS such as the Peng-Robinson (PR) or the Soave-Redlich-Kwong (SRK) equations of state for the estimation of the van der Waals repulsive and attractive pressure terms. Details on this model can be obtained from Cisneros *et al.* (2000).

In a later paper, the group from the Technical University of Denmark (DTU) published results of the application of the model to mixtures containing Carbon Dioxide and of well-defined n-alkane mixtures, representing simple petroleum fractions (Zéberg-Mikkelsen *et al.*, 2000). In this paper, results of viscosity using a well-accepted model within the oil industry, the Lohrenz-Bray-Clark model (LBC) (Lohrenz *et al.*, 1964), are also presented. The comparison presented in this section is based on the results of the mentioned publication. Comparative results are presented in Tables 5.9 and 5.10.

Table 5.9 – Comparison between LJ EoS and f-theory model as reported by Zéberg-Mikkelsen *et al.*, 2000.

			Methane + CO2	n-Decane + CO2	n-Pentane + n-Decane + CO2	n-Butane + n-Hexane + n-Decane + CO2	n-Pentane + n-Hexane + n-Heptane + n-Decane + CO2
		T [K]	323–474	311–403	354–401	324–395	360–395
		P [bar]	34–695	67–347	25–49	25–49	25–49
		NP	132	57	10	10	8
No Kij	f-PR	AAD%	4.49	5.07	4.84	6.24	4.69
		MxD%	17.6	10.9	8.51	14.4	8.74
	f-SRK	AAD%	5.3	5.6	5.01	6.4	4.7
		MxD%	14.6	12.1	8.45	14.5	8.72
With Kij	f-PR	AAD%	3.94	7.35	6.29	6.74	6.23
		MxD%	13	15	10.5	15.1	10.7
	f-SRK	AAD%	5.83	7.92	6.48	6.9	6.27
		MxD%	10.5	16.2	10.5	15.3	10.8
	LJ EOS	**AAD%**	**1.393**	**5.29**	**4.22**	**7.85**	**10.22**
		MxD%	**7.97**	**17.9**	**8.99**	**18.19**	**14.3**
		$\Delta_{Perform\ \%}$	-2.55	0.22	-0.62	1.61	5.53
		$\Delta_{Perform\ MxD\%}$	-2.53	7.00	0.54	3.79	5.58

Table 5.10 – Comparison of LJ EoS with the reported performance of LBC model for the studied systems, as reported by Zéberg-Mikkelsen *et al.*, 2000*.

		Methane + CO2	n-Decane + CO2	n-Pentane + n-Decane + CO2	n-Butane + n-Hexane + n-Decane + CO2	n-Pentane + n-Hexane + n-Heptane + n-Decane + CO2
	T [K]	323–474	311–403	354–401	324–395	360–395
	P [bar]	34–695	67–347	25–49	25–49	25–49
	NP	132	57	10	10	8
LBC*	AAD%	2.29	4.84	35.9	14.4	54
	MxD%	5.2	16.1	41.7	29.7	66.4
LBC-PR*'	AAD%	5.6	28.3	26.4	22.4	21
	MxD%	24	50	29.7	37.8	28
LJ EOS	**AAD%**	**1.393**	**5.29**	**4.22**	**7.85**	**10.22**
	MxD%	**7.97**	**17.9**	**8.99**	**18.19**	**14.3**
	$\Delta_{Perform\ \%}$	-0.897	0.45	-22.18	-6.55	-10.78
	$\Delta_{Perform\ MxD\%}$	2.77	1.8	-20.71	-11.51	-13.7

* - Comparison of the LJ EoS performance is made against the lowest value of f-theory and LBC model in each table presented. Values for AAD% and MxD%, in absolute diference.

The f-theory model was developed in parallel within the EVIDENT project, profiting from the expertise of DTU on corresponding states methodologies for physical properties determination. Due to the fact that the two modelling teams were working within the same project, viscosity data used for development and validation had the same origin, making possible a close comparison. As for "computer code" performance, it was not possible to obtain information about the calculation speed of the f-theory operational code.

Although the f-theory model seems to perform well, one apparent "drawback" of this model is the requirement of using a PVT EoS for the correct phase behaviour prediction (Zéberg-Mikkelsen *et al.*, 2000). In fact, an applicable (in terms of pressure, temperature and density) PVT is required for the f-theory model to work. This fact leads to the requirement of the existence of applicable parameters for the PVT-EoS chosen at the required range of mixture conditions. As it was referred in the introduction of this work, the quite extreme conditions of reservoir fluids, with high temperatures and high pressures, may lead to unavailability of EoS parameters or simply to its inapplicability. In LJ EoS, the PVT EoS is embedded (enhanced KN PVT EoS) and it was incorporated in the model in such a way that no application limitations would arise from its PVT for the desired ranges of applicability.

Another "competitive disadvantage" of the f-theory model is the use of 5 to 7 fitted parameters per pure compound, when compared with the 3 adjustable parameters in the LJ EoS (temperature dependent slopes for ε and σ and the shifting factor F). This will lead to a more difficult parameter fitting process for new compounds. A related "potential disadvantage" of the f-theory model is the (apparent) inexistence of capability of parameter estimation from known general physical parameters, as opposed to the LJ EoS that, in full predictive mode, can infer the pure component parameters from pure compound critical data, as shown in chapter 3.

As shown in chapter 4 and in the present chapter, the Viscosity EoS presented in this work does not suffer from such limitation, as the range of P-T-ρ is wide enough and the "model fluid" is a Lennard-Jones ideal fluid, corrected by the specific ε and σ

parameters for each pure fluid, or its calculation using the critical values methodology, in full predictive mode.
This feature allows the model to be immediately deployed in virtually any deep off-shore petroleum reservoir condition, without limitations on the phase behaviour description or PVT estimation. The results presented in this chapter illustrate the phase behaviour accuracy of the model.

It should also be mentioned that it was not possible to make a comparison regarding the "computer code efficiency" of processor time, as this is a key variable to judge the application of the model to reservoir simulation software.

As a final conclusion to this benchmarking, it can be mentioned that the performance of both models is quite comparable, from the AAD% results presented, whilst the LJ EoS seams to be more "performant" as to the potencial of prediction. It should also be mentioned that, from a "physics" poit of view, the LJ EoS extracts its results from the very nature of molecule dynamics - its basics foundation, MD simulation - whilst the f-theory model seems to rely on more "empirical" models like the PR or SRK PVT EoS's.

As to the comparison with well-known empirical model within the petroleum industry – the LBC model – the results show a considerably better performance of the LJ EoS, for all the systems considered in this work.

5.9 SOFTWARE DEVELOPED

The purpose of the FEUP Team in the EVIDENT Project was to develop a viscosity model, based on Molecular Simulation, and code it into a software package, suitable to application in petroleum reservoir simulators.

As a final "deliverable" presented by the FEUP team, a full program coupled to a general routine for viscosity was assembled. The software allows the calculation of pure compound or mixtures viscosities, using the final LJ EoS model.

The final version of the software was engineered using a strategy of "layer" development, where the base layer – foundation 1 layer – contains the basic algorithm of the model (RP and KN basic equations). Layer 2 contains the coding for the model extensions in temperature and density, while in layer 3 mixing rules and mixture k_{ij} are implemented. In layer 4, user input options are managed, as to p factor, k_{ij} option, as well as input and output data files.

The software package requires the use of pure component basic data as T_C, P_C and molecular weight of each pure compound, as well as an input file with respect of pure component PT data and composition. The pure compounds are treated as single component mixtures for simplicity of operation and inclusion in 3rd party software. As input databases, the software uses a file with k_{ij} binary coefficients matrix and a file with the slopes for ε and σ temperature dependency and the shifting factor F for each pure compound.

Figure 5.26 – Schematic representation of the software package developed

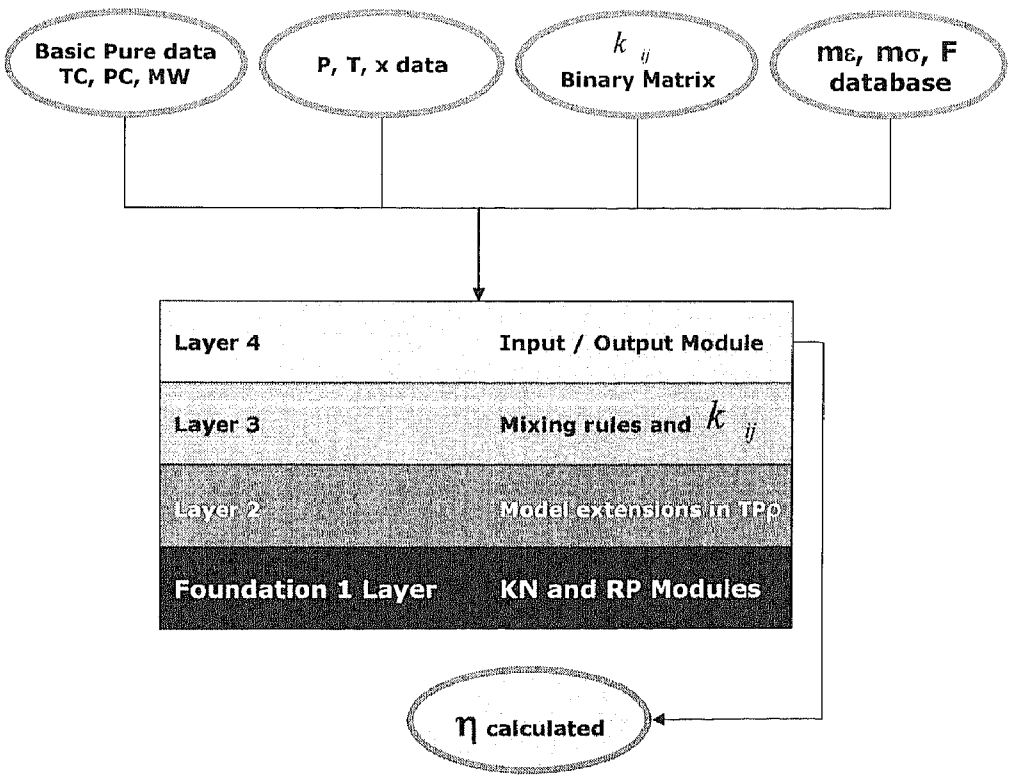

Each layer is composed by FORTRAN subroutines that can be made modular for direct integration on different software applications. Its modularity and layer architecture allows for the further development of alternative solutions in the model, without the need of complete re-programming.

5.10 CONCLUSIONS

In the present chapter, the final development of the LJ EoS was presented, both in terms of the extension of its applicability range in PTρ and its parameters for the temperature dependency. After presenting the results of the application of the model to pure compounds and its validation tests, a strategy for dealing with multi-component was proposed, based on the "One Fluid Approach", using a mixing rule devised to compensate for molecular asymmetries in the mixture, by the use of the p exponent factor in the mixing rules, applied to the model pure component paramenters ε, σ and F. Furthermore, binary interaction coefficients k_{ij} were introduced and *optimized* using binary mixtures data, in order to compensate the model for geometric, electrostatic and unspecified differences among the different molecules in the mixture.

The model was then tested with multi-component mixture data, from binaries to quinary, and as a final test, applied to synthetic reservoir mixtures data, supplied by the Evident Project experimental partners.

The results presented for pure compounds show that the model, as presented in this chapter, works very well for molecules of "sphere-like" molecular geometry – like CO_2, N_2 – having its effectiveness decreased as molecular geometry changes – as for n-C18 – or special electrostatic forces are in action – like water or aromatic compounds.

Nevertheless, the temperature-dependent parameters and shifting factor greatly smooth these geometry effects, acting like an "equivalent molecular diameter" "definer", compensating the geometric deviations from the sphere shape. As referred in early chapters, the present behaviour of the model is a direct consequence of choosing the Lennard-Jones fluid as the model fluid in the MD simulation. In this "fluid", "theoretical molecules" are considered as having sphere-like shapes.

The range of applicability of the model was also "enhanced" by using extrapolation schemes to be able to operate the model in extremer conditions outside the original models of Rowley-Painter and Kolafa-Nezbeda.
The "dangers" of using blindly a model outside its range of applicability are depicted by Machado *et al.* (2001).

The adopted schemes appear to work well, as depicted in Figures 5.6 to 5.12, even taking into account some extreme "Maximum Deviation" values in Table 5.6. Although some errors are quite high in percentage terms, it should be considered that they lie close to the Solid Fluid Equilibrium area, where calculations are quite difficult due to the possibility of solid phase transition, with high fluctuations of viscosity values.

In spite of the errors in this region, the flexibility and range of applicability of the model compensate the potential lack of accuracy of the model in these areas. As will be addressed in the next chapter, the improvement of such results should be the focus of future work.

As far as model performance for mixtures is concerned, results in Tables 5.5 and 5.6 present quite low average errors, for a quite comprehensive mixture database, with a overall maximum error around 25%.

As for results in Table 5.8 and figures 5.18 to 5.21, the values of average deviation depict a good representation behaviour for the analysed multi-component mixtures, with 15 to 20 components.

As mentioned, no mixture-specific parameter were used or adjusted (except for the binary interaction parameter database of k_{ij} values. Bearing this fact in mind, the results presented show a good mixture viscosity representation for the proposed model, with deviations close to the experimental error magnitude.

Again, the highest deviation values occur in the liquid phase, probably close to the SF equilibrium area, constituting another evidence of the need for a improved solution in the SFE region.

The analysis of the comparison made with a recent released viscosity model (f-theory) by the DTU Evident team, presented in Table 5.9, shows a comparative performance on the error side for both models. The f-theory model appears to be slightly better on the higher order mixtures (quinaries), showing slightly worst results on binaries.

The comparison is made using the values reported in the open literature, consequently no data is available regarding the computing time required to make each point calculation. As referred, the main qualitative drawback of the f-theory, when benchmarked against the LJ EoS is that the f-theory model requires the use of an "external" PVT EoS such as PR or SRK. Another apparent drawback is the use of more adjustable parameters per pure compound - 5 to 7, depending on the PVT-EoS used – which decreases the "physical" meaning of each parameter, while making more difficult the optimization of new compound parameter sets.

As a final remark, with reference to the performance against the LBC model – a well known model within the petroleum industry – from the values of average and maximum deviations, it is clear the superior performance of the LJ EoS, specially for higher order mixtures, with absolute differences ranging 10% to 20% in the higher order mixtures.

The benchmark made with the help of the work published by Zéberg-Mikkelsen *et al.* (2000) demonstrates the added value to the petroleum industry of the model proposed in this work and its wide application field.

5.11 LIST OF SYMBOLS

AAD%	average percentual absolute deviation
EAR	Equivalent analytical relationship
EoS	equation of state
k_{ij}	binary interaction parameters
LJ	Lennard-Jones
m	molecular mass
M	molar weight
Max AD %	maximum absolute-value percent relative deviation
MD	Molecular Dynamics
N	number of molecules
N_A	Avogadro's number
NDP	number of data points
P_c	critical pressure
P_r	practical reduced pressure
P_c^+	critical LJ reduced pressure
P^+	LJ reduced pressure
P_{SFE}^+	LJ melting P^+
P	absolute pressure
P	mixing exponent factor transforming mass/mole fractions in Z fractions
PVT	Pressure-Volume-Temperature
RP	Rowley and Painter
SFE	solid-fluid equilibrium
T	absolute temperature
k	Boltzmann's constant
T_c	critical temperature
T_c	critical temperature
T_r	practical reduced temperature
T^+	LJ reduced temperature
T_C^+	critical LJ reduced temperature
$T_{r,LJ,tp}$	triple point LJ reduced temperature
u	potential energy
V	system volume
VAP	Vapour
VLE	vapour-liquid equilibrium
x_i	mole fraction
Z	Z fractions (def. By equation 16)

Greek	**Letters**
σ	LJ separation distance at zero energy
ε	depth of the LJ potential well
η	(Newtonian shear) viscosity
η_0	viscosity at zero density
η_0^+	LJ viscosity at zero density
η_c	(normal) critical viscosity
η_{exp}	experimental viscosity
η_{pred}	predicted viscosity
η_{SFE}	viscosity at SFE
η^+	LJ reduced viscosity
η^+_{SFE}	LJ reduced viscosity at SFE
$\rho^+_{fluid,SFE}$	dimensionless density of the dense LJ fluid in equilibrium with the LJ solid.
ρ	amount-of-substance density (in, e.g., mole cm^{-3})
ρ_c	critical amount-of-substance density (in, e.g., mole cm^{-3} units)
ρ^+	LJ reduced density

5.12 REFERENCES

- Agrawal, R., Kofke, D.A., Mol. Phys. 85: 43,1995.
- Assael, M.J., Karagiannidis, L., Papadaki, M., Int. J. of Thermophys. 12 pp. 811 – 820, 1991.
- Barrufet, M.A., El-Sayed, S.K., Tantawy, M., Iglesias-Silva, G.A., J. Chem. Eng. Data 41 pp. 436 – 439, 1996.
- Baylaucq, A., Boned, C., Dauge, P., Lagourette, B., Int. J. of Thermophys. 18, No.1, 1997.
- Bell, K, Burglass, R., Danesh, A., Gozalpour, F., Todd, A., Tohidi, B., "Evident Report 5", Hariot-Watt University, 2000.
- Ducuolombier, D., Zhou, H., Boned, C., Peyrelasse, J., Saint-Guirons, H. and Xans, P., The J. Phys. Chem. 90 pp. 1692 – 1700, 1986.
- Ducuolombier, D., Zhou, H., Boned, C., Peyrelasse, J., Saint-Guirons, H. and Xans, P., The J. Phys. Chem. 90 pp. 1692 – 1700, 1986.
- Elf ep, "*ELF - Evident Report 3*", Elf ep, Nov. 2000.
- Gonzalez, H., Lee, A.L., J. Chem. Eng. Data, Vol. 13, pp. 66 – 69, 1968.
- Heyes, D.M., Physical Review B, Vol. 37, Number 10, 5677,1988.
- Kolafa, J., Nezbeda, I., Fluid Phase Equilib. 100: 1, 1994.
- Lee, A.L., Ellington, R.T.,J. Chem. Eng. Data, Vol. 10, pp. 346 – 348, 1965.
- Lohrenz, J.; Bray, B.G.; Clark, C.R., Journal of Petroleum Technology, 1171–1176, 1964.
- Machado, J.M. V., Zabaloy, M.S.,Macedo, E.A., Fluid Phase Equilib.,182 75-95,2001.
- Pádua, A.A.H., Faroleira, J.M.N.A., Calado, J.C.G., J. Chem. Eng. Data, Vol. 41, pp. 1488 – 1494, 1996.
- Quiñones-Cisneros, S.E.; Zéberg-Mikkelsen, C.K.; Stenby, E.H., Fluid Phase Equilib., 169, 249–276, 2000.
- Reid, R.C., Prausnitz, J.M., Poling, B.E., " *Properties of Gases and Liquids* ", 4th ed., McGraw-Hill, page 392, 1987.
- Rowley, R.L., Painter, M.M., Int. J. of Thermophys. 18: 1109, 1997.
- «InReferencesAuthorquote_Soave_86» «BookJournal_Info_Soave_86»
- Stephan, K., Lucas, K., Plenum Press, New York and London, 1979.
- Tanaka, Y., Hosokawa, H., Kubota, H. and Makita, T., Int. J. of Thermophys. 12 pp. 245 – 264, 1991.
- Wei, Y. S., Sadus, R. J., AIChE Journal, 46,1,169-196, 2000.
- Zabaloy, M.S., Machado, J.M. V., Macedo, E.A., Int. J. of Thermophys., Vol 22, No 3, 829-858, 2001.
- Zéberg-Mikkelsen, C., Quiñones-Cisneros, S.E.; Stenby, E.H., Petroleum Sci. and Tech., 2000.
- Zéberg-Mikkelsen, C., Cisneros, S., Stenby, H., Petroleum Science and Technology, 20(1&2), 27–42, 2002.

5.13 TABLE OF CONTENTS

5.13.1 List of Tables

5.13.2 List of Figures

APPENDIX 5 – MODEL PARAMETERS USED

Table A1 – List of m_ε and m_σ parameters for application in equations 9, 10 and 11. ID field is presented for reference of k_{ij} in mixtures in Table A2

ID	Compound	m_ε	m_σ	F	ID	Compound	m_ε	m_σ	F
1	Ethane	-0.1903	0.021	1.0979	**21**	n-C14	0.0832	0.8479	1.5312
2	Propane	-0.3494	0.1305	1.1393	**22**	n-C15	0.0786	0.8894	1.6223
3	n-Butane	-0.3709	0.0933	1.0805	**23**	n-C16	0.0799	0.9080	1.6784
4	n-Pentane	-0.2421	0.0773	1.1491	**24**	n-C18	0.0877	1.0598	1.6882
5	n-Hexane	-0.2639	0.0677	1.1896	**25**	2,2-Dimethylpropane	-0.5364	-0.0496	1.4759
6	n-Heptane	-0.0932	0.4897	1.1132	**26**	Butylbenzene	0.0694	0.6859	1.1732
7	n-Octane	-0.1198	0.501	1.1607	**27**	Methylcyclohexane	0.0297	0.4601	1.6816
8	n-Nonane	0.2961	0.8823	1.4535	**28**	1-Methylnaphthalene	0.2007	0.4307	2.1179
9	i-Butane	-0.4603	0.1892	1.2063	**29**	Carbon-Dioxide	-0.2395	0.0364	1.0567
10	i-Pentane	-0.1728	0.0439	1.2172	**30**	Nitrogen	-0.1343	0.0083	1.0682
11	Methane	-0.1415	0.0032	1.1125	**31**	Ethylene	-0.1695	0.0148	1.1062
12	n-Decane	0.0114	0.6835	1.3080	**32**	Propylene	-0.1842	0.0998	1.1684
13	n-Undecane	-0.0252	0.7265	1.2360	**33**	1-Hexene	0.5222	0.9255	1.3291
14	n-Dodecane	-0.0337	0.7551	1.2608	**34**	1-Heptene	0.2950	0.8524	1.1693
15	i-Octane	0.0860	0.6231	1.3851	**35**	1-Octene	0.3196	0.8068	1.3630
16	Benzene	-0.1943	0.2381	1.1591	**36**	Water	-0.0292	-0.4428	1.0697
17	Cyclohexane	0.1973	0.7786	1.9232	**37**	Naphthalene	0.1060	0.5602	1.2435
18	Ethylbenzene	0.2346	0.6109	1.3583	**38**	Phenanthrene	0.0587	0.7047	1.1053
19	Ethylcyclohexane	0.2811	0.7717	1.5839	**39**	Hydrogen-Sulfide	-1.3693	3.4842	2.2431
20	Toluene	0.2683	0.6457	1.2574					

Table A2 – Interaction parameters for binary mixtures, for application on equations. 21, 22 and 23. Please refer to pure compound ID on Table A1 for Binary ID references

Binary ID	K_F	$K\sigma$	$K\varepsilon$
11 , 1	0.050	0.009	0.039
11 , 2	0.056	-0.018	0.111
11 , 3	-0.148	0.009	0.219
11 , 5	0.128	0.299	0.177
11 , 12	-0.984	0.063	0.300
11 , 16	0.466	-0.096	-0.042
11 , 17	0.300	0.150	0.294
11 , 29	-0.105	-0.115	0.400
1 , 29	-0.105	-0.004	0.097
4 , 12	0.277	-0.141	-0.187
5 , 6	0.307	0.452	0.112
5 , 16	-0.504	-0.080	0.078
5 , 17	0.299	0.300	0.258
5 , 20	0.214	0.300	0.252
6 , 8	-0.070	0.017	0.046
6 , 12	0.161	0.131	0.101
6 , 13	-0.160	0.081	0.102
6 , 27	0.322	0.166	0.046
6 , 28	0.300	0.297	0.156
7 , 17	-0.381	0.179	0.210
12 , 5	-0.087	-0.025	0.009
12 , 29	-0.479	-0.335	-0.137
14 , 17	0.075	-0.073	-0.108
15 , 31	0.085	0.257	-0.022
17 , 23	-0.654	-0.247	-0.061
18 , 31	0.220	0.300	0.083
20 , 28	0.220	0.017	-0.057
27 , 28	0.322	0.185	0.042

6. Conclusions and future work

6.1 CONCLUSIONS

A close observation of the evolution of crude oil prices since 2001, presented in Figure 6.1, shows a clear and steady increasing tendency, with more than 100% increase in the period.

The causes for this increase in price of crude are intimately connected with the increase in consumption in the orient, namely in China.

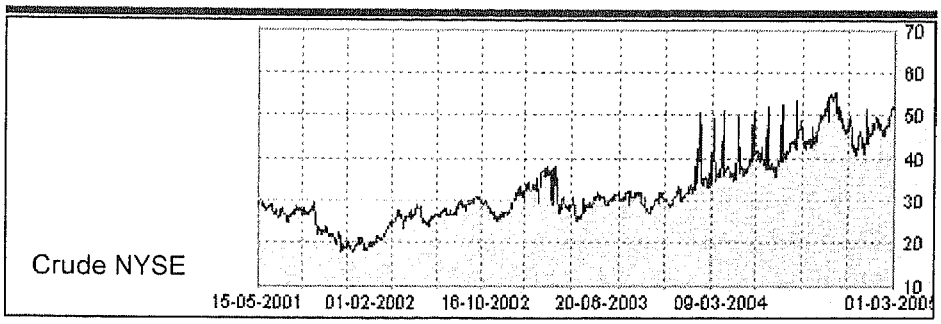

Figure 6.1 – Evolution from 2001 to March 2005 of petroleum crude oil in the New York market. (Jornal de Negócios, 2005)

The work done in chapter 2 allowed the Evident Team to confirm the initial assumption that lead to the implementation of the Evident Project itself: the unavailability of a coherent model for viscosity able to work in a wide range of conditions, along with the unavailability of HPHT viscosity data for a large majority of petroleum fluid compounds.

The simulated data was summarized in the form of Equivalent Analytical Relationships (EARs) - analytical functions that return the same value of the property for the same input data as a computer MD experiments.

This solution allowed us to have the "best of both worlds": The benefits from the microscopic approach from MD in a time frame compatible with the demands of the project. This strategy consisted basically to replace the "engine" – the MD simulator – by an alternative solution that, while containing the original information about the simulations, would not require the computer time to repeat these computer simulations each time the property had to be calculated.

The Rowley and Painter (RP) model (1997) parameters were first re-fitted to allow a better physical behaviour of the simulated viscosity at low temperatures and densities. The first coefficient of the model - b_{11} (see § 4 – equation 15) was set as a function of the remaining *b* parameters. Additionally, as the engineering objective was to calculate viscosities at a given temperature and pressure, the LJ EoS proposed by Kolafa and Nezbeda (1994) was coupled together with RP re-fitted model to generate an Equivalent Analytical Relationship (EAR) connecting temperature, the pressure and the density and yielding the required viscositiy simulation.

Using this methodology, the first approach was to calculate the model parameters – ε and σ – for each pure component using its critical properties. This strategy allows the correction of critical enhancement effects, "setting" the equivalent critical value of viscosity for each pure compound.

This estimation method of pure component model parameters is the "pure predictive mode" of the model, as no experimental data is required for obtaining the model parameters.

The changes done over the original Rowley and Painter model (1997) (equation 15, §4) allowed the model to have a better qualitative behaviour, as the original model showed a relatively complex viscous behaviour at low density and low temperature: a minimum appears for viscosity as a function of density at low temperatures.
This change, coupled with the newly refitted remaining parameters, allowed for the latter establishment of suitable extrapolation schemes, required to operate in areas outside the original PρT envelope, as well as for a better overall qualitative behaviour.

The model presented extraordinary qualitative behaviour, when compared to real viscosity data, presented in the book of Bird *et al.*(1960) (Figures 1.3.1 and 1.3.2 - § 4). Again, no experimental data was used for plotting the referred Figure, demonstrating the realism of the proposed LJ model.

Both qualitative and quantitative model performances were assessed, with good results for simple compounds (e.g. "LJ type molecules"), whilst long chain alkanes would not yield such a good level of accuracy. Fluids like H_2 and Neon also presented high deviations, as they are quantum fluids for which the classical mechanics approach of Molecular Dynamics breaks down at high enough densities and low enough temperatures (Hansen and MacDonald, 1976)

It should be bared in mind that the results presented in chapter 4 are true predictions with the model parameters being calculated from their critical properties. It should also be bared in mind that these results are identical to the results that would be obtained from LJ Molecular Dynamics runs, with input values of ε and σ consistent with the pure compound critical T,P coordinates.

The main limitations of the model, as developed in chapter 4, were its range of applicability in the PρT envelope and the quantitative behaviour for "non-LJ" molecules, like long chain alkanes and molecules with non-spherical geometry. Additionally, the extensions to mixtures had to be developed, in order to meet the goals set in the beginning of this work.

For coping with these problems, two main development strategies were implemented: the development of the extrapolation schemes and the model parameters temperature dependency.

The origin of the range problem was mainly the range of the MD simulation data used for correlating the original Rowley and Painter EAR. Additionally, the behaviour of the LJ fluid close to the Solid-Fluid Equilibrium area, as the LJ (engineering) reduced temperature at the triple point $T_{r,LJ,tp}$ is higher than those found for real fluids (Machado *et al.*, 2001).
Another limitation was the LJ solid-fluid equilibrium (SFE) density $\rho^{+}_{\text{fluid},SFE}$, as the original RP model would only allow for computations up to the SFE line.

A solution for the quantitative behaviour of the model was developed taking into consideration that the LJ model fluid is based on a concept of "soft spheres", with a potential field characterized by these parameters. The solution adopted was then to find an "equivalent sphere" for each compound, characterized by their set of "altered" ε and σ parameters. The parameters were made linearly temperature dependent, and an additional correction parameter was proposed – the F shifting factor. This parameter allowed for the correction of the critical point, and was not made temperature dependent. A large database was used to estimate the 3 model parameters for 39 pure compounds.

As far as extrapolations are concerned, an extrapolation scheme in temperature based on the principle of constant residual viscosity was proposed, where the residual η^+ is considered to be independent of T^+.
An extrapolation scheme on density, for densities higher that the solid-fluid equilibrium (SFE) density was also proposed, based on the second derivative of the VEOS coupled with the information of the viscosity evaluated at the SFE density according to Agrava and Kofkel (1995).

The overall model performance was tested, after estimation by joint optimization both the pure compound temperature dependent slopes of the model parameters ε and σ and of the shifting factor, using a large pure compound database for 39 pure compounds with 3860 data points.

Results obtained showed very good agreement with the experimental data, both qualitatively and quantitatively, with AAD% generally below 5% in most cases. For some long chain alkanes (like n-C18), some aromatic compounds (like 1-Methylnaphthalene) and polar compounds (like water), results were not so satisfactory, with AAD% around 12%. Again, these results show the good behaviour on the LJ model fluid, for compounds with molecular geometry close to sphere-like shape. As mentioned before, the LJ potential function was not "designed" to cope with special inter-molecular forces that appear in aromatic rings or H-bonds.

Additionally to the optimization run, a second pure compound database was compiled, in wide ranges of PT conditions, containing data not used for obtaining the

model parameters. This new database allowed us to test the agreement of the model, with "fresh" data not biased by the optimization procedures.
Results obtained showed equivalent behaviour as of the first database, with AAD% around 6% for the majority of compounds. This fact shows the good agreement of the model and of the pure compound parameters obtained in the optimization run, if the wideness of PT conditions is taken into account. Nevertheless, some of the results obtained, mainly in terms of Max.D%, were quite distant from the experimental value (around 40%). The points showing these high deviations corresponded to low temperature-high density areas data points, well within the extrapolation range. This is a clear indication that the extrapolation schemes devised allowed calculations well outside the original Rowley model range, but with a "price" to pay: Loss of accuracy!

These results showed that, while the proposed model is quite operational in wide ranges of conditions, the extrapolation schemes can surely be improved in the low temperature-high density region.

As for the extension to mixtures, it was decided to apply the One-Fluid approach directly over the model parameters, following the suggestion published by Zéberg-Mikkelsen *et al.*(2000).

For mixtures, three specific binary interaction parameters - $K_{\varepsilon,ij}$, $K_{\sigma,ij}$ and $K_{F,ij}$ - were proposed and obtained by optimization of 3041 datapoints for 28 binary mixtures.
The results obtained showed a quite good agreement with the experimental data, with overall AAD% for binaries, ternaries and quaternaries below 6%, and 10% for the quinaries. The fact that only a fraction of the interaction parameter matrix was complete - 28 out of 760 possible binaries with 39 pure compounds should be taken into account, when analyzing the mixture model performance, and its predictive capabilities.
As referred before, no mixture specific parameters were used, besides the 28 binary interaction parameters.

The runs performed against the multi-component synthetic reservoir mixture data also demonstrated the good predictive capability, even for high-order mixtures with more than 15 compounds.

The comparison with the recent model published by our Evident partner – the F-Theory (Zéberg-Mikkelsen *et al.*, 2000) - revealed an equivalent qualitative and quantitative performance, with a deeper theoretical background, whilst having a simpler implementation (e.g., with less adjustable parameters required by pure compound). Two additional advantages of our LJ VEoS were the independence of 3rd party EOS for pressure calculations, as well as a better predictive capability, as pure compound model parameters can, in our case, be estimated from its critical properties, in the "full predictive mode".
The benchmarking also showed that the LJ VEOS yields more accurate viscosity predictions that the well-accepted LBC model.

As final conclusions, it can be said that the final version of the model presented fulfills well the goal we set for the model at the beginning of the project: the development of a viscosity model, applicable in High-Pressure – High-Temperature deep off shore well conditions, suitable for implementation on reservoir simulators.
Additionally, the model should be able to represent well the viscosity behaviour, both quantitatively and qualitatively, in a wide range of PρT conditions and phases.
Finally, the model should have good predictive capabilities and be applicable to mixtures.

All of the above requirements are satisfactorily fulfilled by the LJ VEOS, with the additional advantage of having its "engine" based on MD simulation, an approximation of the molecular behaviour.

These facts, along with the software implementation strategy, allow for the conclusion that the objectives were successfully achieved.

6.2 FURTHER WORK

Although the LJ VEoS model was fully developed and implemented, some improvements can be made in the sequence of the work done.

The future developments of the model can be performed in two vectors: the development of a new potential function for a new model fluid that can account for more complex molecule interactions (like H-bonds and aromatic rings) and perform the necessary MD simulations in order to substitute the LJ EAR in the model, in wide enough ranges of T+, P+ and ρ+ conditions.

This is the more fundamental vector for development, possibly allowing for the resolution of the range (e.g. extrapolation requirements) and improving the physical behaviour depicting capability, by taking into account more complex intermolecular forces. This work would possibly require the cooperation of a theoretical chemistry researcher.

An alternative vector for further developments would be the study of other extrapolation schemes on temperature and density of the present model, in order to improve the quantitative model performances in the high-density regions.

Additionally, it would be important to complement the team's knowledge about experimental viscosity measurement procedures. Although the Evident project and the visits to all the experimental partners allowed for a good understanding of the techniques applied, it would be important to test alternative HPHT viscosity measurement techniques, as the vibrating wire viscosimeter technology. This technique is known to yield quite accurate values at HPHT conditions, allowing for the extension of the pure compound, as well as for the binaries database.

6.3 REFERENCES

- Agrawal, R., Kofke, D.A., Mol. Phys. 85: 43, 1995.
- Bird, R.B., Stewart, W.E., Lightfoot, E.N., "*Transport Phenomena*", John Wiley & Sons., New York, pp. 16-17, 1960.
- Hansen, J.P. , McDonald, I.R., "*Theory of Simple Liquids*", Academic Press, London, p. 1, 1976.
- Jornal de Negócios, web resource, 2005
- Kolafa, J. , Nezbeda, I., Fluid Phase Equilib. 100: 1, 1994.
- Machado, J.M. V., Zabaloy, M.S., Macedo, E.A., Fluid Phase Equilibria 182 75-95, 2001.
- Powell,R.E, Roseveare,W.E., Eyring,H. Ind. Eng. Chem., 33 430-435, 1941.
- Rowley, R.L., Painter, M.M., Int. J. of Thermophys. 18: 1109, 1997.
- Sun, T. , Teja, A.S., Ind. Eng. Chem. Res., 37: 3151-3158, 1998.
- Zéberg-Mikkelsen, C., Quiñones-Cisneros, S.E.; Stenby, E.H., Petroleum Science and Technology, 2000.

6.4 TABLE OF CONTENTS

THIS PAGE WAS LEFT BLANK INTENTIONALY